UNIVERSIDADE FEDERAL DE MINAS GERAIS

Escola de Engenharia

Programa de Pós-graduação em Engenharia Mecânica

Filipe Nogueira de Carvalho

ENERGETIC, ECONOMIC AND ENVIRONMENTAL ANALYSIS OF A DIRECT-EXPANSION HEAT PUMP ASSISTED BY PHOTOVOLTAIC-THERMAL PANEL FOR DOMESTIC HOT WATER HEATING OPERATING WITH LOW-GWP REFRIGERANTS

Belo Horizonte

2025

Filipe Nogueira de Carvalho

ENERGETIC, ECONOMIC AND ENVIRONMENTAL ANALYSIS OF A DIRECT-EXPANSION HEAT PUMP ASSISTED BY PHOTOVOLTAIC-THERMAL PANEL FOR DOMESTIC HOT WATER HEATING OPERATING WITH LOW-GWP REFRIGERANTS

Submitted in partial fulfillment of the requirements for the degree of Doctorate in Mechanical Engineering in the Programa de Pós Graduação em Engenharia Mecânica of the Universidade Federal de Minas Gerais.

Concentration area: Energy and Sustainability

Advisor: Prof. Dr. Willian Moreira Duarte

Co-advisor: Prof. Dr. Antônio Augusto Torres Maia

Belo Horizonte

2025

Carvalho, Filipe Nogueira de.
C331e Energetic, economic and environmental analysis of a direct-expansion heat pump assisted by photovoltaic-thermal panel for domestic hot water heating operating with low-GWP refrigerants [recurso eletrônico] / Filipe Nogueira de Carvalho**.** - 2025**.**
1 recurso online (107 f. : il., color.) : pdf.

Orientador: Willian Moreira Duarte.
Coorientador: Antônio Augusto Torres Maia.

Tese (doutorado) - Universidade Federal de Minas Gerais, Escola de Engenharia.

Inclui bibliografia.
' Exigências do sistema: Adobe Acrobat Reader.

1. Engenharia mecânica - Teses. 2. Bombas de calor - Teses. 3. Refrigeradores - Teses. 4. Energia - Teses. 5. Sustentabilidade - Teses. 6. Efeito estufa (Atmosfera) - Teses. 7. Evaporadores - Teses. I. Duarte, Willian Moreira. II. Maia, Antônio Augusto Torres. III. Universidade Federal de Minas Gerais. Escola de Engenharia. IV. Título.

CDU: 621 (043)

Ficha catalográfica elaborada pela Bibliotecária Ângela Cristina Silva CRB/6 2361
Biblioteca Prof. Mário Werneck, Escola de Engenharia da UFMG

UNIVERSIDADE FEDERAL DE MINAS GERAIS
ESCOLA DE ENGENHARIA
PROGRAMA DE PÓS-GRADUAÇÃO EM ENGENHARIA MECÂNICA

FOLHA DE APROVAÇÃO

"ENERGETIC, ECONOMIC AND ENVIRONMENTAL ANALYSIS OF A DIRECT-EXPANSION HEAT PUMP ASSISTED BY PHOTOVOLTAIC-THERMAL PANEL FOR DOMESTIC HOT WATER HEATING OPERATING WITH LOW-GWP REFRIGERANTS"

FILIPE NOGUEIRA DE CARVALHO

Tese submetida à Banca Examinadora designada pelo Colegiado do Programa de Pós-Graduação em Engenharia Mecânica da Universidade Federal de Minas Gerais, constituída pelos professores: Dr. Willian Moreira Duarte (Orientador- Departamento de Engenharia Mecânica-UFMG), Dr. Antônio Augusto Torres Maia (Coorientador - Departamento de Engenharia Mecânica-UFMG), Dr. Luis Mauro Moura (Pontifícia Universidade Catolíca do Paraná-PUCPR), Dr. Tiago de Freitas Paulino (Centro Federal de Educação Tecnológica de Minas Gerais - CEFET-MG), Dr. Daniel Dornellas Athayde (Departamento de Engenharia Mecânica-UFMG), Dr. Luiz Machado (Departamento de Engenharia Mecânica-UFMG), como parte dos requisitos necessários à obtenção do título de **"Doutor em Engenharia Mecânica"**, na área de concentração de **" Energia e Sustentabilidade"**.

Tese aprovada no dia 05 de dezembro de 2025.

Documento assinado eletronicamente por **Willian Moreira Duarte**, **Professor do Magistério Superior**, em 14/12/2025, às 11:49, conforme horário oficial de Brasília, com fundamento no art. 5º do Decreto nº 10.543, de 13 de novembro de 2020.

Documento assinado eletronicamente por **Luiz Machado**, **Professor do Magistério Superior**, em 15/12/2025, às 07:43, conforme horário oficial de Brasília, com fundamento no art. 5º do Decreto nº 10.543, de 13 de novembro de 2020.

Documento assinado eletronicamente por **Daniel Dornellas Athayde**, **Professor(a)**, em 15/12/2025, às 08:37, conforme horário oficial de Brasília, com fundamento no art. 5º do Decreto nº 10.543, de 13 de novembro de 2020.

Documento assinado eletronicamente por **Tiago de Freitas Paulino**, **Usuário Externo**, em 15/12/2025, às 08:39, conforme horário oficial de Brasília, com fundamento no art. 5º do Decreto nº 10.543, de 13 de novembro de 2020.

Documento assinado eletronicamente por **Antonio Augusto Torres Maia**, **Professor do Magistério Superior**, em 16/12/2025, às 18:32, conforme horário oficial de Brasília, com fundamento no art. 5º do Decreto nº 10.543, de 13 de novembro de 2020.

Documento assinado eletronicamente por **Luís Mauro Moura**, **Usuário Externo**, em 18/12/2025, às 16:42, conforme horário oficial de Brasília, com fundamento no art. 5º do Decreto nº 10.543, de 13 de novembro de 2020.

A autenticidade deste documento pode ser conferida no site https://sei.ufmg.br/sei/controlador_externo.php?acao=documento_conferir&id_orgao_acesso_externo=0, informando o código verificador **4822014** e o código CRC **7DDB48B5**.

Referência: Processo nº 23072.276348/2025-94 SEI nº 4822014

Preface

This PhD thesis is the result of research conducted in the last four years at the group of refrigeration and heating (GREA) at Universidade Federal de Minas Gerais (UFMG) under the supervision of Prof. Willian Duarte and Prof. Antônio Maia. During this time, one journal paper and two conference/congress papers related to this research were produced and they are listed below:

1. **Nogueira, F.**; Duarte, W. M.; Machado, L.. Review of the recent advances in solar assisted heat pumps integrated with renewable energy sources. - ENCIT2022, 2022, Bento Gonçalves-RS. Proceedings of ENCIT 2022, 2022.

2. **Nogueira, F.**; Maia, A. A. T.; Machado, L.; Duarte, W. M. nergetic, economic and environmental analysis of a direct expansion photovoltaic solar assisted heat pump with low-GWP refrigerants. Solar Energy, v. 302, p. 114042, 2025. ISSN 0038-092X.

3. **Nogueira, F.**; Pinto, G.; Machado, L.; Porto, M.; Maia, A. T.; Duarte, W. Performance evaluation of a PVT-DX-SHAP operating with refrigerants R134a and R290 - COBEM2025. To appear.

This document was written considering the guidelines of Associação Brasileira de Normas Técnicas (ABNT), however, for the decimal separator it was used point (.) instead of comma (,).

To my family, my base.

Acknowledgements

First of all, I would like to thank God for the gift of life and for being with me in all my moments, for giving me strength and confidence.

I would also like to thank my family for their unconditional support, who gave me all the financial and emotional conditions to fulfill my academic career and professional in an ethical and honorable manner.

I would like to thank specially my advisor, Prof. Willian Duarte, for the patience and the quality of the teachings passed on to me, for dedicating his time and for his proactive involvement in the construction of the heat pump at the GREA laboratory. I am also deeply grateful for his meticulous and high-quality reviews of the articles and the thesis.

I would like to thank my co-advisor, Prof. Antônio Maia, for the support and careful reviews of my articles and thesis. I also would like to thank professor Luiz Machado that encouraged and helped me with the working plan of the post graduate program. Thank the professors and staff at UFMG who has always been an institution of excellence in the teaching provided, both in its physical structure and teaching staff.

I would like to thank the professionals who work with me at Fundação Ezequiel Dias for their companionship and professionalism that encourage me in the continuous search for my professional and academic improvement.

Finally, I express my appreciation for the support received by FAPEMIG (Fundação de Amparo à Pesquisa do Estado de Minas Gerais), CNPq (Conselho Nacional de Desenvolvimento Científico e Tecnológico), and CAPES (Coordenação de Aperfeiçoamento de Pessoal de Nível Superior). Additionally, I would like to extend my gratitude to CEMTEC (Centro Multiusuário de Termografia Científica at UFMG/Brazil).

"The only way to do great work is to love what you do." (Steve Jobs)

Abstract

The use of heat pumps may contribute to a substantial reduction in greenhouse gas emissions which is in accordance with climate commitments. A direct expansion photovoltaic thermal solar assisted heat pump (DXPVT-SAHP) is capable to generate both electrical and thermal energy and this work explores the lack of studies of DX-PVT-SAHP using refrigerants with low Global Warming Potential (GWP). The main objective of this work is to evaluate the performance of low GWP refrigerants from an energy, economic, and environmental (3E) perspective when used in a DX-PVT-SAHP. To achieve this objective, a mathematical model was developed to simulate the heat pump operation under different operating conditions. A bench test was constructed to validate the proposed model. The numeric model that employs a moving boundary model for the heat exchangers and a semiempirical model for the compressor was used to compare the refrigerants coefficient of performance (COP) and power output of R134a, R1234yf, R290, R600a, R513A, R454C and R455A. Additionally, the seasonal performance factor (SPF) and total equivalent warming impact (TEWI) were calculated considering the hourly mean solar irradiation, ambient temperature, dew point temperature and wind speed from 07:00 a.m. to 6:00 p.m. in 2024 for Belo Horizonte-MG, Florianópolis-SC and São Luís-MA. R1234yf presented the best results of COP among the compared low GWP pure refrigerants, increasing the COP value from 2.21 at 50 W/m^2 to 4.06 at 1,000 W/m^2, additionally the best TEWI value was presented by R1234yf due to its low GWP value combined with the best SPF among the low GWP fluids. The payback for R1234yf was 2.8 years. The highest solar fraction (SF) was 1.0 in September in São Luís-MA with the DX-PVT-SAHP operating with R1234yf and the worst SF of 0.59 occurred with R454C in the city of Florianópolis in June. The results confirm that the refrigerant achieving the highest COP, combined with the highest solar irradiation, yielded the greatest SF. Conversely, the fluid with the lowest COP under the lowest solar irradiation conditions resulted in the smallest SF.

Keywords: heat pump; photovoltaic thermal evaporator; low GWP refrigerants; TEWI.

Resumo

O uso de bombas de calor pode contribuir para uma redução substancial nas emissões de gases de efeito estufa. Uma bomba de calor de expansão direta utilizando um evaporador fotovoltaico-térmico assistida por energia solar (DX-PVT-SAHP) é capaz de gerar simultaneamente energia elétrica e térmica. Este trabalho explora a lacuna de estudos sobre as DX-PVT-SAHP utilizando refrigerantes com baixo potencial de aquecimento global (GWP). O principal objetivo deste estudo é avaliar o desempenho de refrigerantes de baixo GWP sob as perspectivas energética, econômica e ambiental (3E) quando aplicados em uma DX-PVT-SAHP. Para atingir esse objetivo, desenvolveu-se um modelo matemático para simular a operação da bomba de calor em diferentes condições de funcionamento. Um protótipo foi construído para validar o modelo proposto. O modelo numérico, que emprega um modelo de fronteira móvel para os trocadores de calor e um modelo semiempírico para o compressor, foi utilizado para comparar o COP e a potência gerada com R134a, R1234yf, R290, R600a, R513A, R454C e R455A. Além disso, o SPF e o TEWI foram calculados considerando a média horária da irradiação solar, temperatura ambiente, temperatura do ponto de orvalho e velocidade do vento das 7h00 às 18h00 no ano de 2024 para Belo Horizonte-MG, Florianópolis-SC e São Luís-MA. O R1234yf apresentou os melhores resultados de COP entre os refrigerantes puros de baixo GWP, elevando o valor do COP de 2,21 a 50 W/m^2 para 4,06 a 1.000 W/m^2. Adicionalmente, o melhor valor de TEWI também foi obtido com o R1234yf, devido ao seu baixo GWP aliado ao melhor SPF entre os fluidos de baixo GWP. O tempo de retorno (payback) para o R1234yf foi de 2,8 anos. O maior SF foi de 1,0 em setembro na cidade de São Luís-MA, com o DX-PVT-SAHP operando com R1234yf, enquanto o pior SF de 0,59 ocorreu com o R454C em Florianópolis no mês de junho. Os resultados confirmam que o refrigerante que alcançou o maior COP, associado à maior radiação solar, apresentou o maior SF. Por outro lado, o fluido com o menor COP sob as menores condições de radiação solar resultou no menor SF.

Palavras-chave: bomba de calor; evaporador fotovoltaico-térmico; refrigerante de baixo GWP; TEWI.

List of abbreviations and acronyms

3E	Energy, economic, and environmental
AC	Alternating current
ANN	Artificial neural network
ASHP	Air source heat pump
BH	Belo Horizonte-MG
CFC	Chlorofluorocarbon
COP	Coefficient of performance
COP21	21st Conference of the Parties
DC	Direct current
DHW	Domestic heat water
DX	Direct expansion
EES	Engineering Equation Solver
Exp.	Experimental
EU	European Union
FL	Florianópolis-SC
FS	Fixed speed
Gl	Glazed
GREA	Grupo de Refrigeração e Aquecimento - UFMG
GWP	Global warming potential
HFC	Hydrofluorocarbon

HP	High pressure
HSEU	Heat storage and exchange unit
HTC	Heat transfer coefficient
ID	Identification
IMST-ART	Instituto de Ingeniería Energética Simulation Tool for Refrigeration and Air Conditioning
IX	Indirect expansion
LCCP	Life cycle climate performance
LCOE	Levelized cost of energy
LINMAP	Linear Programming Technique for Multidimensional Analysis of Preference
LP	Low pressure
MA	Maranhão-SL
MAD	Mean absolute deviation or mean absolute relative deviation
Max.	Maximum
MD	Mean deviation or mean relative deviation
NTU	Number of Transfer Units
ODP	Ozone depletion potential
PV	Photovoltaic panel
PVT	Photovoltaic thermal panel
R	Refrigerant
R12	Refrigerant dichlorodifluoromethane known as Freon-12
R1270	Code used to identify propene when used as refrigerant
R134a	Refrigerant also known as HFC-134a

R1234yf	Refrigerant 2,3,3,3-Tetrafluoropropene
R1234ze(E)	Refrigerant 1,3,3,3-Tetrafluoropropene
R152a	Refrigerant 1,1-Difluoroethane
R22	Refrigerant chlorodifluoromethane or 22 Freon
R245fa	Refrigerant 1,1,1,3,3-Pentafluoropropane
R290	Code used to identify propane when used as refrigerant
R32	Refrigerant difluoromethylene
R404A	Refrigerant blend (44% of R125, 52% of R143a and 4% of R134a)
R407C	Refrigerant blend (23% of R32, 25% of R125 and 52% of R134a)
R410A	Refrigerant blend (50% of R125, 50% of R32)
R454C	Refrigerant blend (21.5% of R32, 78.5% of R1234yf)
R455A	Refrigerant blend (75.5% of R1234yf, 21.5% of R32 and 3% of CO_2)
R513A	Refrigerant blend (56% of R1234yf, 44% of R134a)
R600	Code used to identify butane when used as refrigerant
R600a	Code used to identify isobutane when used as refrigerant
R717	Code used to identify ammonia when used as refrigerant
REFPROP	Reference fluid thermodynamic and transport properties database
SAHP	Solar assisted heat pump
SF	Solar fraction
SL	São Luís-MA
SH	Space heating
SLCCP	Specific life cycle climate performance
SPF	Season performance factor

TEWI	Total equivalent warming impact
TRNSYS	Transient system simulation tool
Ung	Unglazed
VS	Variable speed

List of symbols

Greek and special symbols

α	Absorptivity [$dimensionles$]
α'	Void fraction [$dimensionless$]
β	Temperature coefficient [K^{-1}]
χ	Electricity tariff [USD/kWh]
δ	Thickness [m]
ϵ	Average emittance [$dimensionles$]
ε	Effectiveness [$dimensionles$]
η	Efficiency [$dimensionles$]
λ	Annual refrigerant leakage rate [$dimensionles$]
μ	Dynamic viscosity [$Pa \cdot s$]
π	Pi [$dimensionless$]
ρ	Density [kg/m^3]
σ	Stefan–Boltzmann constant [$W/(m^2K^4)$]
σ'	Surface tension [N/m]
τ	Transmittance [$dimensionles$]
Φ	Emission factor [$g\ CO_2/kWh$]
Ψ	Payback period [$years$]
ω	Rotational speed [s^{-1}]
ζ	Annual inflation rate [$dimensionles$]

$\forall$	Displacement volume [m^3]

Latin symbols

A	Area [m^2]
B	Linear regression coefficient [$dimensionless$]
C	Specific heat capacity at constant pressure [$J/(kgK)$]
$\dot{C}$	Heat capacity [J/K]
D	Diameter [m]
e	Error [$dimensionless$]
E	Total energy demand [J]
G	Solar irradiation [W/m^2]
h	Heat coefficient [W/m^2K]
i	Specific enthalpy [J/kg]
I	Difference of initial investment [USD]
k	Thermal conductivity [$W/(m^2K)$]
L	Length [m]
m	Mass [kg]
$\dot{m}$	Mass flow rate [kg/s]
n	Number of data points [$dimensionless$]
N	System lifetime [$years$]
P	Pressure [Pa]
q''	Heat flux [W/m^2]
Q	Energy heating demand [J]

$\dot{Q}$	Heat transfer rate [W]
R^2	Coefficient of determination [$dimensionless$]
S	Annual savings [USD]
T	Temperature [K]
U	Overall heat transfer coefficient [W/m^2K]
v	Velocity [m/s]
V	Voltage [V]
$\dot{W}$	Power [W]
x	Vapor quality [$dimensionless$]

Dimensionless numbers

Bo	Boiling
De	Dean
Pr	Prandtl
Re	Reynolds
We	Weber

Common subscripts

1	Refrigerant state at the compressor inlet
2	Refrigerant state at the compressor outlet
3	Refrigerant state at the expansion valve inlet
4	Refrigerant state at the expansion valve outlet
5	Refrigerant state at the heat exchanger inlet

6	Refrigerant state at the heat exchanger outlet
7	Refrigerant state at the surface of the photovoltaic panel
A, B, C, D, E	Reference letters of linear regression coefficients
a	Ambient
atm	Atmospheric
bo	Boiling region
c	Condensation
cd	Condensation flow region
cmp	Compressor
co	Copper
$coil$	Coil
cr	Critical
con	Convective
d	Desuperheating region
e	Evaporation
ele	Electrical
exp	Experimental
fg	Latent
h	Hydraulic
i	Inlet
ii	Inner diameter of inner tube
inv	Inverter
io	Outer diameter of inner tube

l	Liquid
max	Maximum
min	Minimum
o	Outlet
ov	Overall
p	Plate
$pred$	Predicted
pv	Photovoltaic panel
r	Refrigerant
rad	Radiation
ref	Refrigeration
rv	Reference value
s	Solar irradiation
sub	Subcooling
sup	Vapor region
v	Vapor
vol	Volumetric
w	Water
wd	Wind

List of Figures

List of Tables

Contents

1 INTRODUCTION

According to EPE (2023) the electricity generation in the Brazilian public service and self-producers power plants reached 677.1 TWh in 2022, an amount 3% higher than the result for 2021. Additionally the electricity generation from nonrenewable sources accounted for 12.3% of the national total, compared with 22.6% in 2021 which indicates the trend towards energy production with fewer pollutant emissions and less harmful effects on the environment. Brazil has an electric matrix of predominantly renewable origin, with emphasis on the hydroelectric source that accounts for 69.1% of the total electricity supply as stated by EPE (2023). Furthermore the solar energy supply is in fifth position of the energy sources production corresponding to 4.4% of the total electricity supply as shown in Fig. 1.

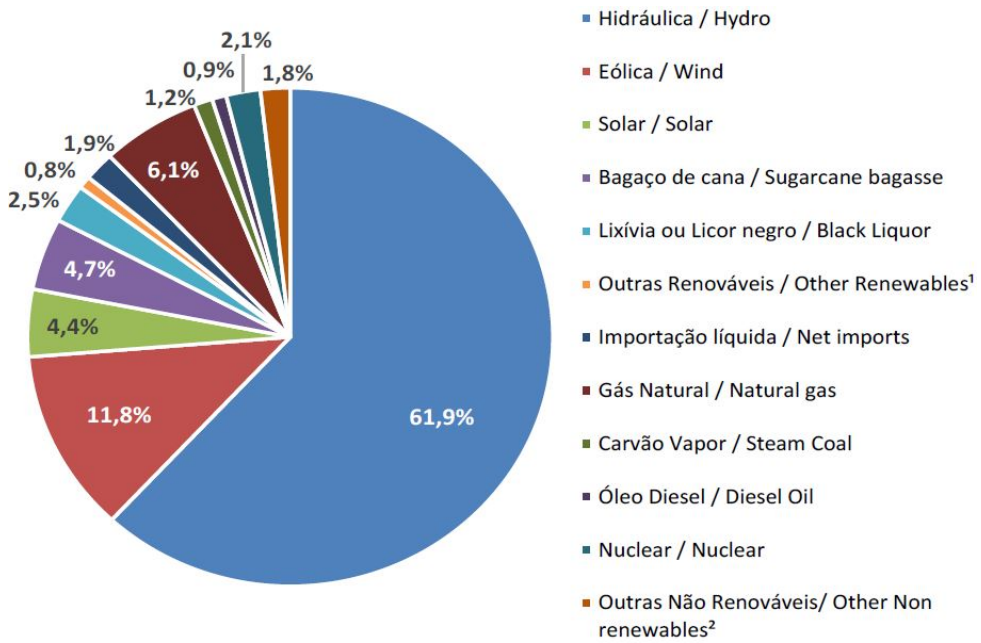

Figure 1 – Total Electricity Supply by Source in Brazil.

Source: EPE (2023)

In the report of EPE (2020) it was stated that in Brazil, the latest available data shows that approximately 50% of electrical energy consumption in houses occurs in thermal systems: close to 35% is used in the production of cold and approximately 15% is used to produce heat in electric showers. Clearly, the significance of energy consumption within the building sector cannot be overstated. Embracing alternative and renewable energy sources in building infrastructure is imperative for reaching sustainability goals.

According to UNEP (2017) the original aims of the Montreal Protocol to protect the ozone layer were fulfilled and a new agreement to phase-down the production and consumption of hydrofluorocarbons (HFCs) called the Kigali Amendment was established. Moreover, During the 21^{st} United Nations Climate Change Conference (COP21) under the UNFCCC (United Nations Framework Convention on Climate Change), the Paris Agreement was put forth, outlining obligations to mitigate emissions of greenhouse gases. Subsequently, the Brazilian Congress ratified this agreement in September 2016 establishing official targets. Brazil aims to cut greenhouse gas emissions by 37% by 2025 and by 43% by 2030 compared to 2005 (Agreement (2015)).

The DX-PVT-SAHP represents a promising solution for reducing both energy consumption and greenhouse gas emissions. However, a major drawback of the currently used equipment is the use of refrigerants which contribute significantly to global warming. The scientific literature contains only a limited number of studies addressing heat pumps operating with low-GWP refrigerants. Furthermore, PVT-SAHPs offer the advantage of decreased CO_2 emissions compared to conventional heat pumps according to Kamel and Fung (2014).

Heating in buildings is responsible for 4 gigatonnes of CO_2 emissions annually which corresponds to 10% of global emissions as informed in OECD/IEA (2022). Replacing fossil-fuel-based boilers with heat pumps offers a substantial reduction in greenhouse gas emissions which is in accordance with climate commitments. Furthermore the heat pump technology is also economically advantageous, according to OECD/IEA (2022) household savings range from USD 300 per year in the United States to USD 900 in Europe compared to traditional heating technologies.

Carrying out a broad literature review demonstrates that the refrigerant most used in heat pumps is R134a that has a high Global Warming Potential (GWP) of 1430. However, there are few studies comparing the performance of the HPs operating with ecological refrigerants with low GWP as the researches conducted by Chaichana, Aye, and Charters (2003); Chata, Chaturvedi, and Almogbel (2005); Ghoubali *et al.* (2014); Makhnatch and Khodabandeh (2014); Botticella and Viscito (2015); Duarte, Paulino, Pabon, *et al.* (2019); Bellos and Tzivanidis (2019); Yıldız and Yıldırım (2021); Kim *et al.* (2023); Yogaraja *et al.* (2024); Arnesson *et al.* (2025).

To address the operational aspects of the DX-PVT-SAHP, two main approaches can be adopted. The first is the experimental strategy, which is generally considered costly due to the high expenses associated with implementation, the demand for skilled labor, and the

extended time required for conducting tests. The second approach is the development of a mathematical model, which provides a more accessible means of obtaining results by employing well-established correlations that have been experimentally validated and are widely reported in the literature.

Knowledge gaps were identified throughout the development of this thesis regarding the limited number of comparative studies involving low-GWP refrigerants operating in heat pump systems. Furthermore, up to the date of publication of this work, only one study had examined a low-GWP refrigerant operating in a DX-PVT-SAHP configuration. In addition, no studies comparing R513A, R454C, and R455A with other refrigerants were found in the literature. The present work aims to address these gaps, thereby contributing original insights to the field of heat pumps operating with low-GWP working fluids.

1.1 General objective

The general objective of this work is to perform an energy, economic and environmental analysis of a DX-PVT-SAHP operating with low-GWP refrigerants.

1.2 Specific objectives

The first specific objective of the present thesis is to build a prototype of an R134a DX-PVT-SAHP at UFMG to obtain the experimental data required for validation. Then, elaborate a mathematical model based on assumptions widely used in the literature and on correlations tested for different refrigerants. Next, validate the model using the experimental data collected from the R134a DX-PVT-SAHP prototype. Afterward, compare the Total Equivalent Warming Impact (TEWI) and the COP of the DX-PVT-SAHP running with different refrigerants. Subsequently, perform an economic analysis of the DX-PVT-SAHP operating with the refrigerant with the lowest TEWI in order to calculate the payback and to compare it with the payback of an electric heater assisted by a PV system. Finally, compare the monthly solar fraction (SF) of the DX-PVT-SAHP in the selected cities of Belo Horizonte–MG, Florianópolis–SC, and São Luís–MA.

2 PVT-SAHP STATE OF THE ART

This chapter is organized into three sections. The first subsection presents the different types of solar-assisted heat pumps. The second subsection describes the operating principles and configurations of heat pumps coupled with PVT panels. Finally, the third subsection reviews comparative studies involving low-GWP refrigerants operating in heat pump systems.

2.1 Solar Assisted Heat Pumps

Solar assisted heat pumps (SAHP) integrates solar energy with heat pumps that are devices in which heat is taken from a heat source at one location and transferred to a heat sink at another location. SAHPs main applications are water heating, space heating and cooling, drying and desalination. According to Buker and Riffat (2016) SAHPs have enhanced performance of the system as a whole compared to conventional air source heat pumps (ASHP).

SAHPs are classified into three different constructive configurations as stated by Fan *et al.* (2021): (i) Parallel; (ii) Series direct expansion (DX-SAHP); (iii) Series indirect expansion (IX-SAHP). In addition to these possible configurations there are also combined systems that integrate constructive aspects of series and parallel configuration as well as the use of auxiliary sources of renewable energy such as wind, geothermal, among others which are not the scope of this thesis.

Parallel SAHP integrate a conventional ASHP with a solar collector to transfer heat independently for the heat sink as shown in Fig. 2. Parallel configuration is composed of a conventional solar heating system where the fluid passing through the solar collector transfers heat to the heat sink as a priority. When solar energy is insufficient to heat the heat sink to the set point temperature a heat pump is activated in parallel to supply the energy needed in the process.

Direct Expansion SAHP (DX-SAHP) that was first proposed by Sporn and Ambrose (1955) is composed of a solar collector evaporator integrated with the heat pump and the refrigerant expands directly without the need of a secondary fluid as represented in Fig. 3. According to M. Mohanraj *et al.* (2018), in DX-SAHPs the incidence of problems related to corrosion is lower and the disadvantage of secondary fluid freezing is eliminated when compared

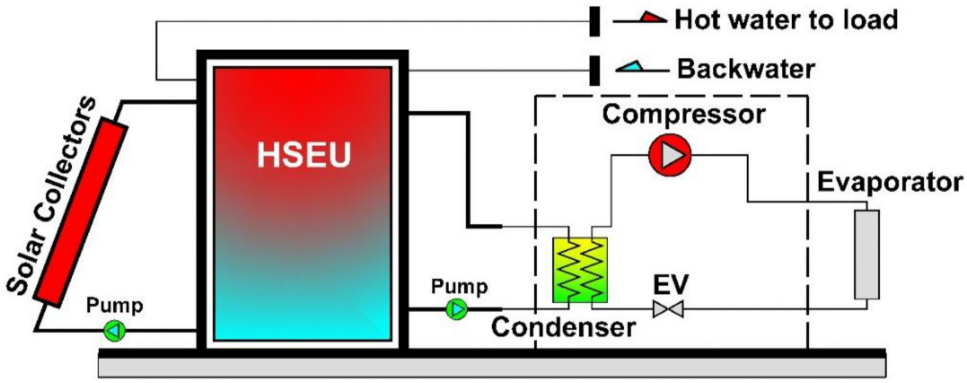

Figure 2 – Example of parallel SAHP.

Source: Fan *et al.* (2021)

to Indirect Expansion SAHP (IX-SAHP).

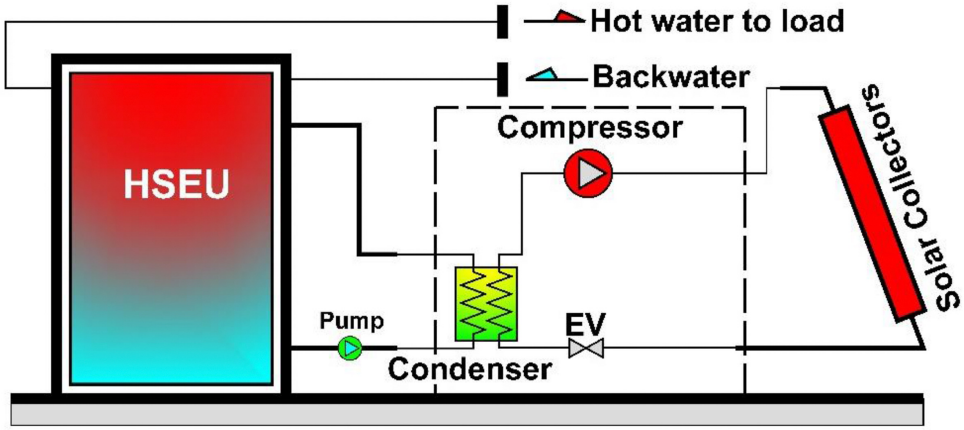

Figure 3 – Example of DX-SAHP.

Source: Fan *et al.* (2021)

In IX-SAHP the thermal energy from the solar collector is transferred by a secondary fluid (water, ethylene glycol, etc.) to vaporize the heat pump refrigerant through an intermediate heat exchanger as illustrated in Fig. 4.

2.2 Photovoltaic-Thermal SAHPs

SAHPs integrated with photovoltaic-thermal collector (PVT-SAHP) are equipment that a solar collector type evaporator is coupled to a photovoltaic module as represented in Fig. 5. This arrangement enables the cogeneration of thermal and electrical energy in the collector evaporator.

Drop of electricity production efficiency by photovoltaic cells related to the increase in its operating temperature can be minimized due to the decrease in the operation temperature

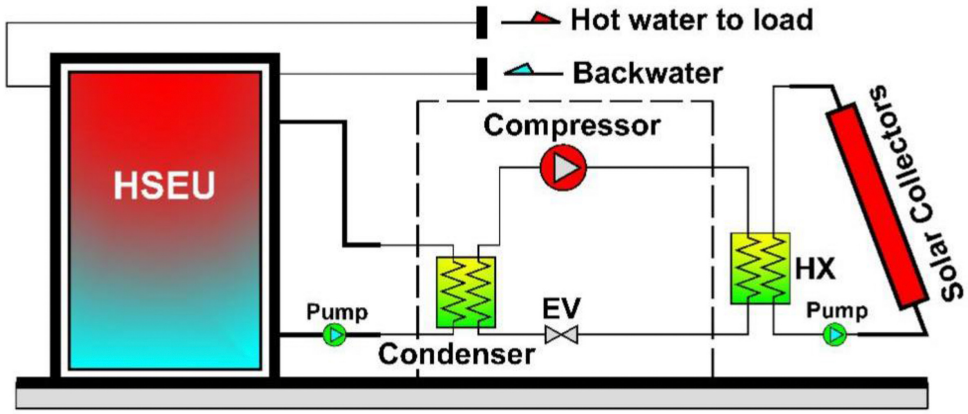

Figure 4 – Example of IX-SAHP.

Source: Fan *et al.* (2021)

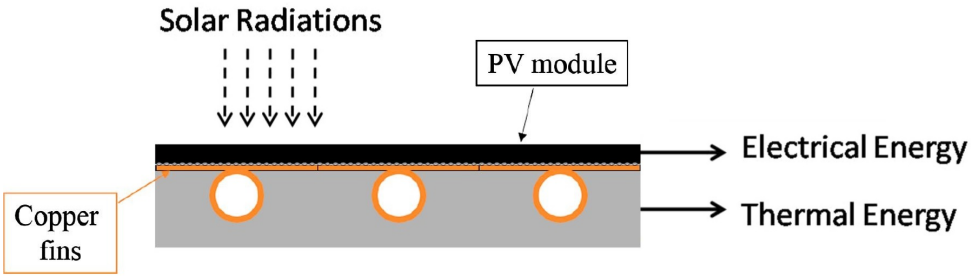

Figure 5 – PVT collector schematic.

Source: Adapted from Guarracino *et al.* (2019)

caused by the absorption of heat in the evaporator of the PVT-SAHP and also benefits from a higher evaporation temperature. Ji *et al.* (2009) developed a PVT-SAHP with 12% increase in the efficiency of photovoltaic energy production compared to other systems operating separately. Furthermore, PVT-SAHPs offer the advantage of decreased CO_2 emissions compared to conventional heat pumps as stated by Kamel and Fung (2014).

PVT was established to optimize the solar energy harvesting. The area utilized by PVT is smaller than that used by traditional PV or thermal collectors separately installed. PVT evaporators are manufactured according to the type of photovoltaic cells, thermal collector, working fluid, glazing and thermal absorber. Herez *et al.* (2020) classified these equipments according to Fig. 6.

PVT-SAHP systems do not yet have a standardized manufacturing approach. Depending on the intended application, they may incorporate different types of components—for example, collectors can be either glazed (gl.) or unglazed (ung.); electrical energy can be stored in batteries, fed into the grid, or supplied directly to the system; compressors may operate at variable speed

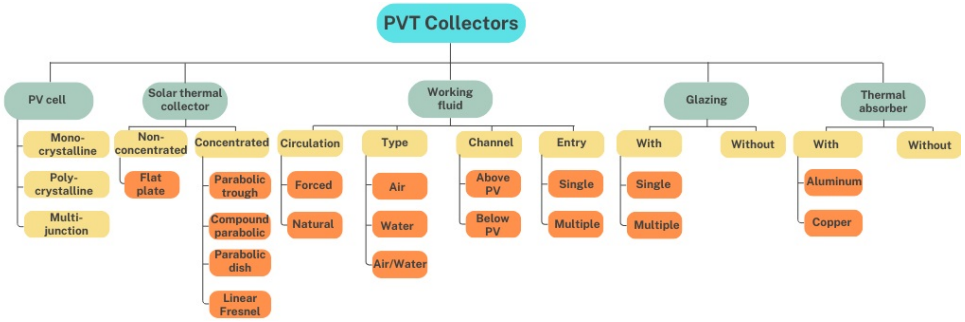

Figure 6 – PVT classification.

Source: Adapted from Herez *et al.* (2020)

(VS) or fixed speed (FS) and use either alternating current (AC) or direct current (DC); and the system can be designed for space heating (SH) or domestic hot water (DHW).

A review in the latest researches concerning the operational and performance parameters of DX-PVT-SAHP and IX-PVT-SAHP was summarized in Tab. 1 and Tab. 2. Analysis of the researches yields the conclusion that most of the experimental and theoretical studies about PVT-SAHP were performed with non-ecological refrigerants such as R134a and R22 corresponding to 50% and 23% respectively of the studies presented in Tab. 1 and Tab. 2. The refrigerant R22 has very low ozone depletion potential (ODP), R134a has null ODP and both refrigerants still have high global warming potential (GWP) according to Chaichana, Aye, and Charters (2003).

Table 1 – Studies on DX-PVT-SAHP

Authors	Collector		Electrical energy	Compressor		Refrigerant	COP	Type of study	Load	Location	Tank	Water
	Cover	A (m^2)		Speed	Current						(L)	Temp. (^oC)
Pei *et al.* (2008)	Gl./Ung.	5.49	Storage / System	VS	AC	R-22	3.41-4.85	Exp.	SH, DHW	China	-	15-55
Xu, Deng, *et al.* (2009)	Gl.	2.25	Grid	VS	AC	R-22	4.8	Theo.	DHW	China	150	25-50
Chow *et al.* (2010)	Ung.	12	System / Grid	FS	-	R-134a	4.97-6.89	Theo.	DHW	Hong Kong	2,500	16-29
Fang, Hu, and Liu (2010)	Ung.	1.2	Storage / System	-	AC	-	2.75-2.85	Exp.	DHW	China	-	20-42
Hu, Wang, and Fang (2010)	-	7.5-11.3	Storage / System	-	AC	R-134a	6.0-7.9	Theo.	SH, DHW	China	-	-
Chen, Riffat, and Fu (2011)	Gl.	0.42	Grid	-	AC	R-134a	3.8-4.3	Exp.	SH	U.K.	-	25-45
Zhao *et al.* (2011)	Gl.	10	Storage / System	-	AC	R-134a	-	Theo.	SH, DHW	U.K.	-	-
Xu, Zhang, and Deng (2011)	Gl.	3.17	Storage / System	-	DC	R-134a	4.8	Exp.	DHW	China	80	30-70
Zhang, Guanb, and Guo (2012)	Ung.	61	Storage / Grid	-	-	-	4.86	Theo.	DHW	China	8,000	5-55
Zhang, Zhao, *et al.* (2013)	Gl.	0.61	Storage / System / Grid	-	AC	R-134a	8.7	Theo. / Exp.	DHW	China	100	-
Tsai (2015)	Ung.	8.5	Grid	VS	AC	R-134a	-	Theo. / Exp.	DHW	Taiwan	200	26-48
Mohanraj *et al.* (2016)	Ung.	1.92	Storage	FS	-	R-134a	2.8-4.1	Exp.	SH	India	-	-
Manzolini *et al.* (2016)	Gl.	100	System	VS	AC	R-134a	3.00-6.05	Exp.	SH, DHW	Italy	1,000	max. 35
Li and Sun (2018)	Gl.	1.87	Storage	FS	-	R-22	3.1	Theo.	DHW	China	150	10-50
Zhou *et al.* (2019)	Gl.	1.2	Grid	-	AC	R-22	6.16	Exp.	DHW	China	150	25-55
Yao, Chen, *et al.* (2020)	Gl.	2	System / Grid	-	-	R-134a	3.2-6.0	Theo.	DHW	China	200	-
James *et al.* (2021)	Gl.	5.39	System	VS	AC	R-32	6.4	Exp.	DHW	India	150	30-63
Yao, Liu, *et al.* (2021)	Gl.	1.14	System / Grid	VS	AC	R-134a	4.37	Exp.	DHW	China	-	-
Sanz *et al.* (2022)	Ung.	4.80	System / Grid	VS	DC	R-134a	2.3-3.4	Exp.	DHW	Czech Rep.	300	max. 50
Zanetti *et al.* (2023)	Ung.	1.64	Storage / System	VS	AC	R-744	3.31-4.29	Theo. / Exp.	DHW	Italy	200	-
Liang *et al.* (2023)	Gl.	4.80	Grid	-	-	R-22	4.32	Theo. / Exp.	DHW	China	150	5-58
Sharma *et al.* (2024)	Gl.	0.65	Grid	-	-	R-134a	3.75	Theo. / Exp.	DHW	India	60	20-50
Petrucci *et al.* (2024)	Gl.	2.83	Storage / Grid	FS	AC	-	2.5 - 7.5	Theo.	DHW	Brazil	300	25-65
Liu, Quan, *et al.* (2024)	Gl.	-	Grid	FS	AC	-	4.28 - 4.62	Theo. / Exp.	DHW	China	200	-
Hu, He, *et al.* (2024)	-	-	Grid	VS	DC	R410A	5.30	Theo. / Exp.	DHW	China	500	28.8 - 52.64
Anastas and Mwesigye (2025)	-	5	-	-	-	-	3.83-4.08	Theo.	DHW	Canada	180	max. 50

Source: Adapted from Nogueira, Machado, *et al.* (2025)

Table 2 – Studies on IX-PVT-SAHP

Authors	Collector		Electrical energy	Compressor		Refrigerant	COP	Type of study	Load	Location	Tank	Water
	Cover	A (m^2)		Speed	Current						(L)	Temp. (^oC)
Wang *et al.* (2015)	Gl.	2.56	-	-	-	R-22	3.07	Theo. / Exp.	DHW	China	64	15-50
Qu *et al.* (2016)	Ung.	8.68	Grid	-	-	R-134a	2-5	Exp.	DHW	China	500	30-50
Fine, Friedman, and Dworkin (2017)	Gl.	8.4	System	VS	-	R-134a	-	Theo.	DHW	Canada, USA	-	24-65
Chen, Zhang, *et al.* (2017)	Gl.	1.3	-	FS	AC	R-134a	3.23	Theo.	DHW	China	200	25-55
Dannemand, Perers, and Furbo (2019)	Ung.	3.1	System	VS	AC	R-407C	2.3-3.4	Exp.	DHW	Denmark	160	max. 50
Vallati *et al.* (2019)	-	1.67	System / Grid	-	-	-	4.82-4.95	Theo.	SH, DHW	Italy, Czech Rep.	4,000	7-25
Leonforte *et al.* (2020)	Gl.	1.69	Grid	VS	-	-	-	Exp.	SH, DHW	Italy	300	max. 40
Liu, Zhang, and Chen (2020)	Gl.	0.73	Storage	-	-	R-22	3.51	Exp.	SH, DHW	China	1,000	-
Rijvers, Rindt, and Keizer (2021)	-	5-35	-	-	-	R-410A	3.0-3.9	Theo.	SH, DHW	Netherlands	175-250	10-60

Source: Adapted from Nogueira, Machado, *et al.* (2025)

2.3 Comparative studies on refrigerants selection of heat pumps

Wu, Hu, and Wang (2021) divided the refrigerants development into four different stages with different development requirements, as presented in Fig. 7.

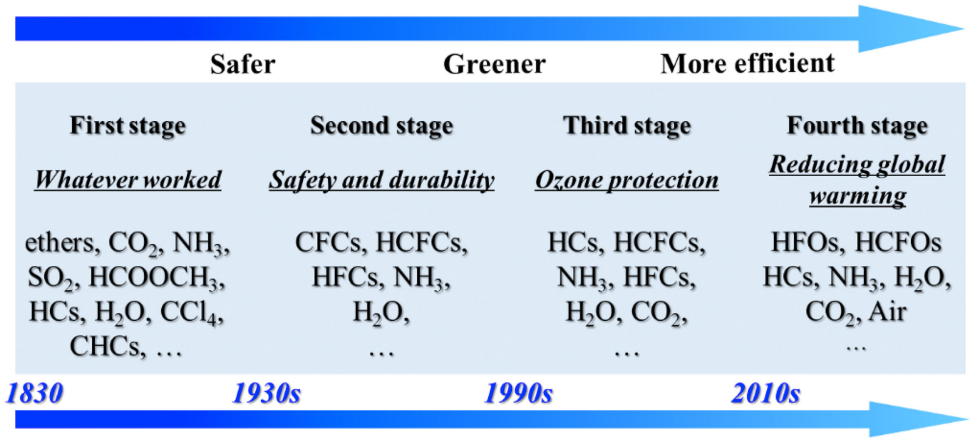

Figure 7 – Development of refrigerants.

Source: Wu, Hu, and Wang (2021)

At the beginning of HP technology development the refrigerant selection was based on COP and in the hazardous rating. CFCs were broadly used due to their safety compared to natural refrigerants according to Chaichana, Aye, and Charters (2003). The hazard classification is defined according to the Standard 34 ASHRAE standards for refrigerants as shown in Fig. 8.

As a consequence of the Montreal protocol agreement in 1987 the phase out of the high ODP refrigerants, such as the broadly used R12 and R22 was established and research on new refrigerants like R134a for HP application started as reported by Chata, Chaturvedi, and Almogbel (2005). In Tab. 3 is presented the ODP and GWP among other information from some refrigerants operating in HPs.

According to Duarte, Paulino, Pabon, *et al.* (2019) the refrigerant selected for a HP must present some characteristics such as (i) non-toxic and non-flammable; (ii) easy leak detection; (iii) suitable thermodynamic properties; (iv) high chemical stability in the refrigeration system; (v) miscible in the lubricating oil; (vi) compatibility with refrigeration system materials; (vii) low cost; and (viii) low environmental impact.

In a comparative research conducted by Chaichana, Aye, and Charters (2003) based on a commercially available R22 SAHP water heater, the refrigerants R22, R290, R600, R600a,

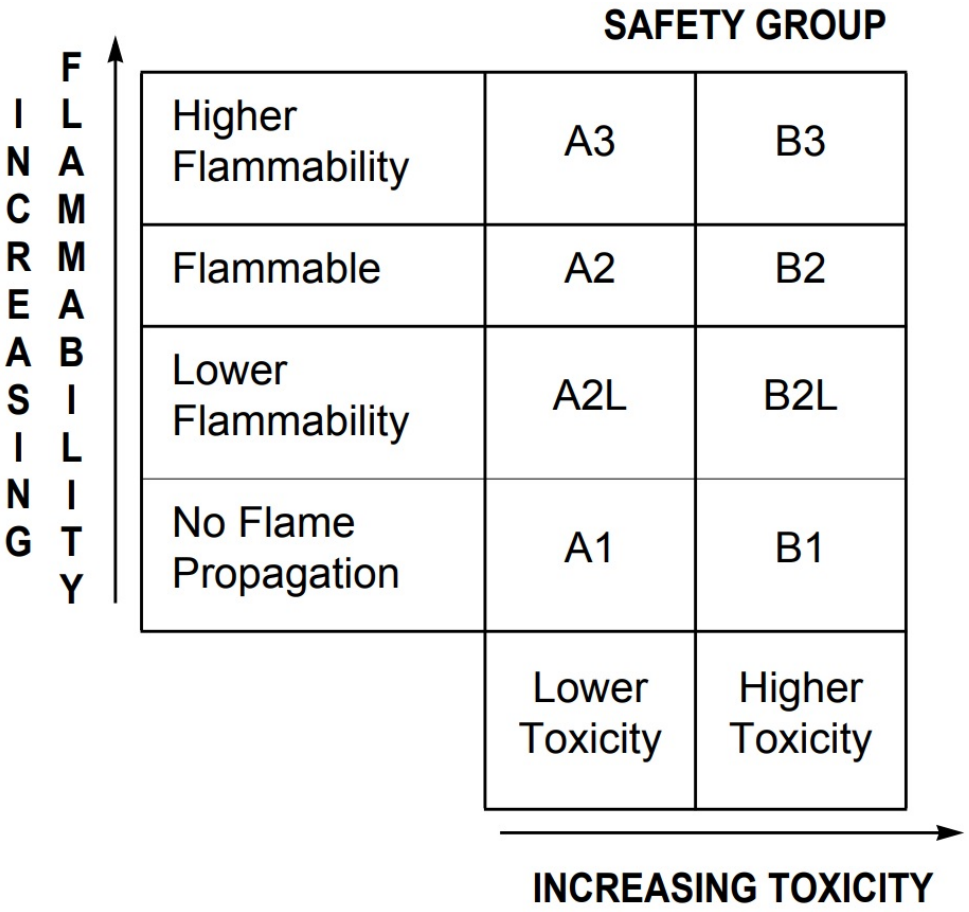

Figure 8 – Refrigerants safety groups classification by ASHRAE.

Source: ASHRAE (2013)

R1270 and R717 were selected and compared according to the COP, ODP and GWP. The fluids properties were estimated using REFPROP. It was concluded that R717 was the prime candidate to substitute R22 and it was highlighted that the mass of R717 is only 20% of the R22 that helps to minimize the global warming effects.

Chata, Chaturvedi, and Almogbel (2005) compared the COP of R12, R22, R134a, R404A, R410A and R407C of a DX-SAHP. The fluids properties were obtained from REFPROP and a program in C++ was written. The conclusion of the study was that R12 produced the highest COP value followed by R22 and R134a, respectively. The system's performance decreases by approximately 2-4% within the collector temperature range of 0–20 ^{o}C when R12 is substituted with R-134a.

A comparative research between R407C, R290 and R1234yf with a numerical model method performed in EES and TRNSYS by Ghoubali *et al.* (2014) was developed for a simultaneous ASHP that operates in three modes: heating, cooling and simultaneous. An environmental

Table 3 – Refrigerants properties operating in heat pumps

Refrigerant	ODP	GWP	Normal Boiling Point (^oC)	Critical Temp. (^oC)	Safety Group	Refrigerating effect (kJ/m^3)
R12	0.82	10900	-30	111.97	A1	2833
R22	0.04	1790	-41	96.145	A1	4529
R32	0	675	-51.7	78.1	A2L	7240
R134a	0	1300	-26	101.6	A1	2972
R404A	0	3700	-46.6	72.046	A1	4797
R407C	0	1700	-43.8	86.034	A1	4215
R410A	0	2100	-51.6	74.67	A1	6729
R454C	0	146	-45.6	85.7	A2L	4080
R455A	0	146	-52.0	85.6	A2L	4286
R1234yf	0	<4.4	-29.4	94.7	A2L	2840
R1270	0	20	-48	91.061	A3	4653
R152a	0	133	-24	113.26	A2	2757
R290	0	20	-42	96.74	A3	3867
R513A	0	573	-29.2	96.5	A1	3058
R600	0	20	0	151.98	A3	1143
R600a	0	20	-12	134.66	A3	1573
R717	0	<1	-33	132.25	B2L	5003
R744	0	1	-78	30.98	A1	14909

Source: Adapted from ASHRAE (2013)

and performance analysis was done considering the TEWI and COP, respectively. The conclusion was that R290 was the best option and had also the additional advantage of components suitable and available on the market.

In another research conducted by Makhnatch and Khodabandeh (2014) of a 30 kW ASHP a Life Cycle Climate Performance (LCCP) analysis was carried out. The LCCP analysis take into account the estimation of direct and indirect green house gas emissions of the system. In that study the fluids with GWP values lower than 150 such as R152a, R1234yf, R290, R1270 were compared to the R410A. The authors concluded that the natural refrigerant R290 was the best option because of its low lifetime emissions and satisfactory COP.

Botticella and Viscito (2015) developed a simulation model of an ASHP for space heating using IMST-ART software to compare the COP of R1234yf and R290. The results showed a better COP of R290 for both climate conditions tested. Additionally, the largest difference in SPF (7.5%) occurs under the colder reference climate, where the test conditions specified by the European Standard result in a higher pressure ratio and reduced performance of the R1234yf heat pump.

Duarte, Paulino, Pabon, *et al.* (2019) conducted a refrigerant selection study of a DX-SAHP according to the experimental setup presented in Fig. 9. The R134a DX-SAHP is composed of a tank to store hot water with 200 L, a collector evaporator of 1.65 m^2 area, a hermetic reciprocating compressor, a thermostatic expansion valve and two different condensers: an

immersed condenser and a coaxial condenser. The experiments were made of 20 tests to heat 200 L of water from ambient temperature to approximately 45 ^oC considering indoor and outdoor environments.

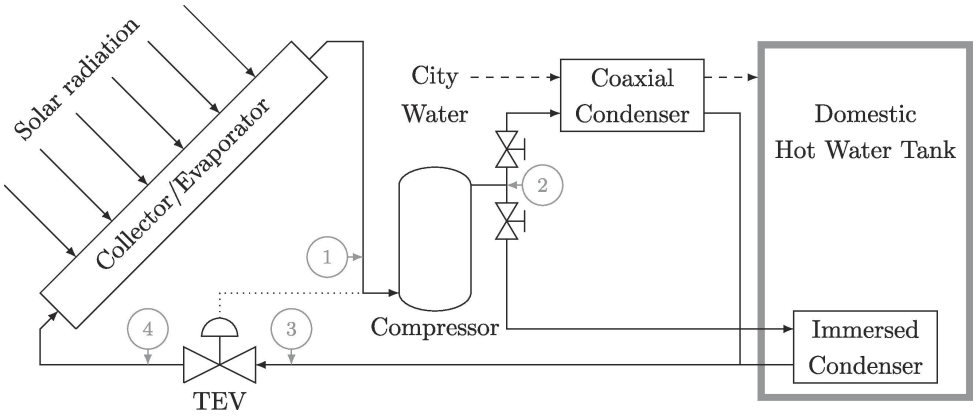

Figure 9 – Experimental setup used in the model validation of DX-SAHP.

Source: Adapted from Duarte, Paulino, Pabon, *et al.* (2019)

The comparison was made between the R134a that is a broadly used refrigerant in DX-SAHP. The R290 selection was made because of its high evaporating temperature and its use by many manufacturers. In addition, R600a was selected due to its lower noise levels and good compressor efficiency. The R744 choice was made because of the good match between the water temperature profile in applications with conventional heaters. Lastly, R1234yf was chosen based on its suitability to replace the R134a and to be considered an ecological alternative. The DX-SAHP model was developed using a quasi-steady-state model in the EES with the purpose to determinate the TEWI and the COP of the system. The model validation compared the measured COP with the calculated COP and it was found a mean difference of 1.6% for both immersed and coaxial condensers. The conclusion was that in general the lower the TEWI value, the higher the COP value of a refrigerant. Another conclusion was that R290 has better COP than others refrigerants for solar irradiation between 300 W/m^2 and 700 W/m^2 considering the coaxial condenser and for solar irradiation between 50 W/m^2 and 700 W/m^2 for the immersed condenser, R290 has also better COP as shown in Fig. 10.

Bellos and Tzivanidis (2019) developed a theoretical study of an IX-PVT-SAHP according to Fig. 11. The IX-PVT-SAHP is composed of a tank to store hot water with 500 L and a PVT of 10 m^2 area. The IX-PVT-SAHP aim is to warm up air from 20 ^oC to 30 ^oC and the produced electricity from the PV cells is delivered to the inverter. A part of this electricity is given to the heat pump and the remaining part goes to the grid or to the building.

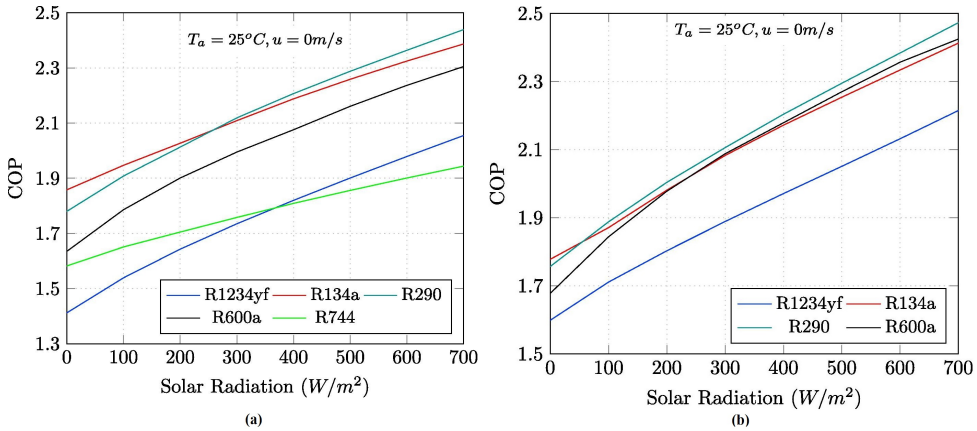

Figure 10 – The variation of COP function of solar irradiation for coaxial (a) and immersed (b) condenser.

Source: Adapted from Duarte, Paulino, Pabon, *et al.* (2019)

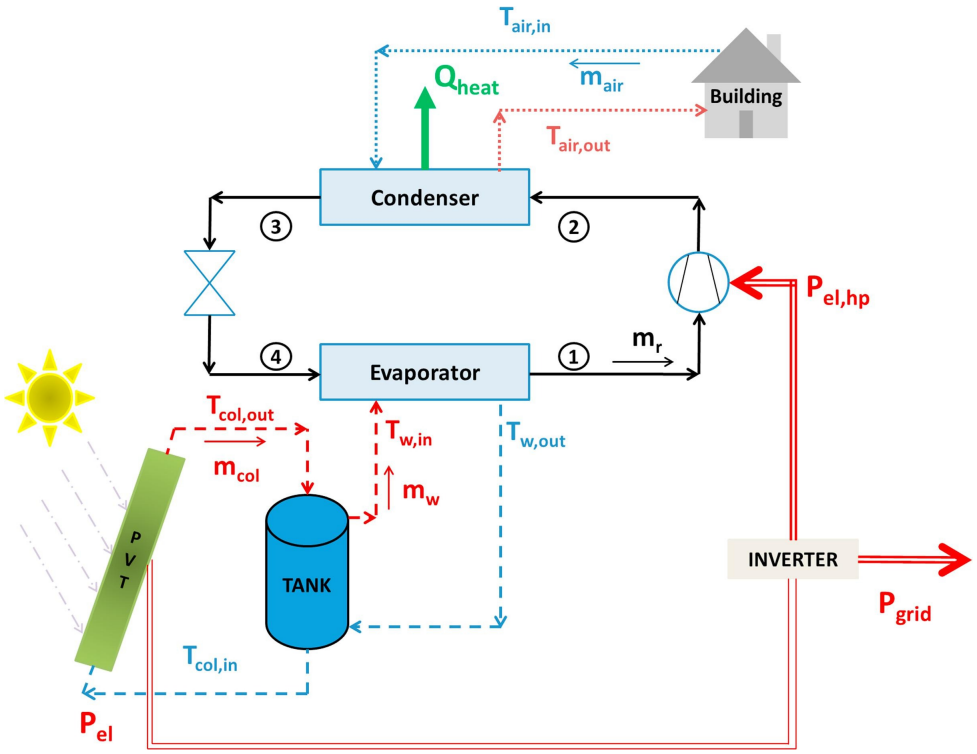

Figure 11 – Theoretical setup of the IX-PVT-SAHP.

Source: Bellos and Tzivanidis (2019)

The developed model was examined under steady-state condition comparing seven refrigerants: R32, R1234yf, R245fa, R404A, R290, R152a and R600a. In the investigation different mass flow rate and evaporator temperature were simulated in order to obtain an optimized value of heating production (Q_{heat}) and net electricity production (P_{grid}) using the EES. The result was that for all the cases, the same optimum design conditions were found. The obtained mass flow rate was 0.3222 kg/s and the evaporator temperature of 12.5 ^oC. According to Fig. 13 the

optimum point is the one which has the lowest geometrical distance to the ideal one point. In that study the best option was R32 followed by R1234yf. It can also be stated that R245fa leads to the maximum electricity production and to the minimum heating production. Alternately, R404A is the fluid with the maximum heating production and the minimum electricity production.

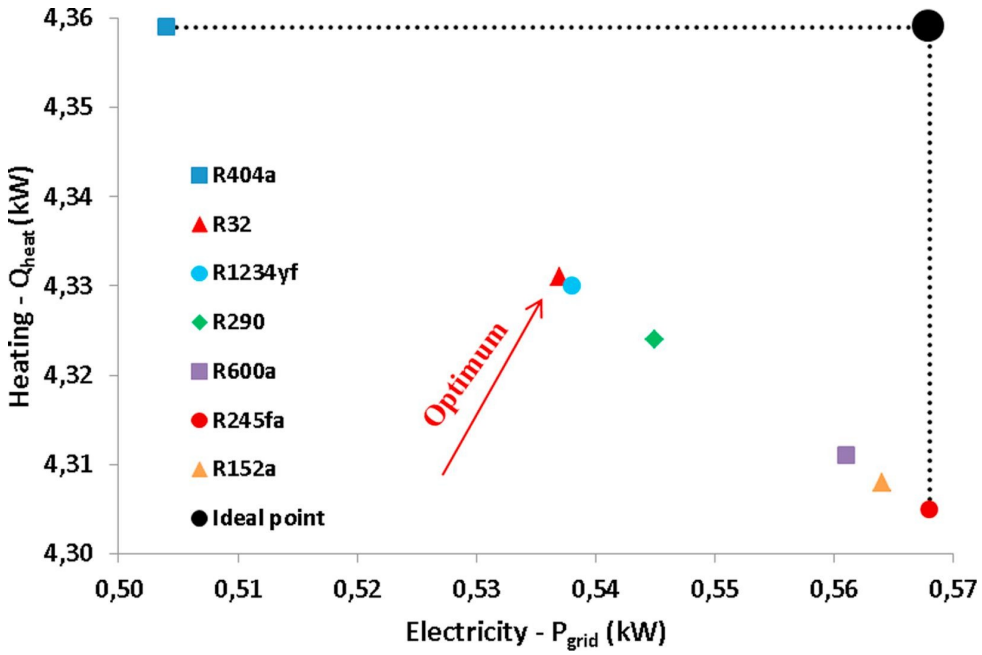

Figure 12 – Comparison of the optimum design points for all the working fluids.

Source: Bellos and Tzivanidis (2019)

The last analysis was the system performance evaluation during the winter period from November to April for the climate conditions of Athens (Greece). According to Fig. 13 (a) in December occurs the minimum daily heating production of 16.55 kWh and also the minimum daily electricity production of 2.28 kWh. On the other hand, in April occurs the maximum daily heating production of 37.73 kWh and also the maximum daily electricity production of 3.88 kWh. According to Fig. 13 (b) in January the energy efficiency is maximized resulting in 60.53% and in the same month the exergy efficiency is minimized resulting in 9.26%. The authors concluded that the energy and exergy efficiencies have reverse variations among the examined months. This behavior occurs due to the variation of the ambient temperature. Higher ambient temperature levels lead to lower electricity production and lower exergy efficiency. Higher ambient temperature is also related to higher heating production and higher energy efficiency.

Yıldız and Yıldırım (2021) developed a comparative theoretical and experimental study in a R134a ASHP shown in Fig. 14 to compare the performances of R134a, R1234yf and R513A.

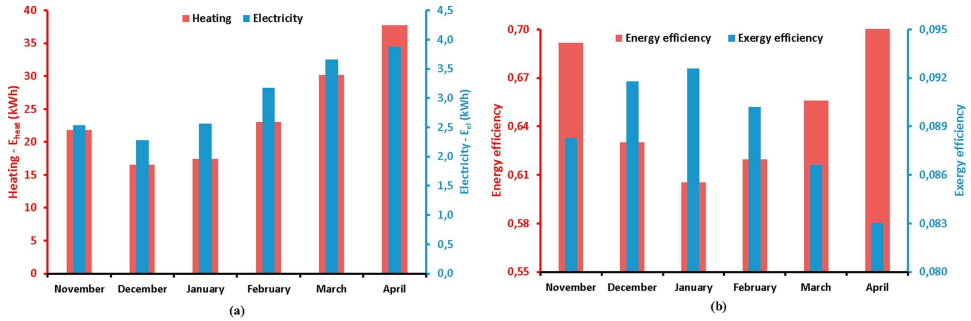

Figure 13 – Daily performance for all the months (a) heating and electricity production (b) mean energy and exergy efficiency.

Source: Adapted from Bellos and Tzivanidis (2019)

In their study they compared the selected refrigerants based on the energetic parameter COP and environmental parameter LCCP. The tests were performed under constant condenser temperature of 35 ^oC and three different evaporator temperatures of -10 ^oC, -5 ^oC and 0 ^oC.

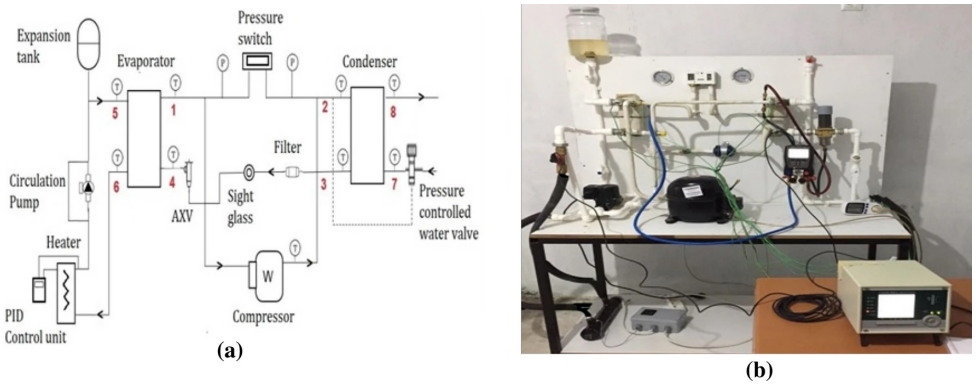

Figure 14 – Schematic view (a) and heat pump test system (b).

Source: Yıldız and Yıldırım (2021)

Although the authors concluded that in theoretical analysis, R134a always has a higher COP value than R513A and R1234yf according to Fig. 15 (a), in the experimental results it was stated that when the evaporator temperature is -10 ^oC and -5 ^oC, R513A has higher COP than R134a despite high compressor energy consumption. Furthermore in the LCCP analysis R134a presented the worst environmental results according to Fig. 15 (b.). Considering the environmental aspects the authors found that direct emission values of refrigerants are negligible compared to total emission values, the majority of indirect emission values of refrigerants are due to energy consumption and increasing the energy efficiency of the heat pump system is necessary to decrease the emission value. In addition, using renewable energy for electricity generation will reduce the emission value.

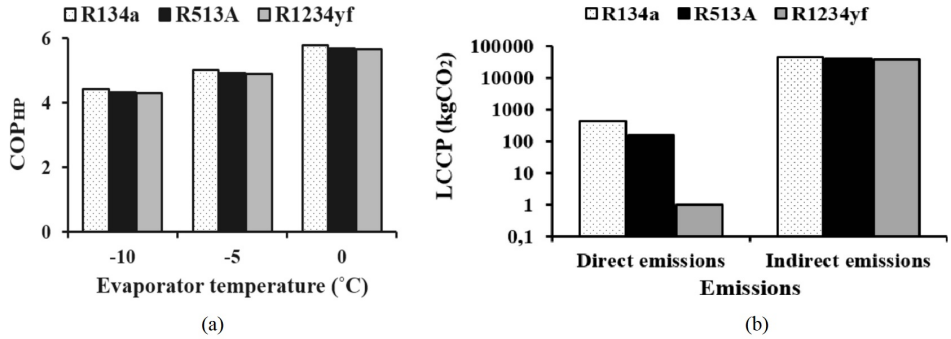

Figure 15 – COP (a) and LCCP (b) results.

Source: Adapted from Yıldız and Yıldırım (2021)

A recent research about IX-PVT-SAHP applying the energy, economic, and environmental (3E) analysis was performed by Kim *et al.* (2023) to replace the refrigerant R134a. The authors developed an IX-PVT-SAHP that produces DHW and SH to residential buildings. The produced electricity by the PVT of 10 m^2 area is self-consumed by the building or it can be stored in an energy storage system and when the system is fully charged, electricity is sent to the grid. The produced heat by the HP is stored in a DHW tank and the heat produced by the PVT is stored in a solar heat storage tank that assists the HP to operate continuously at night. The schematic of the system is presented in Fig. 16.

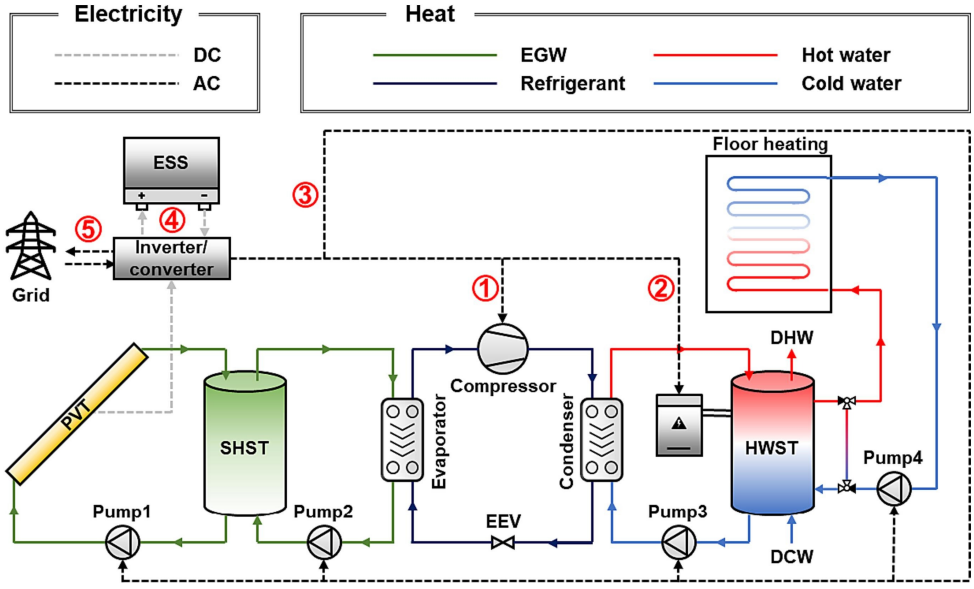

Figure 16 – Schematic of an IX-PVT-SAHP.

Source: Kim *et al.* (2023)

The candidates to substitute the refrigerant R134a were the R1234yf, R1234ze(E), and R152a based on their GWP lower than 150. The experiments were performed in temperatures of heat source from 0 ^oC to 30 ^oC and temperatures of heat sink from 35 ^oC to 50 ^oC. The

optimization of the system was made by a multi-objective decision-making method to determine the optimal alternative among the low-GWP refrigerants to replace R134a. This method aimed to minimize the levelized cost of energy (LCOE) and the specific life cycle climate performance (SLCCP) performance that are economic performance and environmental performance indexes respectively. A COP and heating capacity comparison measured at optimal refrigerant charge amounts was made between R1234yf, R1234ze (E), and R152a in relation to R134a. As shown in Fig. 17 (a), all low-GWP refrigerants exhibited a degraded heating capacity compared to R134a. Additionally, R152a showed a moderate degradation in heating capacity, ranging from 4.8% to 8.4%. Moreover, R152a enhanced the COP by up to 10.3% compared to R134a as shown in Fig. 17 (b).

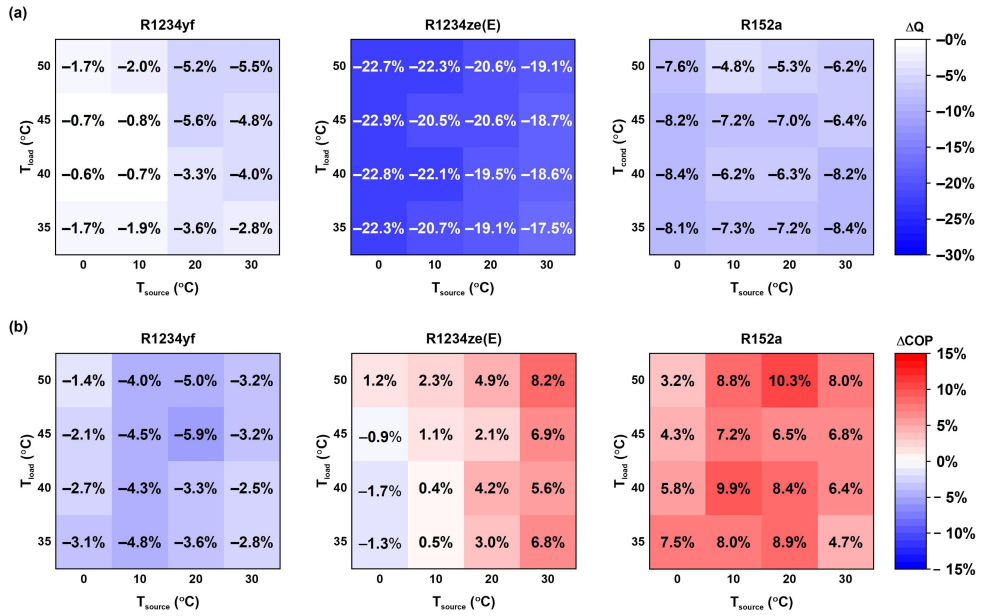

Figure 17 – Variations in the (a) heating capacity and (b) COP of the heat pump using low-GWP refrigerants to replace R134a according to the heat source and load temperature.

Source: Kim *et al.* (2023)

The authors also investigated the LCOE comparing R1234yf, R1234ze (E), and R152a in relation to R134a it was concluded that the most economical refrigerant was R152a, which showed a 50% reduction in the LCOE compared to R134a as shown in Fig. 18 (a). They stated that this reduction was due to the lower electricity purchase cost and higher sale cost of R152a. Additionally, compared to R134a all refrigerants exhibited a reduction in SLCCP according to Fig. 18 (b). R152a presented the best result with a LCCP reduction of 20.8% compared to R134a.

Kim *et al.* (2023) concluded that R152a was the most suitable refrigerant to replace R134a owing to its superior economic and environmental performance. Accordingly, in Fig. 19

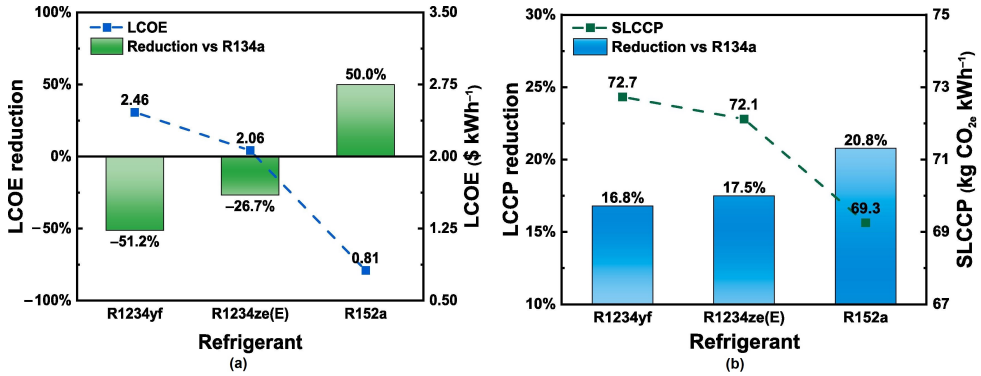

Figure 18 – LCOE reduction of (a) IX-PVT-SAHP compared to R134a and (b) SLCCP reduction of IX-PVT-SAHP compared to R134a.

Source: Adapted from Kim *et al.* (2023)

R152a showed the shortest distance from the ideal point, that corresponds to minimum SLCCP and LCOE values. Moreover, when R1234yf and R1234ze(E) are used as alternatives to R134a in IX-PVT-SAHP, CO_2 emissions can be reduced, but costs will increase.

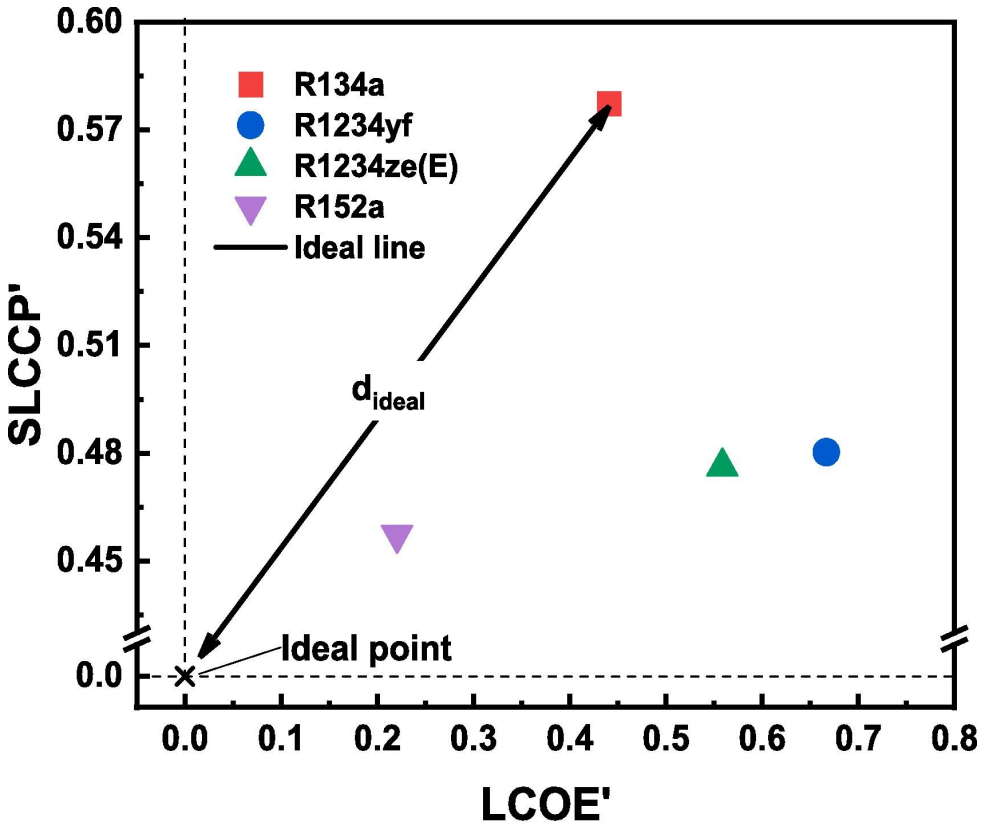

Figure 19 – Determination of alternative refrigerants through the LINMAP method.

Source: Kim *et al.* (2023)

Another contemporary research developed by Yogaraja *et al.* (2024) investigated the feasibility to substitute R134a for R290/R600a zeotropic mixture in a DX-PVT-SAHP employing

an Artificial Neural Network (ANN) model that was validated with the experimental setup installed in Coimbatore in India as shown in Fig. 20.

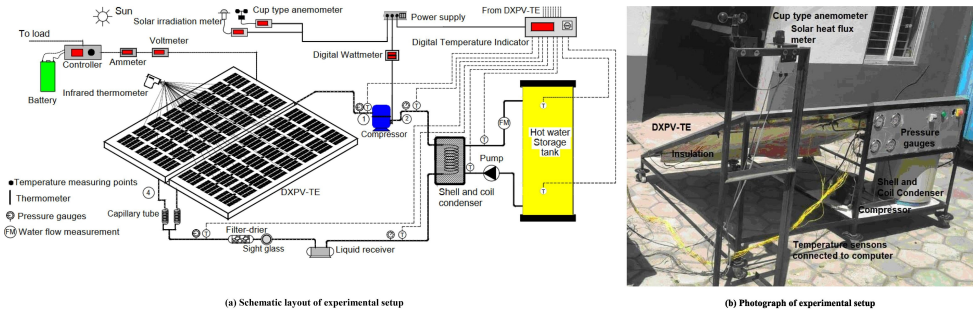

Figure 20 – Details of experimental setup.

Source: Adapted from Yogaraja *et al.* (2024)

The experimental setup is composed of a sealed reciprocating compressor (Emerson Copeland; Model: KCE444HAG) and of two photovoltaic panels with total area of 1.3 m^2 and rated power of 250 W each. Moreover, the quantity of refrigerant was determined based on the maximum COP observed under radiation values above 800 W/m^2 that resulted in 750 ± 10 g for R134a and 380 ± 10 g for the R290/R600a zeotropic mixture. The authors found that the COP of R290/600a is 3.5–7.9 % higher than R134a and the R290/R600a mixture has 4.2–5.7 % higher condenser heating capacity than R134a owing to its higher latent heat according to Fig. 21, that illustrates the experimental results.

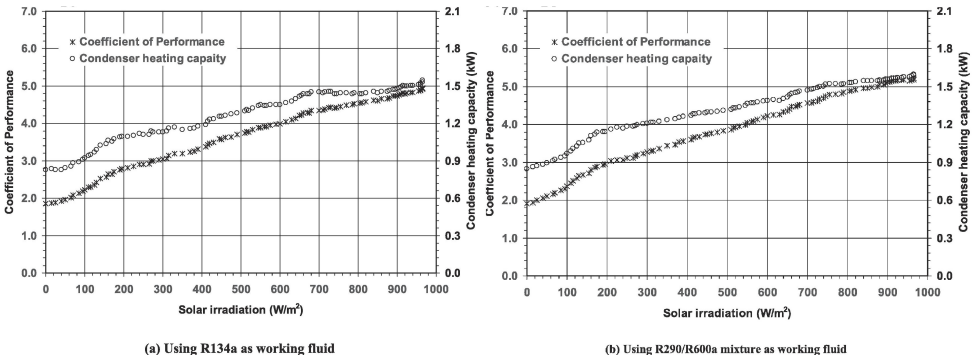

Figure 21 – COP and Heating capacity of the PVT-DX-SAHP.

Source: Adapted from Yogaraja *et al.* (2024)

Additionally compressor power consumption of R290/600a is 1.1–2.5 % lower than R134a, owing to its improved physical properties and it is noticed that the electrical power output of the DX-PVT-SAHP using R290/R600a mixture was greater than R134a, owing to better panel cooling of the mixture as represented in Fig. 22.

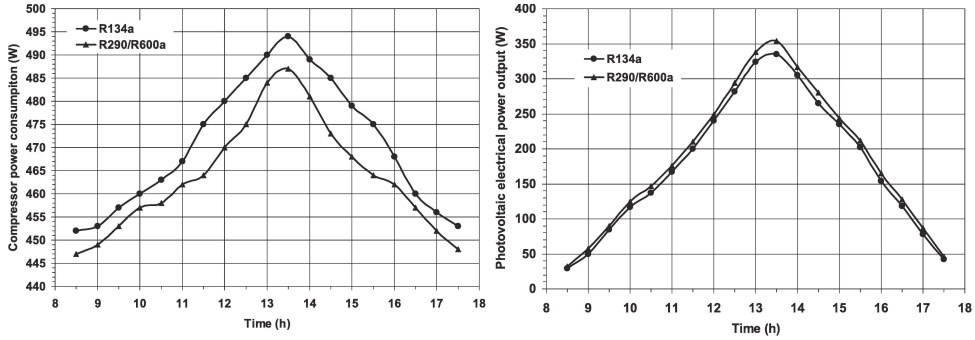

Figure 22 – Compressor power consumption and photovoltaic electrical power output of the PVT-DX-SAHP.

Source: Adapted from Yogaraja *et al.* (2024)

The results in comparative studies about refrigerants selection of heat pumps are summarized on Tab. 4. In the analysis of the previous mentioned table it is evident that the researches are concentrated on refrigerants comparison of low GWP and to the best of the authors knowledge, studies on refrigerants comparison of fluids R454C and R455A are focused on replacement of R404A and R22 in refrigeration systems according to the studies of Mostafa, Hassanain, and Elgendy (2021), Braga *et al.* (2025), Mota-Babiloni, Giménez-Prades, *et al.* (2022), Llopis *et al.* (2019), while research applied to DX-PVT-SAHP have not been described in the existing literature yet.

Table 4 – Comparative studies on refrigerants selection of HPs

Authors	Type	Compared refrigerants	Selection criteria	Selected refrigerant
Chaichana (2003)	SAHP	R22, R290, R600, R600a, R1270, R717	COP, ODP, GWP	R717
Chata (2005)	DX-SAHP	R134a, R404A, R410A, R407C	COP	R134a
Ghoubali (2014)	ASHP	R407C, R290, R1234yf	COP, TEWI	R290
Makhnatch (2014)	ASHP	R152a, R1234yf, R290, R1270, R410A	LCCP	R290
Botticella (2015)	ASHP	R290, R1234yf	COP	R290
Duarte (2019)	DX-SAHP	R134a, R290, R600a, R744, R1234yf	COP, TEWI	R290
Bellos (2019)	IX-PVT-SAHP	R404A, R32, R1234yf, R290, R600a, R245fa, R152a	Q_{heat}, P_{grid}	R32, R1234yf
Yıldız (2021)	ASHP	R134a, R1234yf, R513A	COP, LCCP	R513A
Kim (2023)	IX-PVT-SAHP	R134a, R1234yf, R1234ze(E), R152a	3E	R152a
Yogaraja (2024)	DX-PVT-SAHP	R134a, R290/R600a	COP	R290/R600a
Arnesson (2025)	IX-PVT-SAHP	R32, R290, R410A	COP,LCOE	R32

Source: Adapted from Nogueira, Maia, *et al.* (2025)

3 METHODOLOGY

This chapter is organized into six parts. First, the selection criteria for the low-GWP refrigerants included in the comparison are presented. Next, the prototype and the experimental tests conducted on the DX-PVT-SAHP are described. Subsequently, the input data used in the mathematical model are detailed. Following this, the development of the mathematical model is explained. In the fifth subsection, the uncertainty analysis and the statistical methods employed are outlined. Finally, the sixth subsection presents the numerical procedure adopted in the study.

3.1 Selected refrigerants

The low GWP refrigerants selected for the comparative study were chosen based on two criteria: The first criteria is the choice of refrigerants of GWP < 750 due to the EU Regulation No 517/2014 that prohibits single split air-conditioning systems containing less than 3 kg of fluorinated greenhouse gases, that contain, or whose functioning relies upon, fluorinated greenhouse gases with GWP ≥ 750 from 1 January 2025. The second criteria is the choice of refrigerants that work with commercially available compressors.

Taking into account the above criteria the refrigerants R290, R600a, R1234yf, R454C, R455A and R513A were selected to be compared with R134a. Although there are other refrigerants with GWP lower than 750 listed in Tab. 3, the reason for choosing the selected refrigerants will be discussed next.

R290 was selected because of the good results of environmental and energetic performance in the comparative studies presented by Ghoubali *et al.* (2014), Duarte, Paulino, Pabon, *et al.* (2019), Makhnatch and Khodabandeh (2014), Botticella and Viscito (2015). Although R290 is a flammable refrigerant, the PVT-DX-SAHP of this work is a small equipment and it will be installed in an open ventilated location.

The choice of R600a refrigerant was based on its compact circuit, fitting well within the dimensions of household refrigerators as stated in Protocol and Layer (2022). Additionally, R600a boasts reduced noise levels, a crucial factor for domestic appliances, while its compressor demonstrates satisfactory efficiency according to Palm (2008).

R1234yf was selected due to the the good results presented in the comparative study of an IX-PVT-SAHP performed by Bellos and Tzivanidis (2019). Furthermore, R1234yf has been implemented as a direct substitute for R134a across various systems as stated by Lee and Jung (2012) and Belman-Flores *et al.* (2017). While both refrigerants exhibit comparable COP values, R134a's COP marginally outperforms that of R1234yf. Despite concerns regarding the classification of R1234yf as a polyfluoroalkyl substance, it was included in the analysis. This choice was made even in light of reports that some states are already considering enacting restrictions on its use.

R454C is a low-GWP blend composed of 21.5% R32 and 78.5% R1234yf. Although any comparative study for R454C operating in solar assisted heat pumps was found, the selection of R454C was done due to the good thermodynamic performance presented in the investigation study conducted by Oruç and Devecioğlu (2021) to substitute R404A in refrigeration systems operating at condensing temperature from 30 ^oC to 50 ^oC.

The selection of R455A that is a low-GWP blend composed of 75.5% of R1234yf, 21.5% of R32, and 3% of CO_2 was made based on the investigation done by Mota-Babiloni, Haro-Ortuno, *et al.* (2018) that corroborates the feasibility of R455A to replace R404A in a refrigeration system operating at condensing temperature from 32 ^oC to 47 ^oC. Furthermore to the best of the authors knowledge, studies on R455A operating in heat pumps have not been described in the existing literature.

R513A is a low-GWP blend composed of 56% of R1234yf and 44% of R134a. The selection of R513A was done due to the satisfactory results of COP and LCCP compared to R134a found by Yıldız and Yıldırım (2021) in an ASHP in which tests were performed under constant condenser temperature of 35 ^oC and three different evaporator temperatures of -10 ^oC, -5 ^oC and 0 ^oC.

Although R32 was one of the selected fluids in the comparative studies conducted by Bellos and Tzivanidis (2019) and Arnesson *et al.* (2025), it was not found a commercially available compressor for the heating capacity evaluated in the present work. For that reason it was not part of the selected fluids.

3.2 System design and experiment

The experimental setup of the DX-PVT-SAHP for hot water applications was built at UFMG in Belo Horizonte, MG, Brazil, coordinates $19^o54'46''$ S and $43^o56'27''$ W shown in Fig. 23. The rear section of the PVT panel, which consists of the solar collector, is shown in Fig. 24.

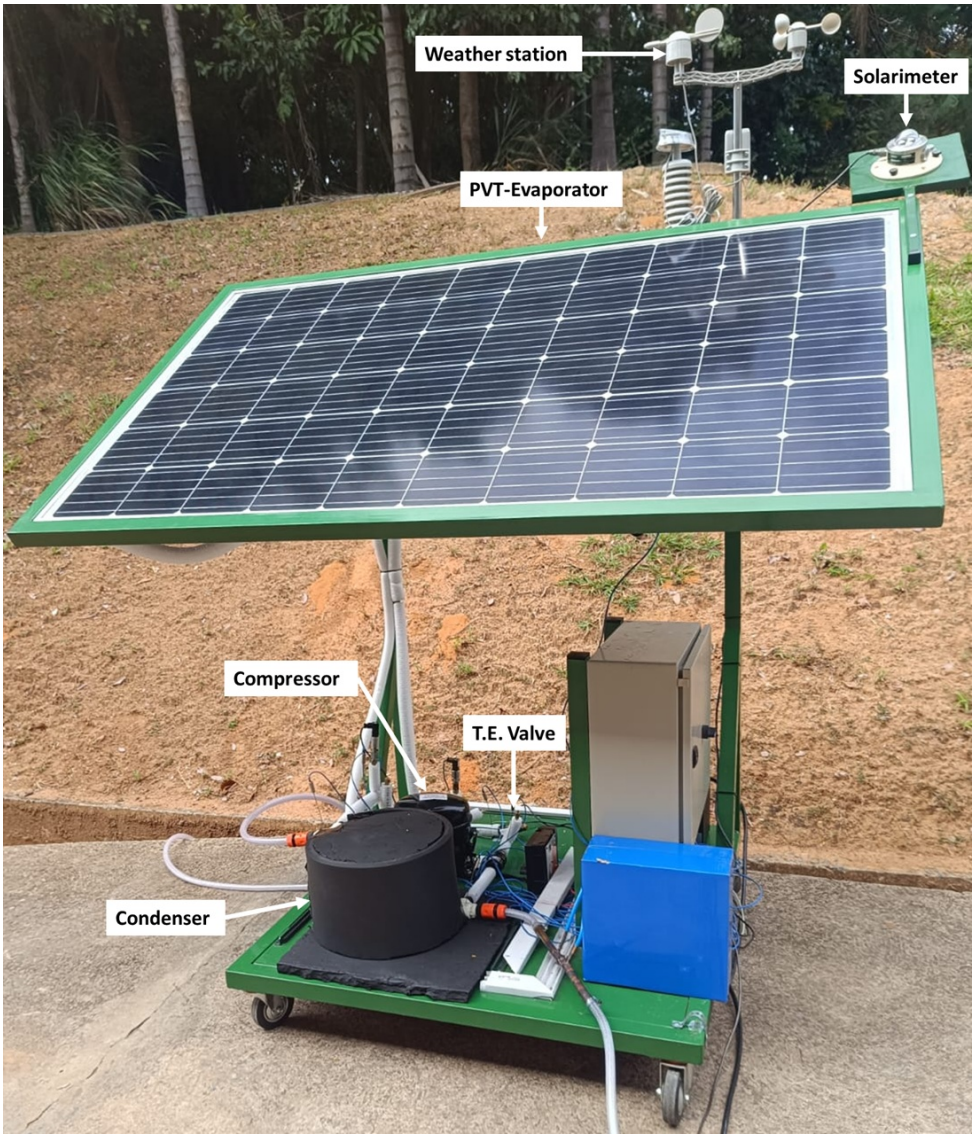

Figure 23 – Photo of the experimental device

The DX-PVT-SAHP operates with R134a and comprises an hermetic reciprocating variable speed compressor, manufactured by Embraco model VEGT8HB, a counterflow coaxial helical coil composed of an outer polymer tube and inner stainless steel tube where the water flows in annular region, and R134a flows in the inner tube, a solar evaporator formed by a flat aluminum plate welded to a serpentine copper tube, which is positioned on the rear side of the polycrystalline photovoltaic panel manufactured by Kript model KRPF-320W5B and mechanically pressed

Figure 24 – Photo of the solar collector

into contact using crossbars to ensure effective coupling and a thermal expansion valve. The compressor operates at a fixed speed and the heating capacity varies according to environmental conditions. The condensed liquid refrigerant enters the expansion valve, and then it is directed to the PVT evaporator. Within the PVT evaporator, it is vaporized by the thermal energy absorbed from solar irradiation and surrounding ambient air. Additionally, electrical energy is produced by the PV cells through the photovoltaic effect, the direct current is converted into alternative current by a micro-inverter manufactured by Growatt model NEO 2000M-X to the grid. The evaporated fluid is then raised to the condenser pressure by the compressor, achieving the required temperatures. The resultant high pressure superheated refrigerant flows to the coaxial coil heat exchanger (condenser), where it undergoes condensation and transfer energy to heat water. The schematic configuration and the sensors position are illustrated in Fig. 25.

The temperature measurements were indicated by seven T-type thermocouples: four refrigerant temperature measurements at the compressor inlet (T_1), compressor outlet (T_2), expansion valve inlet (T_3), and expansion valve outlet (T_4). Two water temperature measurements were recorded at the heat exchanger inlet (T_5) and heat exchanger outlet (T_6). One temperature measurement was evaluated at the surface of the photovoltaic panel (T_7). Additionally, two pressure transducers measure the low pressure at the compressor inlet (LP) and high pressure at

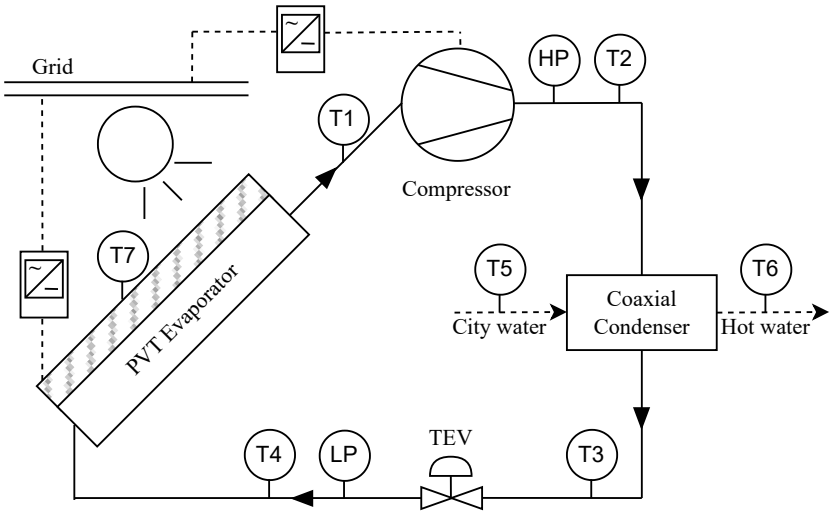

Figure 25 – Scheme of DX-PVT-SAHP

the compressor outlet (HP). Ambient conditions of temperature, dew point, atmospheric pressure, and wind speed were measured by the weather station, the solar irradiation was measured by the solarimeter, the electrical energy consumed by the compressor was measured by a wattmeter manufactured by Novus model DigiRail VA and the energy produced by the photovoltaic panel is measured by the micro-inverter. The measuring range of instruments and their uncertainty are shown in Tab. 5.

Table 5 – Instruments range of measurements and accuracy

Instruments	**Range**	**Uncertainty**
Thermocouple (T-type) [^oC]	-270 to 400	$\pm 0.44\ ^oC$
Gauge pressure transducer [bar]	0 to 100	$\pm 0.25\ bar$
Weather station Temperature [^oC]	-40 to 65	$\pm 1\ ^oC$
Weather station Pressure [hPa]	300 to 1100	$\pm 3\ hPa$
Weather station Wind [m/s]	0 to 44	$\pm 1\ m/s$
Scale [kg]	0 to 13	$\pm 1\ g$
Chronometer [s]	–	$\pm 1\ s$
Pyranometer [W/m^2]	–	$\pm 5\%$
Wattmeter [W]	–	$\pm 0.5\%$

The methodology for carrying out the experimental tests followed the steps below: the first step consisted of positioning the DX-PVT-SAHP in the uncovered outdoor area of the GREA laboratory. After placing the equipment in the sunny location, all the air inside the DX-PVT-SAHP piping was removed with the aid of a vacuum pump for fifteen minutes, in order to prevent air from contaminating the refrigerant and impairing the operational efficiency of the DX-PVT-SAHP. Next, using a scale to accurately measure the refrigerant mass, R134a

from the cylinder was used to fill the DX-PVT-SAHP piping. The following step consisted of pumping water to the DX-PVT-SAHP condenser through a variable-speed brushless DC pump model QR30E, DC 12V, 4.8 W, controlled by a frequency inverter that adjusted the frequency and voltage supplied to the pump's electric motor, thereby controlling its rotational speed and, consequently, the mass flow rate and pressure of the pumped water. The water tank that was not shown, had three openings located at different height levels. The tank was supplied with city water through the lower opening, and water was pumped to the condenser through the middle opening. The upper opening served to drain water and keep the tank level constant, since the mass flow rate of city water was higher than the mass flow of water delivered by the pump to the DX-PVT-SAHP. Finally, the compressor was switched on initiating the operation of the DX-PVT-SAHP that occurred from 8:00 a.m. to 12:00 p.m. Once the outlet water temperature reached steady temperature, the water mass flow rate was adjusted to a new setpoint using the frequency inverter. Throughout the process, data were continuously acquired to identify and analyze the system steady-state operating points. The steady-state condition was achieved when the water outlet temperature reached a constant value and the other measured heat pump variables presented negligible variation as shown in Fig. 26.

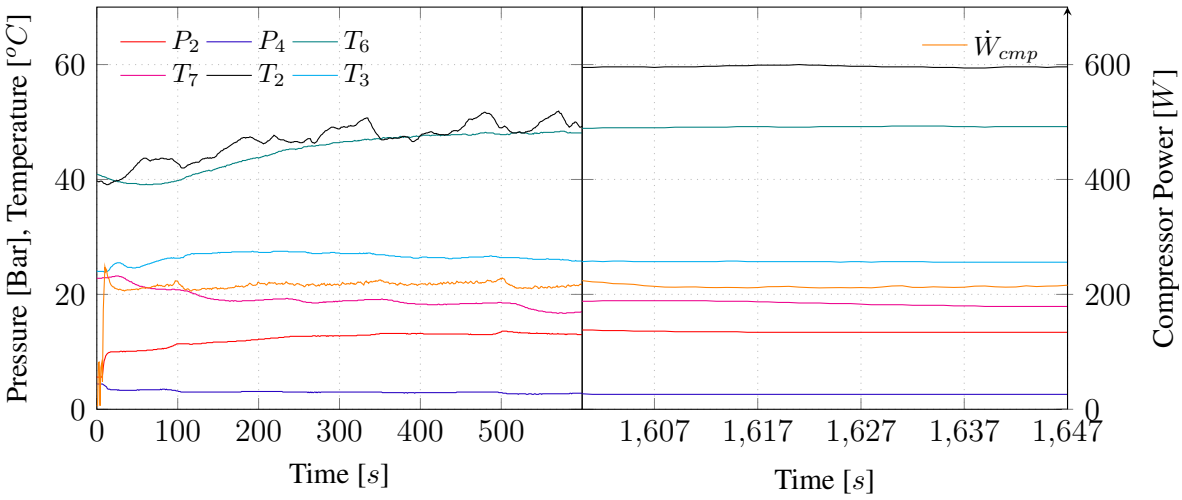

Figure 26 – Gauge pressures, temperatures and compressor power during the start-up (left plot) and after reached steady-state condition (right plot).

3.3 Input values of DX-PVT-SAHP simulation

In order to simulate the performance results the values of the input variables shown in Tab. 6 were adopted. A superheating temperature of 15 ^oC was adopted to ensure convergence of the computational model when using the refrigerant R600a. Additionally a frequency of 50

Hz was adopted for the compressors because this is the value used in the manufacturers tests reported in the equipment catalog.

Table 6 – Input values of DX-PVT-SAHP simulation

Parameter	Value	Unit	Parameter	Value	Unit
Collector emissivity	0.95		Coil diameter	0.25	m
Collector absorptivity	0.95		Evap. tube length	17.28	m
Collector transmittance	1		Cond. tube length	7.5	m
Contact resistance	0.02		Collector area	1.552	m^2
System years lifetime	15		DX-PVT-SAHP cost	1372	USD
Temp. coefficient of PV	0.0039	$^oC^{-1}$	Compressor speed	50	Hz
Reference efficiency of PV	17.14	$\%$	Electric heater cost	21.59	USD
Electric heater efficiency	97	$\%$	PV + inverter cost	645.21	USD
Annual leakage rate	3	$\%$	Electricity tariff	0.21	USD/kWh
Annual inflation rate	10	$\%$	Emission factor	54.5	gCO_2/kWh
Collector thickness	1	mm	Ambient temp.	25.0	^oC
D_i, evaporator tube	4.77	mm	Water inlet temp.	25.0	^oC
D_o, evaporator tube	6.35	mm	Water outlet temp.	50.0	^oC
Thickness of evap. tube	0.79	mm	Superheating	15.0	^oC
D_{ii}, condenser tube	8.32	mm	Wind speed	0.3	m/s
D_{io}, condenser tube	9.52	mm	Atm. pressure	93.4	kPa
D_{oi}, condenser tube	16	mm	Solar irraditaion	500	W/m^2

3.4 Mathematical modelling

The initial step in preparing the DX-PVT-SAHP model is to identify the input and output variables. The list of input and output variables are shown in Fig. 27.

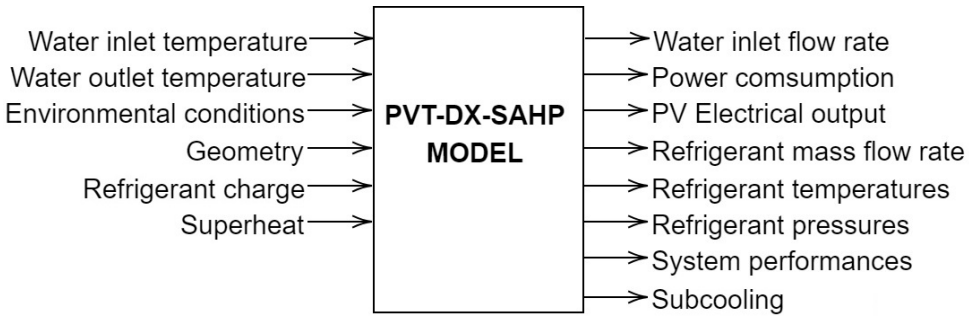

Figure 27 – Input and output variables of PVT-DX-SAHP model

The environmental conditions are the ambient temperature, the dew point temperature, the wind speed, the solar irradiation, the sky temperature, the atmospheric pressure and the gravitational acceleration. Additionally, the geometry parameters are the collector area, PV area, capillary coil diameter, inner diameter of evaporator tube, thickness of evaporator tube, inner

diameter of inner condenser tube, outer diameter of inner condenser tube, inner diameter of outer condenser tube, length between components, evaporator tube length, condenser length, collector length, collector width.

The PVT-DX-SAHP model is formulated based on several assumptions that ensure mathematical tractability and consistency with established modeling practices. First, the heat pump system is considered to operate under quasi–steady-state conditions, allowing transient effects to be neglected. In addition, the kinetic and potential energy variations of the refrigerant are assumed to be negligible, thereby simplifying the energy balance. Pressure drops within the heat exchangers and in the connecting tubes are also disregarded, which enables the use of uniform pressure conditions along each component. Moreover, the refrigerant superheat is taken to be constant throughout the operation, and water is treated as an incompressible fluid. Finally, the vapor quality is assumed to vary linearly along the condenser and evaporator lengths, providing a simplified yet representative description of the phase-change process.

The indicator of energetic performances are the coefficient of performance (COP), seasonal performance factor (SPF) and solar fraction (SF) calculated according to Eq. 1, 2 and 3, respectively as predicted by Rees (2016):

$$COP = \dot{m}_w C_w \left(\frac{T_{wo} - T_{wi}}{\dot{W}_{cmp}} \right) \tag{1}$$

$$SPF = \frac{Q}{E_{ele}} \tag{2}$$

$$SF = 1 - \frac{1}{SPF} \tag{3}$$

where the subscripts w, o, i, cmp refers to water, outlet, inlet and compressor, respectively. Additionally, $\dot{m}$ is the mass flow rate and $\dot{W}$ is the power, Q is the annual energy heating demand, E_{ele} is the total Energy Demand. The selection of refrigerants was primarily guided by three key environmental metrics: GWP, TEWI, and LCCP. LCCP is a comprehensive metric used to assess the impact of a refrigerant on a system total lifetime emissions. However, in practice, LCCP is more complex than TEWI, and the additional emissions it accounts for have a minimal impact in the final result Khliyeva *et al.* (2023),Andrade, Zapata-Mina, and Restrepo

(2024). GWP is a valuable metric for comparing different refrigerants, but it can sometimes overstate the environmental benefits of low-GWP refrigerants, as it does not consider many other influencing factors according to Makhnatch and Khodabandeh (2014). An environmental performance assessment based solely on GWP is insufficient to provide a comprehensive and reliable evaluation. For this reason, the present study adopted the TEWI metric. This parameter considers the global warming impact from both direct and indirect emissions and is composed of two factors: the direct effect of refrigerant emissions over the equipment lifetime and the indirect impact of CO_2 emissions resulting from fossil fuel consumption for energy generation during operation, it is calculated as:

$$TEWI = GWP \cdot \lambda \cdot N + \frac{Q \cdot \Phi \cdot N}{SPF} \tag{4}$$

where λ is the annual refrigerant leakage rate , N is the system lifetime, both parameters values adopted according to the authors Makhnatch and Khodabandeh (2014), Rees (2016), Duarte (2018) and Φ is the emission factor to the electricity consumed, according to MCTI: Ministry of Science and Innovation (2024). The economic performance can be assessed by comparing the payback period (Ψ) of the DX-PVT-SAHP with that of an electrical heater according to Rabelo *et al.* (2019):

$$\Psi = \frac{I}{S(1+\zeta)^{(\Psi-1)}} \tag{5}$$

$$S = \chi \left(\frac{Q}{\eta_{ele}} - \frac{Q}{SPF} \right) \tag{6}$$

where I is the difference of initial investment between DX-PVT-SAHP and an electrical heater, ζ is the annual inflation rate, S the annual savings, χ is the electricity tariff and η_{ele} is the efficiency of the electrical heater.

3.4.1 Photovoltaic-thermal collector model

The PVT collector model was developed to predict both the heat gained by the refrigerant and the electrical power output, and its formulation relies on several simplifying assumptions.

Specifically, the thermal resistance of the evaporator tube wall due to conduction is taken as zero, heat transfer at the evaporator edges is considered negligible, and the thermal resistance associated with the bond between the tube and fin is also assumed to be zero. Additionally, the vapor quality is assumed to vary linearly along the flow direction in the boiling region, and the electrical energy generated by the photovoltaic panel is assumed to be entirely supplied to the grid. The schematic of the PVT collector is represented in Fig. 28.

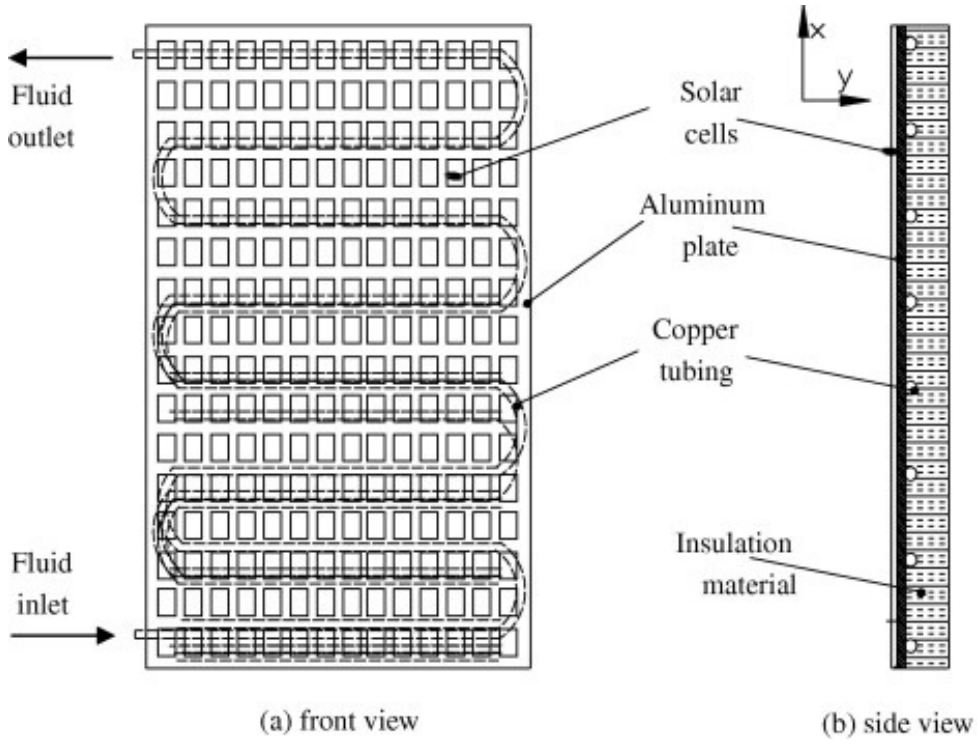

Figure 28 – PVT evaporator.

Source: Chow *et al.* (2010)

The useful thermal energy of the PVT evaporator used in this study ($\dot{Q}_e$) can be evaluated according to Xu, Deng, *et al.* (2009):

$$\dot{Q}_e = \dot{Q}_s - \left(\dot{Q}_{con} + \dot{Q}_{rad}\right) - \dot{W}_{pv} \tag{7}$$

$$\dot{Q}_s = \tau\alpha G A_p \tag{8}$$

$$\dot{Q}_{con} = h_a \left(T_p - T_a\right) A_p \tag{9}$$

$$\dot{Q}_{rad} = h_{rad} \left(T_p - T_a\right) A_p \tag{10}$$

$$\dot{W}_{pv} = \tau_{pv}\eta_{pv}GA_{pv} \tag{11}$$

$$\eta_{pv} = \eta_{rv}\left[1 - \beta\left(T_p - 25\right)\right] \tag{12}$$

where $\dot{Q}_s$ is the solar irradiation collected by absorber, $\dot{Q}_{con}$ and $\dot{Q}_{rad}$ are the heat losses induced by the convective and radiation heat transfer between the surface of PVT evaporator and ambient air, $\dot{W}_{pv}$ the electrical power output per unit time from PV cells, $\tau\alpha$ is the effective absorptivity-transmittance product, G is the solar irradiation, A_p is the plate area, T_p is the plate surface temperature, T_a is the ambient temperature, η_{pv} is the photovoltaic efficiency of solar cells, η_{rv} is the photovoltaic efficiency reference value at the standard condition, β is the temperature coefficient, h_a is the convective heat loss coefficient calculated according to Kuang, Sumathy, and Wang (2003), h_{rad} is the radiant heat coefficient calculated according to Kong, Zhang, *et al.* (2011):

$$h_a = 2.8 + 3.0v_{wd} \tag{13}$$

$$h_{rad} = \epsilon\sigma T_a^3 \tag{14}$$

where v_{wd} is the wind speed, ϵ is the average emittance, σ is the Stefan–Boltzmann constant. The thermal energy absorbed by the refrigerant is calculated as the enthalpy variation:

$$\dot{Q}_e = \dot{m}_r\left(i_1 - i_4\right) \tag{15}$$

where $\dot{m}_r$ is the refrigerant mass flow rate, i is the refrigerant specific entalphy, and the subscripts from 1 to 4 are related to the points shown in Fig 25. The heat gained by refrigerant in evaporator ($\dot{Q}_e$) is the same as the heat harvested in the PVT according to Xu, Deng, *et al.* (2009). Furhtermore the refrigerant flows through the copper tube that was divided into two regions to apply the balance of energy: flow boiling region (bo) and superheated flow vapor region (sup). The balance of energy of the refrigerant in each region are expressed as:

$$\dot{Q}_{bo} = \dot{m}_r\left(i_v - i_4\right) \tag{16}$$

$$\dot{Q}_{sup} = \dot{m}_r \left(i_1 - i_v\right) \tag{17}$$

the evaporator has a fixed total length (L_e) and the length of regions bo and sup are expressed as

$$L_{bo} = \frac{\dot{Q}_{bo}}{\dot{Q}_e} L_e \tag{18}$$

$$L_{sup} = \frac{\dot{Q}_{sup}}{\dot{Q}_e} L_e \tag{19}$$

the average refrigerant temperature (T_r) and the photovoltaic panel temperature (T_{pv}) are expressed as:

$$T_r = \frac{[(T_4 + T_v)/2]L_{bo} + [(T_v + T_1)/2]L_{sup}}{L_e} \tag{20}$$

$$T_{pv} = \dot{Q}_e \left(\frac{1}{\bar{h}_r A_i} + \frac{\delta_{co}}{k_{co} A_i}\right) + T_e \tag{21}$$

$$A_i = \pi D_{e,i} L_e \tag{22}$$

$$\bar{h}_r = \frac{h_{bo} L_{bo} + h_{sup} L_{sup}}{L_{sup}} \tag{23}$$

where the subscript co refers to copper tube, A_i is the internal surface heat transfer area of refrigerant, $\bar{h}_r$ is the convection heat transfer coefficient of refrigerant, h_{bo} is the boiling heat transfer coefficient of refrigerant calculated according to Sun and Mishima (2009) and h_{sup} is the vapor heat transfer coefficient of refrigerant calculated using Dittus and Boelter equation according to Rohsenow, Hartnett, Cho, *et al.* (1998):

$$h_{bo} = \frac{6 Re_l^{1.05} Bo^{0.54}}{We_l^{0.191} \left(\rho_l / \rho_v\right)^{0.142}} \frac{k_l}{D_h} \tag{24}$$

$$h_{sup} = 0.023\, Re^{0.8}\, Pr^n \frac{k_l}{D_h} \tag{25}$$

$$Re_l = \frac{\rho_l v D_i}{\mu_l} \tag{26}$$

$$Bo = \frac{q''}{\frac{\dot{m}_r}{A_i} h_{fg}} \tag{27}$$

$$We_l = \frac{(\frac{\dot{m}_r}{A_i})^2 D_i}{\rho_l \sigma'} \tag{28}$$

$$Pr = \frac{\mu C}{k} \tag{29}$$

$$q'' = \frac{\dot{Q}_e}{A_i} \tag{30}$$

where the subscripts l refers to liquid, v vapor, h hydraulic, fg latent, i internal, p constant pressure, Re is the Reynolds number, Bo is the Boiling number, k is the thermal conductivity, We is the Weber number, ρ is the density, D is the diameter, Pr is the Prandtl number, n is a constant of 0.4 for heating of the fluid and 0.3 for cooling of the fluid, μ is the dynamic viscosity, q'' is the heat flux at the wall, σ' is the surface tension and c is the specific heat.

3.4.2 Compressor model

In a refrigeration machine or heat pump, the suction and discharge pressures can be determined by the secondary fluid in the hot and cold sources, respectively. The compressor impact on these variables is indirect. As Paula *et al.* (2021) pointed out, there are several techniques to model a compressor, some of which are relative complex as stated by Yang, Bradshaw, and Groll (2013), Duarte, Pabon, *et al.* (2019) and Fonseca *et al.* (2022). Hermetic compressor manufacturers typically do not give the necessary specifications, geometric details, or enough data for more complex models. Additionally, the compressor model used in a refrigeration system is typically simplified according to Kong, Li, *et al.* (2017), Reis *et al.* (2024) and A. Santos *et al.* (2024).

The compressor model is formulated as a gray-box representation and is developed under several simplifying assumptions. Specifically, refrigerant leakage is considered negligible, the compression process is assumed to be adiabatic and isentropic, and the compressor operates at a constant rotational speed.

The volumetric efficiency η_{vol} and the overall efficiency η_{ov} are expressed as Maia, Koury, and Machado (2013):

$$\dot{m}_{cmp} = \rho_1 \omega \forall_{cmp} \eta_{vol} \tag{31}$$

$$\dot{W}_{cmp} = \frac{\dot{m}_{cmp}\,(i_2 - i_1)}{\eta_{ov}} \tag{32}$$

where $\dot{m}_{cmp}$ is the mass flow rate of compressor, $\dot{W}_{cmp}$ is the compressor electric power ρ_1 is the suction density, ω is the rotational speed, $\forall_{cmp}$ is the compressor displacement volume. The mass flow rate and the compressor electric power are function of the mean evaporating temperature (T_e) and mean condensing temperature (T_c) provided by manufacturer in the performance map. In order to calculate η_{vol} and η_{ov} for the $\overline{T}_e$ and $\overline{T}_c$ values provided by manufacturer, the Eq. 31 and Eq. 32 were employed. Furthermore, to predict an equation of η_{vol} and η_{ov} as a function of any $\overline{T}_e$ and $\overline{T}_c$, Eq. 33), proposed by ISO 9309 and described by Rasmussen and Jakobsen (2000) were employed.

$$\eta = B_A \overline{T}_e + B_B \overline{T}_c + B_C \overline{T}_e \overline{T}_c + B_D \overline{T}_e^2 + B_E \overline{T}_c^2 \tag{33}$$

A multiple linear regression using the least square method was used to calculate the coefficients B_A to B_E to predict the function of the calculated values of η_{vol} and η_{ov} based on the catalog values according to Chapra (2018).

3.4.3 Condenser model

According to Duarte, Paulino, Tavares, Cançado, *et al.* (2023) there are many studies that employed distributed heat exchangers models as presented by Laughman *et al.* (2015), Paulino *et al.* (2019) and Humia *et al.* (2025), these models require much computational effort if compared with the lumped models. Additionally, some studies demonstrate that the lumped model can be used to quickly assess system performance according to Li, Chu, *et al.* (2017), Paula *et al.* (2020) and Martins *et al.* (2024) but has limited results. The alternative is the moving boundaries technique as adopted by Esbrí *et al.* (2015), Resende *et al.* (2025) and Braga *et al.* (2025) that was used in the present work.

The condenser is a coaxial type and it was divided into three regions to apply the equations of energy balance: desuperheating region (d), condensation flow region (cd) , and liquid flow region (l). The balance of energy of the refrigerant in each region is expressed as

$$\dot{Q}_d = \dot{m}_r \left(i_2 - i_v\right) \tag{34}$$

$$\dot{Q}_{cd} = \dot{m}_r \left(i_v - i_l\right) \tag{35}$$

$$\dot{Q}_l = \dot{m}_r \left(i_l - i_3\right) \tag{36}$$

The heat transfer rate in the condenser was calculated separately in the regions using the effectiveness-NTU method. The effectiveness (ε) of a concentric heat exchanger was calculated according to Eq. 42, except for pure substance refrigerants in the condensation region that was calculated according to Eq. 43, the Number of Transfer Units (NTU) and the product between the overall heat transfer coefficient (U) and the heat transfer surface area (A) were evaluated according to Incropera and DeWitt (2008):

$$\varepsilon_d = \dot{Q}_d / \dot{C}_{min} \left(T_2 - T_9\right) \tag{37}$$

$$\varepsilon_{cd} = \dot{Q}_{cd} / \dot{C}_{min} \left(T_c - T_8\right) \tag{38}$$

$$\varepsilon_l = \dot{Q}_l / \dot{C}_{min} \left(T_c - T_5\right) \tag{39}$$

$$T_8 = T_5 + \dot{Q}_l / (\dot{m}_w C_w) \tag{40}$$

$$T_9 = T_8 + \dot{Q}_{cd} / (\dot{m}_w C_w) \tag{41}$$

$$\varepsilon = \frac{1 - exp\left[-NTU\left(1 - \dfrac{\dot{C}_{min}}{\dot{C}_{max}}\right)\right]}{1 - exp\left[-NTU\left(1 - \dfrac{\dot{C}_{min}}{\dot{C}_{max}}\right)\right]\dfrac{\dot{C}_{min}}{\dot{C}_{max}}} \tag{42}$$

$$\varepsilon = exp\left(-NTU\right) \tag{43}$$

$$UA = \dot{C}_{min} NTU \tag{44}$$

where $\dot{C}_{min}$ and $\dot{C}_{max}$ are equal to $\dot{C}_r$ or $\dot{C}_w$, whichever is smaller and bigger, respectively. Additionally, the refrigerant and water heat capacities rate were expressed as $\dot{C}_r = \dot{m}_r C_r$ and $\dot{C}_w = \dot{m}_w C_w$. The length of each region was calculated as

$$L = UA \left[\frac{1}{\bar{h}_r \pi D_{ii}} + \frac{ln\left(\frac{D_{ii}}{D_{io}}\right)}{2\pi k} + \frac{1}{\bar{h}_w \pi D_{io}} \right] \tag{45}$$

where the subscript w refers to water, D_{ii} is the inner diameter of inner tube, D_{io} is the outer diameter of inner tube. The $\bar{h}_r$ is the heat transfer coefficient of refrigerant in the desuperheating and liquid flow regions calculated according to Eq. 25 as proposed by Rohsenow, Hartnett, Cho, *et al.* (1998). The work of Shah (2022), which contrasted correlations with experimental results of pure refrigerants and mixtures, was taken into consideration when selecting a correlation for condensation. Additionally, the correlation of Shah (1979) produced acceptable results under the flow conditions encountered in the simulations of the equipment:

$$\bar{h}_r = h_l \left[(1-x)^{0.8} + 3.8 \frac{x^{0.76}(1-x)^{0.04}}{(P_c/P_{cr})^{0.38}} \right] \tag{46}$$

where h_l is the liquid-only heat transfer coefficient, calculated according to Eq. 25, x is the vapor quality, P_c is the condensing pressure, and P_{cr} is the critical pressure. The heat transfer coefficient of water (h_w) in annular region is calculated according to Dravid *et al.* (1971):

$$h_w = \left(0.76 + 0.65\,\mathrm{De}_w^{0.5}\right)\,\mathrm{Pr}_w^{0.175} \frac{k_w}{D_h} \tag{47}$$

$$De = \mathrm{Re}\sqrt{\frac{D_h}{D_{coil}}} \tag{48}$$

where De is the Dean number, D_{coil} is the coil curvature diameter.

3.4.4 Expansion device model

The expansion device required for a PVT-DX-SAHP is the electronic valve or a thermostatic valve, due to the large variations in solar irradiation. The expansion valve is used to control the superheat at evaporator outlet and it is modeled as an isenthalpic device.

3.4.5 Refrigerant charge

The charge of refrigerant (m_r) is calculated according to Eq. 49 for single phase flow and the correlation for void fraction (α') of Zivi (1964) in Eq. 50 is employed to calculate the charge of refrigerant for two-phase flow according to Eq. 51.

$$m_r = \bar{\rho_r} \frac{\pi D_i^2}{4} L \tag{49}$$

$$\alpha' = \frac{1}{1 + \left(\frac{1-x}{x}\right)\left(\frac{\rho_v}{\rho_l}\right)^{0.5}} \tag{50}$$

$$m_r = \int \left[\alpha' \rho_v + (1 - \alpha')\, \rho_l\right] dV \tag{51}$$

The numerical integration method chosen to solve Eq. 51 was the 1/3 Simpson's rule according to Chapra (2018).

3.5 Uncertainty and statistical analysis

Since various measuring instruments were used in the study, it is essential to verify the accuracy of the collected data. In the present work the EES software was employed to calculate the overall uncertainty according to Taylor, Kuyatt, *et al.* (1994). If y is expressed as a function of n independent variables, $y = f(x_1, x_2, x_3, \ldots, x_n)$, where the relative uncertainties of these variables are $\delta x_1, \delta x_2, \delta x_3, \ldots, \delta x_n$, the overall uncertainty can be determined using the error propagation equation, given by Eq. 52.

$$\partial y = \sqrt{\left(\frac{\partial y}{\partial x_1}\,\partial x_1\right)^2 + \left(\frac{\partial y}{\partial x_2}\,\partial x_2\right)^2 + \ \ldots\ + \left(\frac{\partial y}{\partial x_n}\,\partial x_n\right)^2} \tag{52}$$

The accuracy of the correlation data with the mathematical model can be evaluated according to the Mean Absolute Deviation (MAD) and Mean Deviation (MD) calculated according to:

$$MAD = \frac{1}{n}\sum_{n}^{j=1}\left|\frac{\eta_{pred} - \eta_{exp}}{\eta_{exp}}\right| \tag{53}$$

$$MD = \frac{1}{n}\sum_{n}^{j=1}\left(\frac{\eta_{pred} - \eta_{exp}}{\eta_{exp}}\right) \tag{54}$$

where η is the efficiency, n is the number of data points, the subscripts $pred$ and exp are the predicted and experimental results, respectively.

3.6 Numerical procedure

In order to solve the set of equations previously presented, the platform chosen was the Python programming language. The Python library CoolProp (Bell *et al.* (2014)) was used to connect to REFPROP 10, according to Lemmon *et al.* (2018) to compute thermodynamics properties. The first step consists of entering the input data. Next, initial values are assigned for the subcooling temperature, followed by the assignment of values for the condensation temperature. The enthalpy at the condenser outlet is then calculated. Subsequently, values for the evaporation pressure are assigned, after which the enthalpy at the compressor inlet and outlet is computed. The refrigerant mass flow rate is then determined, followed by the calculation of the heat absorbed by the refrigerant. Next, the heat absorbed in the solar collector is evaluated, and the evaporator error is computed. The subsequent stage involves calculating the heat absorbed by the water, followed by determining the condenser length and evaluating the condenser error. The next step is the estimation of the refrigerant charge, after which the error associated with the subcooling temperature is computed. The final step consists of generating the results. The evaporator error (e_e) was evaluated by comparing the heat transfer heat of Eq. 15 and 7. The condenser error (e_c) was evaluated by comparing the condenser length calculated using Eq. 45 with the real condenser length (L_c). The subcooling error (e_{sub}) was evaluated by comparing the real and calculated refrigerant mass. The algorithm of the numerical model is represented in Fig. 33.

Additionally, for the environmental parameters two strategies were adopted. Similar to some studies of Hawlader, Chou, and Ullah (2001), Deng and Yu (2016) and Kong, Li, *et al.* (2017), the first simulation considered fixed values of solar irradiation, ambient temperature, atmospheric pressure, and wind speed. In addition, a case study was also carried out considering the average environmental conditions of three specific cities in a similar way to that performed by some authors as Lazzarin (2012), Chaturvedi, Gagrani, and Abdel-Salam (2014) and Duarte, Paulino, Tavares, Maia, *et al.* (2021). To carry out a case study, analysis of the hourly mean solar irradiation, ambient temperature, dew point temperature and wind speed from 07:00 a.m. to 6:00 p.m. for the cities Belo Horizonte-MG (BH), Florianópolis-SC (FL) and São Luís-MA (SL) in Brazil at the meteorological station code Pampulha-A521, Florianópolis-A806 and São Luís-A203, respectively, were obtained using the weather data in the months of the year 2024 of the meteorological institute of Brazil INMET (2024). Fig. 29 and Fig. 30 demonstrate the typical solar irradiation and ambient temperature during January to represent the summer conditions in the selected cities, while Fig. 31 and Fig. 32 demonstrate the typical solar irradiation and ambient temperature during July to represent the winter conditions in the selected cities. The prices were derived from the July 2025 market for the Brazilian city of Belo Horizonte. The mean inflation rate of electricity in Brazil was obtained from J. O. Santos *et al.* (2018). Throughout the day, the price of electricity was considered to be constant and the tax is included in the price value.

In the present chapter, the methodology adopted for performing the calculations used to develop the mathematical model was presented and the convergence of the results obtained will be examined in the following chapter.

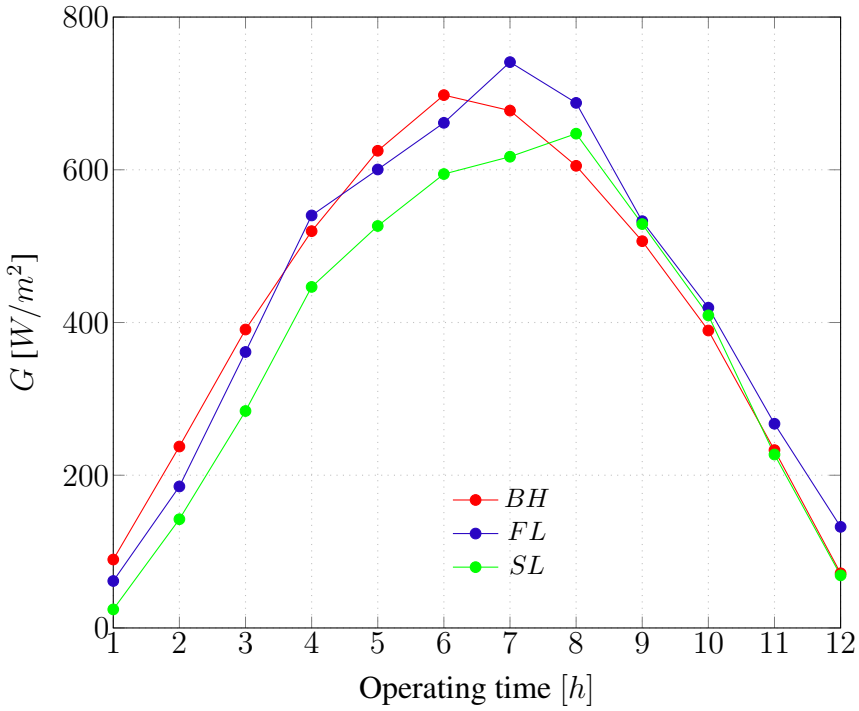

Figure 29 – Solar irradiation in January

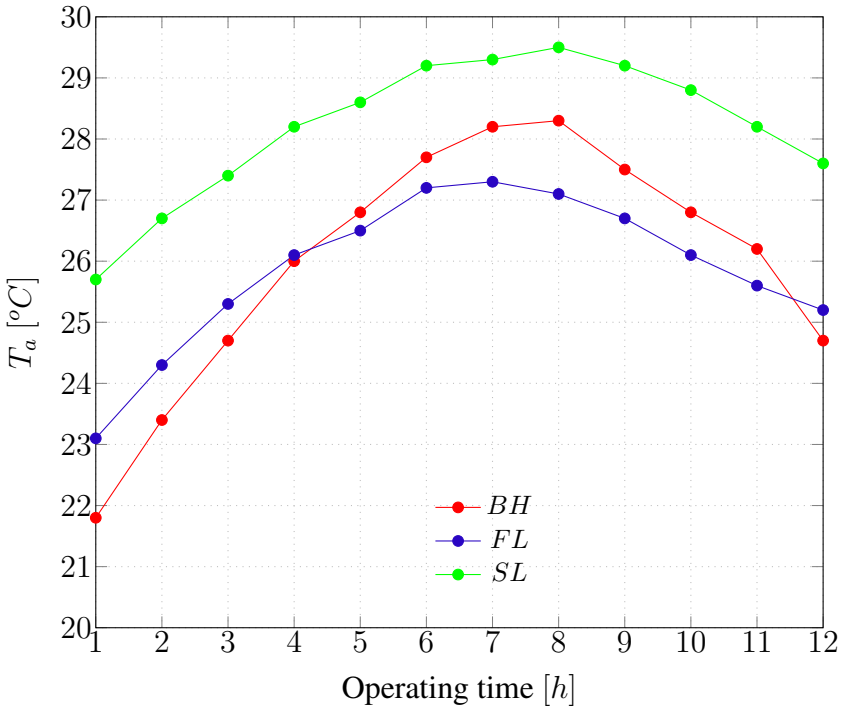

Figure 30 – Ambient temperature in January

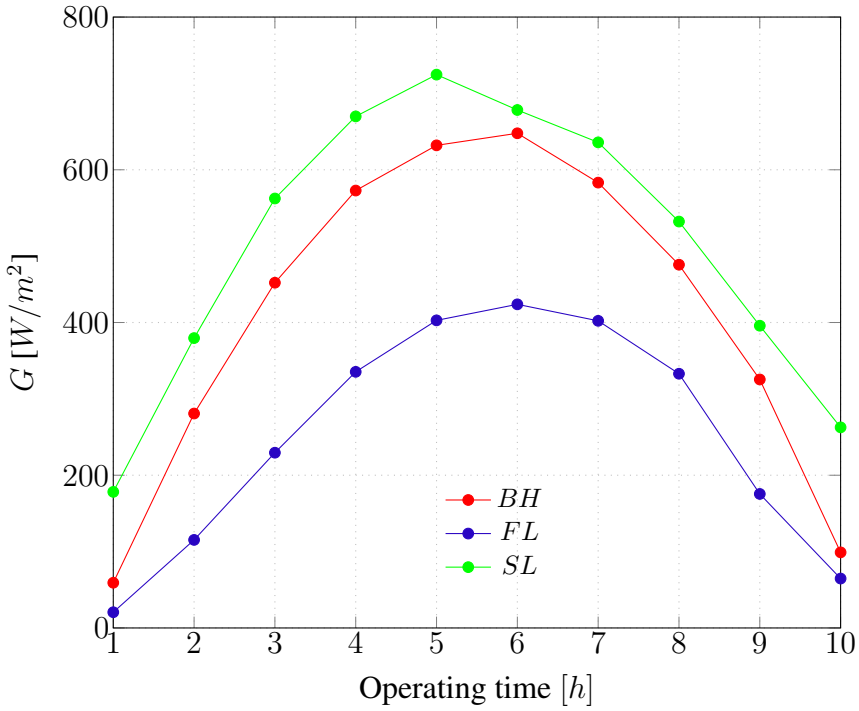

Figure 31 – Solar irradiation in July

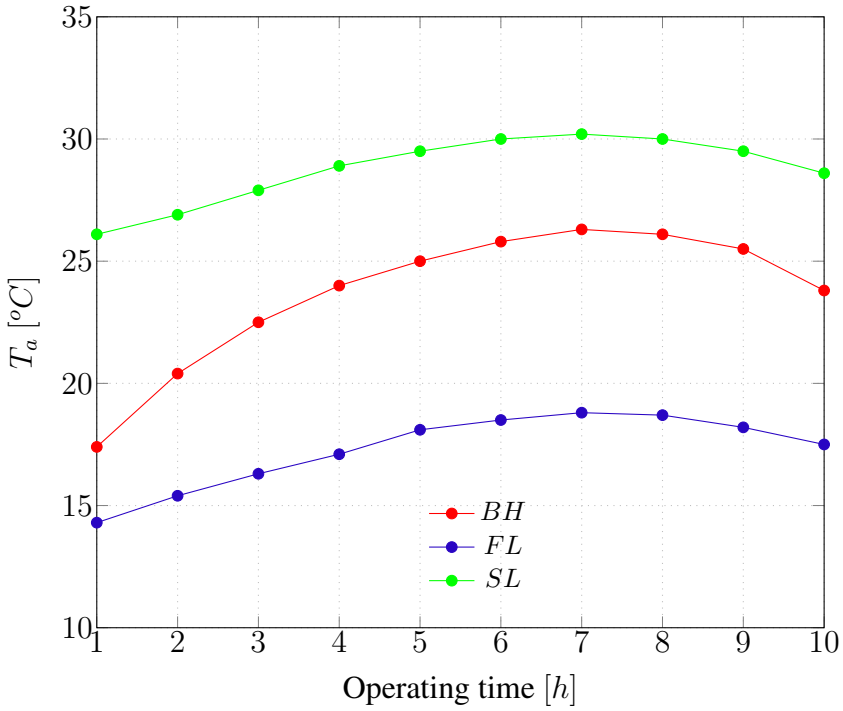

Figure 32 – Ambient temperature in July

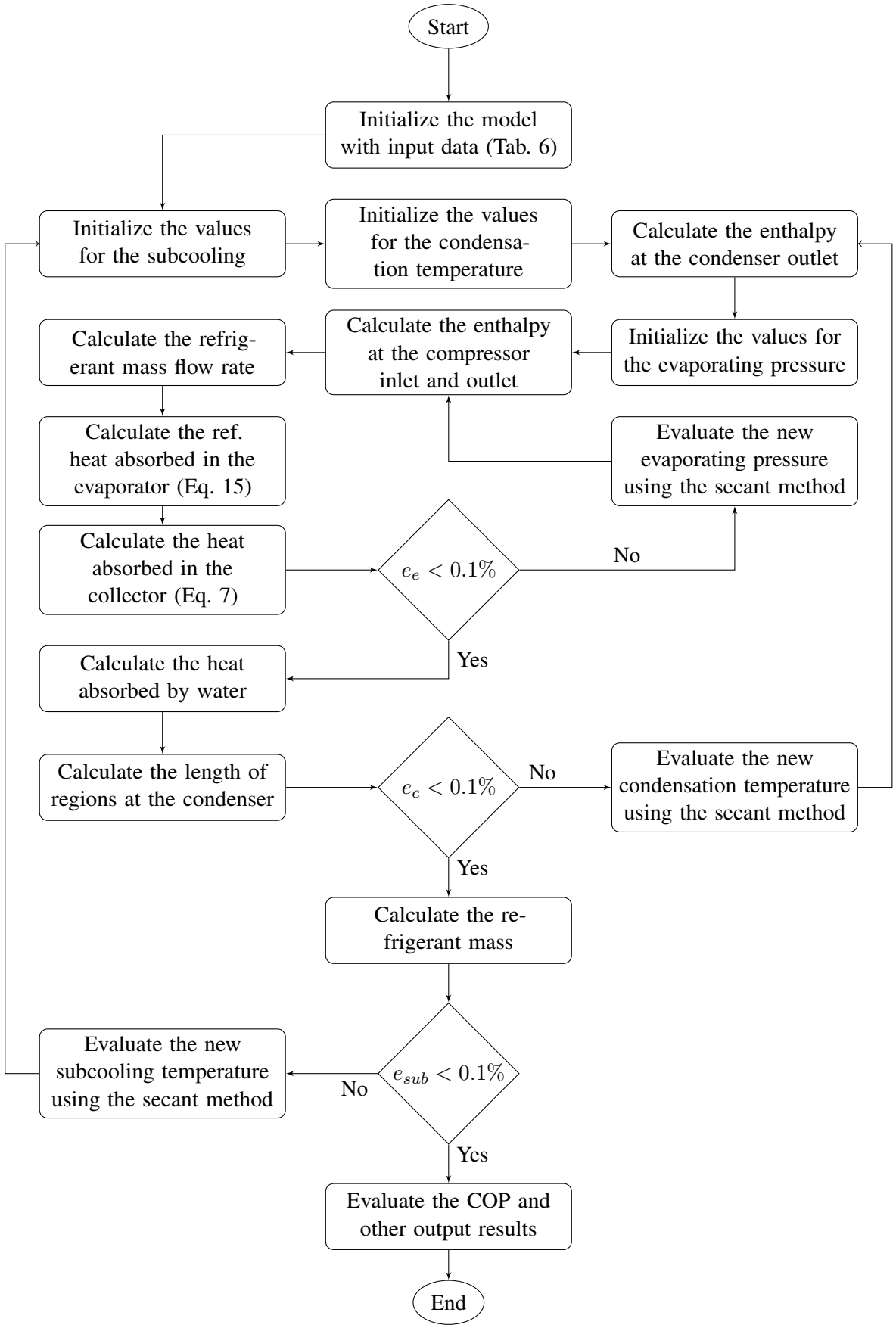

Figure 33 – Model algorithm

4 EXPERIMENTAL VALIDATION

This chapter is divided into two parts. In the first subsection, the validation data for the compressors are presented, along with the convergence between the results obtained from the mathematical model and the values provided by the manufacturers. In the second subsection, a comparison is presented between the model predictions and the experimental data obtained during the operation of the DX-PVT-SAHP.

4.1 Compressor model validation

The commercial compressors selected to perform the refrigerant selection were fixed speed compressors of refrigeration capacity from $814W$ to $1160W$. The experimental setup is comprised of a variable-speed compressor (Embraco VEGT8HB). Since its efficiency under the tested conditions is higher than that of the fixed-speed models used in the simulations, it was only applied for DX-PVT-SAHP model validation. For comparison purposes, it was replaced with a fixed-speed compressor (Embraco FFU100HAK) to ensure a fair evaluation between the selected compressors. Two R1234yf compressors were evaluated according to their refrigeration capacity since there were no commercial available options that matched exactly the refrigeration capacity for the simulated conditions. The refrigeration capacity ($\dot{Q}_r$) of the selected compressors were determined according to test standard of ASHRAE: T_e of 7.2 ^oC, T_c of 54.5 ^oC, Return Gas (T_1) of 35 ^oC, Subcooling of 8.1 ^oC and T_a of 35 ^oC. A multiple linear regression using the least square method was used to calculate the coefficients B_A to B_E to predict the function of the calculated values of η_{vol} and η_{ov} based on the catalog values according to Chapra (2018). The obtained coefficients for Eq. 33 are listed in Tab. 7.

The experimental results and calculated results obtained for the compressor volumetric efficiency and overall efficiency showed good agreement according to Fig. 34 and Fig. 35. The accuracy of the results of volumetric efficiency and overall efficiency are shown in Tab. 8. N is the number of data points and the R^2 is the coefficient of correlation which the best value is 100%. The efficiency model result can vary significantly if it is compared to the experimental measured data from manufacturer.

Table 7 – Compressors coefficients B_A to B_E

Refrig. / Model	$\forall$ $[cm^3]$	$\dot{Q}_{ref}$ $[W]$	Eq.	B_A	B_B	B_C	B_D	B_E
R134a / Embraco	7.95	861	η_{vol}	-0.00497	0.03850	0.00016	-0.00020	-0.00044
VEGT8HB$^{(VS)}$			η_{ov}	-0.00452	0.02502	0.00007	0.00013	0.00026
R134a / Embraco	7.95	865	η_{vol}	-0.00213	0.03030	0.00009	-0.00011	-0.00033
FFU100HAK$^{(FS)}$			η_{ov}	-0.00706	0.01517	0.00012	-0.00004	-0.00013
R1234yf /Embraco	7.15	815	η_{vol}	0.00241	0.02846	0.00005	-0.00006	-0.00029
FGS80LAS$^{(1)}$			η_{ov}	0.00196	0.01632	-0.00002	-0.00005	-0.00014
R1234yf /Embraco	10.85	1160	η_{vol}	-0.00225	0.03197	0.00010	-0.00011	-0.00036
FMFT411L$^{(2)}$			η_{ov}	-0.00255	0.01927	0.00001	-0.00007	-0.00021
R290 / Tecumseh	8.02	1055	η_{vol}	0.00393	0.03387	-0.00002	-0.00005	-0.00038
AE4440U-FZ1A			η_{ov}	-0.00137	0.02121	0.00002	-0.00006	-0.00021
R600a / Embraco	14.28	814	η_{vol}	0.00344	0.03390	0.00003	-0.00005	-0.00040
NEK6170Y			η_{ov}	-0.00278	0.01452	0.00005	-0.00006	-0.00012
R513A / Tecumseh	10.33	1113	η_{vol}	0.00367	0.02838	-0.00004	-0.00002	-0.00025
AE4440Y-FZ1A			η_{ov}	-0.00443	0.01390	0.00002	-0.00010	-0.00010
R454C / Tecumseh	6.69	853	η_{vol}	0.00346	0.04107	-0.00001	-0.00002	-0.00054
AE4440P-FZ1A			η_{ov}	-0.00373	0.01937	0.00007	-0.00006	-0.00023
R455A /Tecumseh	6.69	929	η_{vol}	0.00307	0.04311	-0.00001	0.00001	-0.00057
AE4440P-FZ1A			η_{ov}	-0.00110	0.02499	0.00002	-0.00001	-0.00030

$^{(VS)}$ Compressor of variable speed used in the experimental setup
$^{(FS)}$ Compressor of fixed speed selected to the model comparison between refrigerants
$^{(1)}$ Compressor selected in the model comparison between refrigerants
$^{(2)}$ Compressor for comparison performance purpose of R1234yf

Table 8 – Metrics on the adjustment of compressor efficiencies curves

			η_{vol}			η_{ov}	
Refrigerant	N	R^2 [%]	MD [%]	MAD [%]	R^2 [%]	MD [%]	MAD [%]
R134a$^{(VS)}$	20	99.92	-0.06	2.48	99.94	-0.05	2.23
R134a$^{(FS)}$	13	100.00	0.0003	0.07	99.99	0.01	0.92
R1234yf$^{(1)}$	12	99.97	-0.03	1.66	99.98	-0.02	1.37
R1234yf$^{(2)}$	6	99.94	-0.06	2.35	99.95	-0.06	2.10
R290	25	99.96	-0.03	1.89	99.98	-0.02	1.15
R600a	12	99.93	-0.06	2.47	99.97	-0.06	1.71
R513A	35	99.81	-0.08	3.92	99.97	-0.06	1.41
R454C	25	99.89	-0.05	3.12	99.98	-0.03	1.42
R455A	26	99.89	-0.05	3.11	99.95	-0.04	1.96

The correlation developed through linear regression to determine volumetric efficiency and overall efficiency as a function of evaporation and condensation temperatures obtained satisfactory results. The only refrigerant that presented values outside the $\pm 5\%$ error range in the volumetric efficiency values was R513A, in 8 points out of 35 (22.86%) with a maximum deviation of 8.67%. The worst results regarding volumetric efficiency of MD and MAD were -0.08% and 3.92%, respectively, obtained by R513A. The best MD result of 0.0003% and MAD

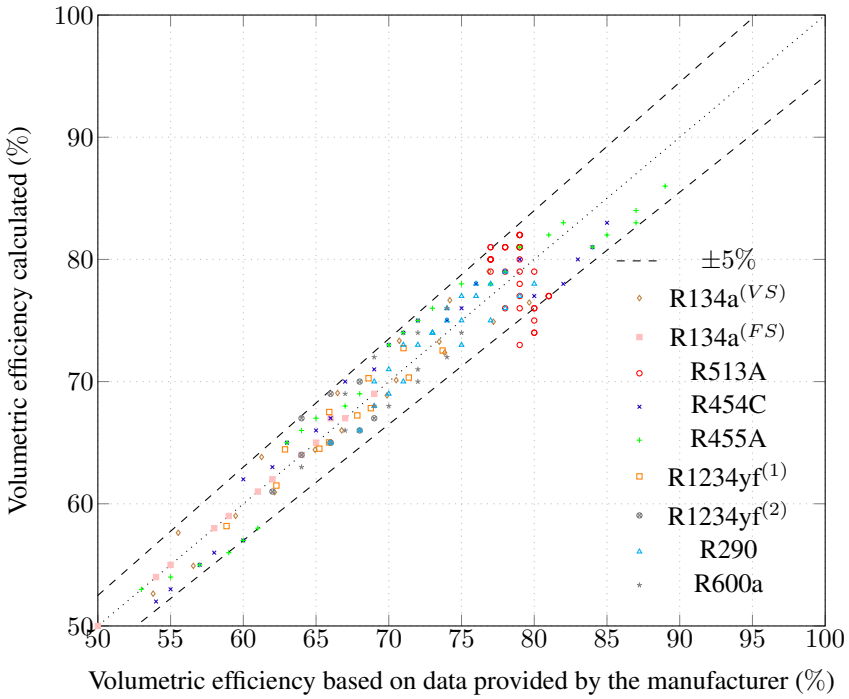

Figure 34 – Compressor volumetric efficiencies

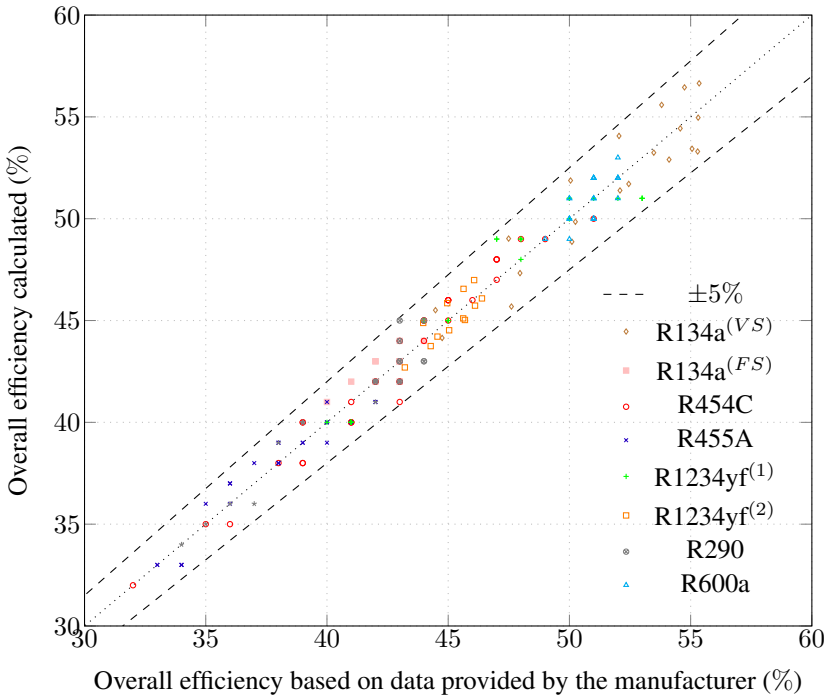

Figure 35 – Compressor overall efficiencies

result of 0.07% were both obtained by R134a$^{(2)}$. Regarding overall efficiency, the worst MD result of -0.06% was obtained by R513A and R600a and the worst MAD result of 2.23% was obtained by R134a$^{(1)}$. The best MD result of 0.01% and MAD result of 0.92% were both obtained by R134a$^{(2)}$.

4.2 DX-PVT-SAHP model validation

In order to evaluate the accuracy of the results calculated in the model with the results obtained in the experimental device, seven different tests in steady state condition were performed in June 16^{th}, 2025 at UFMG located in Belo Horizonte, MG, Brazil, coordinates $19^o54'46''$S and $43^o56'27''$ W. The tests were performed with mass of $375g$ of R134a and superheating of 5^oC. The experimental results are shown in the Tab. 9 and Tab. 10. The COP mean uncertainty value was ± 0.10 and the maximum value was ± 0.15 that corresponds to 3.4% of the measured result. The mass flow rate of water mean uncertainty value was $\pm 0.13 g/s$ and the maximum value was $\pm 0.21 g/s$ that corresponds to 1.67% of the measured result. The pressure-enthalpy diagram for experimental results ID 1 and ID 5 are presented in Fig. 36. Between Test 1 and Test 5, two significant changes were observed: the solar irradiation increased, while the outlet water temperature decreased. The increase in solar irradiation led to a higher evaporation pressure, whereas the reduction in outlet water temperature resulted in a lower condensation temperature of the heat pump. This behavior is evident in Fig. 36, as Test 5 shows a closer approach between the evaporation and condensation temperatures compared to Test 1.

Table 9 – Temperatures measured

ID	T_1 $[^oC]$	T_2 $[^oC]$	T_3 $[^oC]$	T_4 $[^oC]$	T_5 $[^oC]$	T_6 $[^oC]$	T_7 $[^oC]$	T_a $[^oC]$	T_{dp} $[^oC]$
1	18.7	58.9	25.5	9.3	21.9	48.7	18.1	20.2	13.0
2	15.3	60.9	26.8	11.2	22.7	50.2	24.7	21.7	12.0
3	14.9	58.9	26.1	10.1	22.9	44.8	27.3	22.7	11.8
4	23.4	63.5	25.7	14.0	22.9	41.6	29.4	23.9	12.6
5	24.2	59.4	26.3	14.4	23.4	40.4	30.1	23.1	10.9
6	22.0	59.1	26.4	13.9	23.2	44.0	30.2	23.7	11.4
7	21.0	61.5	27.3	15.4	22.7	46.6	34.9	25.3	10.8

Table 10 – Other experimental parameters

ID	G $[W/m^2]$	v_{wd} $[m/s]$	P_{atm} $[hPa]$	P_e $[bar]$	P_c $[bar]$	$\dot{m}_w$ $[g/s]$	$\dot{W}_{pv}$ $[W]$	V_{inv} [V]	$\dot{W}_{cmp}$ $[W]$	COP
1	452.8	0.7	934	2.9	13.0	6.25	147.3	223.1	217.5	3.24
2	594.0	0.3	934	3.1	13.9	6.84	168.0	223.5	234.1	3.38
3	641.9	0.3	934	3.0	12.0	9.04	184.8	222.0	216.3	3.85
4	671.4	0.0	934	3.5	10.6	11.6	195.8	222.4	219.2	4.16
5	648.6	0.3	934	3.6	10.3	12.8	196.8	219.7	214.7	4.27
6	713.7	0.3	933	3.5	11.4	10.4	172.9	219.7	221.6	4.09
7	771.9	0.0	933	3.6	12.4	9.04	185.4	223.1	235.3	3.86

Figures 37, 38 and 39 showed the comparison between experimental and theoretical results with 69% of data inside of $\pm$10% range and 97% of data inside of $\pm$15% range. The

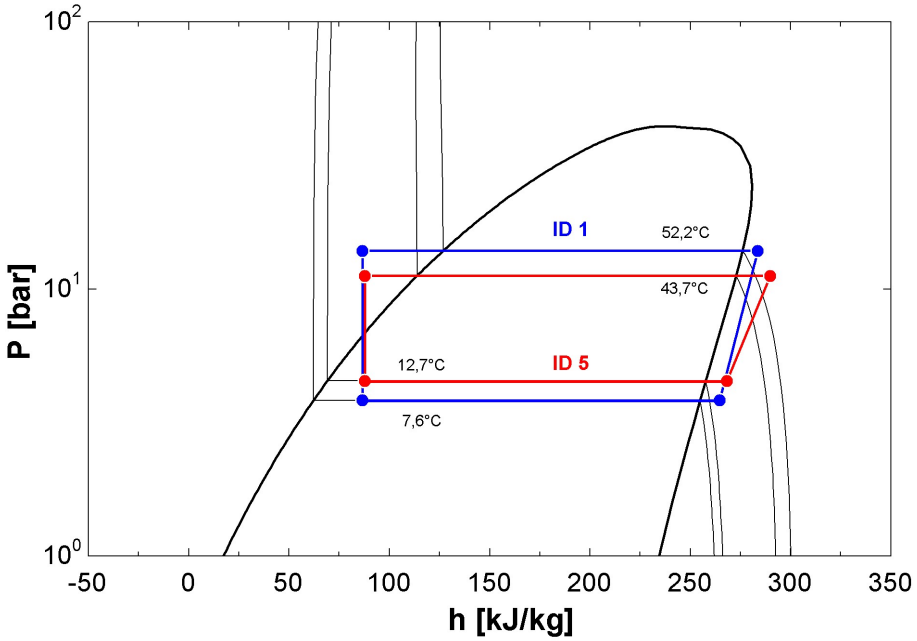

Figure 36 – Pressure-enthalpy diagram for experimental results ID 1 and ID 5.

statistical parameters of mean deviation (MD), mean absolute deviation (MAD), maximum deviation (Max.) for the DX-PVT-SAHP model validation showed a good agreement according to Tab. 11. The values presented in the Tab. 11 are compatible with values typically found in the literature: Sharma *et al.* (2024) presented a validation of a model of PVT system considering two experimental tests and five different variables with a maximum error in the range of $\pm 10\%$; Liang *et al.* (2023) validated their model of PVT-SAHP with maximum difference of 14.93% and 20.15% for COP and photovoltaic power, respectively. In the heat pump model validation some authors as Abbasi, Li, and Mwesigye (2024), Zanetti *et al.* (2023) and Li, Li, and Zhang (2015) presented an average difference between experimental and theoretical COP of 4.2%, 5.0% and 5.5%. Additionally, data points corresponding to the DX-PVT-SAHP tests (represented by squares in Fig. 39) were complemented with points validated for a DX-SAHP operating with a solar collector without a photovoltaic panel (represented by circles in Fig. 39) with experimental data published by Duarte (2018). The operational difference between the two systems is that the DX-PVT-SAHP employs a PVT-type evaporator, whereas the DX-SAHP uses a solar-collector-type evaporator. These additional points were obtained using the mathematical model developed in this thesis, with the following modifications: the photovoltaic panel efficiency and the contact resistance were set to zero in the DX-SAHP.

The procedure presented in this chapter demonstrated the accuracy and flexibility of

the proposed mathematical model in simulating the operation of the heat pump with different constructive configurations. In the next chapter, the numerical model will be applied considering a range of environmental conditions and operating scenarios.

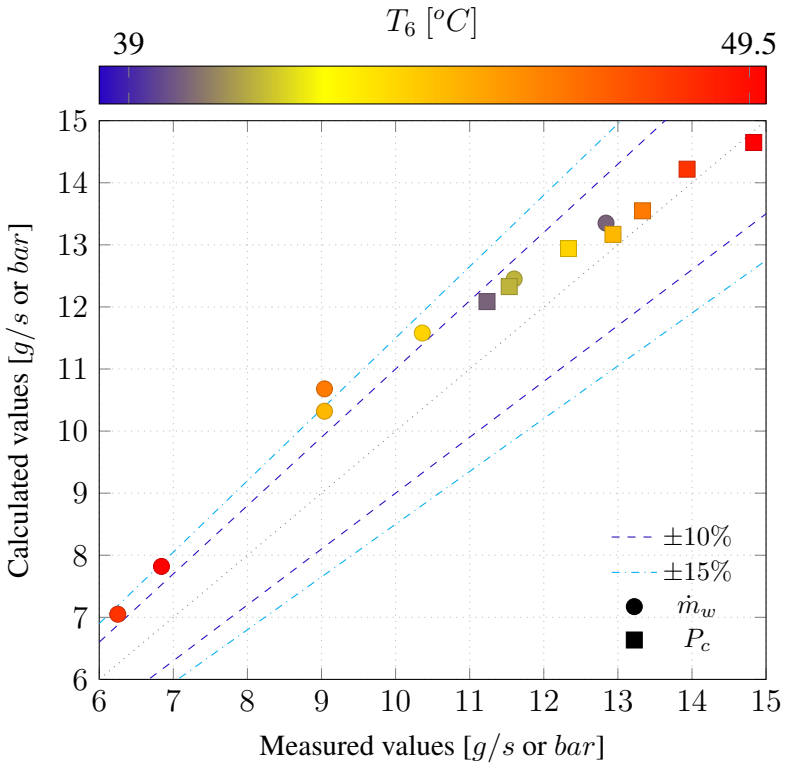

Figure 37 – Water mass flow rate ($\dot{m}_w$) and pressure (P_c) at condenser obtained in the model and experimentally for the same environmental conditions.

Table 11 – Statistical parameters on the modelling validation

	MD	MAD	Max.
Condensing pressure [%]	3.4	3.7	7.6
Power generation [%]	-3.4	9.0	14.4
Compressor power [%]	11.8	11.8	15
COP [%]	-0.6	3.4	6.6
Water mass flow rate [%]	11.8	11.8	18.2
All data [%]	4.6	8.0	18.2

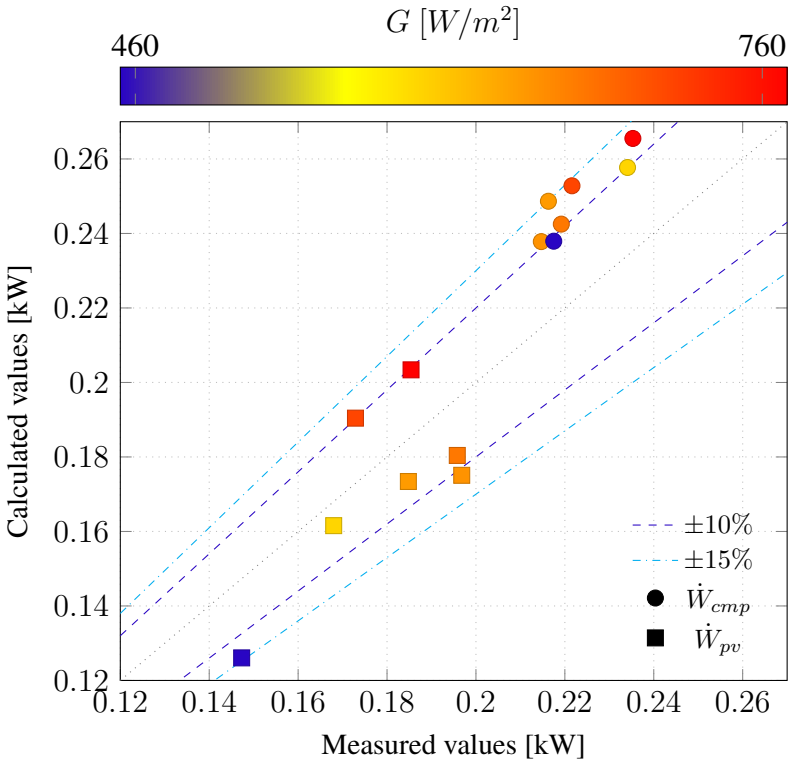

Figure 38 – Power consumed by the compressor ($\dot{W}_{cmp}$) and power produced by photovoltaic cells ($\dot{W}_{pv}$) obtained in the model and experimentally for the same environmental conditions.

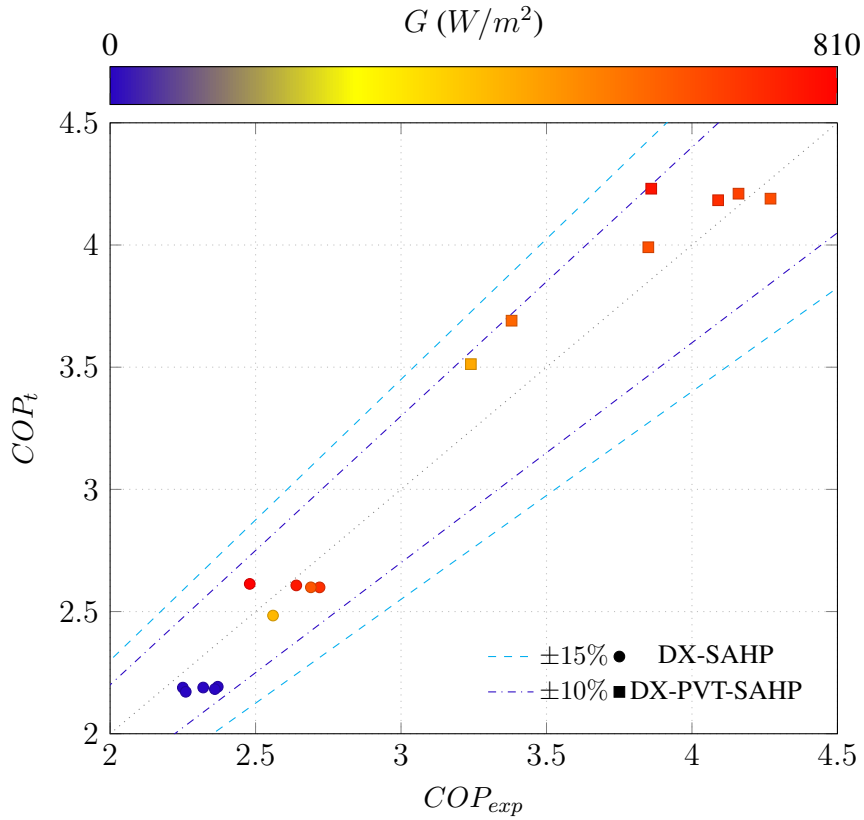

Figure 39 – Coefficient of performance (COP) obtained in the model and experimentally for the same environmental conditions.

5 RESULTS

This chapter presents the main results obtained from the numerical model. First, the optimized refrigerant charge for the DX-PVT-SAHP operating with seven different refrigerants is discussed. Subsequently, the coefficient of performance (COP) as a function of ambient temperature is analyzed. Following this, the variation of COP, the power output of the PV cells, and the compressor's electrical consumption as a function of solar irradiance are examined. Next, the operational performance of the DX-PVT-SAHP using R134a during January 2024 is presented. In addition, the annual SPF and TEWI values calculated for the city of Belo Horizonte–MG are reported. The section also includes the payback analysis of the DX-PVT-SAHP operating with R1234yf in Belo Horizonte–MG. Finally, the variation of the monthly solar fraction (SF) in the selected cities is compared, and the importance of the compressor selection criteria for systems operating with different refrigerants is highlighted.

5.1 Optimized refrigerant charge

The refrigerant charge of the system can be optimized due to the behavior described as follows. The degree of subcooling is governed by the refrigerant charge, with higher charge leading to greater subcooling. Increasing the subcooling enhances the enthalpy variation in the condenser without affecting that of the compressor, thereby improving the COP. However, excessive subcooling may lower the refrigerant outlet temperature below that of the water at the condenser outlet, requiring a higher condensation temperature and consequently reducing the COP as represented in Fig. 40.

The first step to obtain the energetic performance results for each refrigerant was to determine the amount of mass that resulted in the best COP considering three solar irradiation values: 500 W/m^2, 700 W/m^2, 900 W/m^2 and the conditions presented in Tab. 6, as shown in Fig. 41 for R134a. The optimized refrigerant mass quantity does not vary with changes in solar irradiation conditions. Furthermore, the optimized refrigerant charge considering the COP is illustrated in Tab. 12.

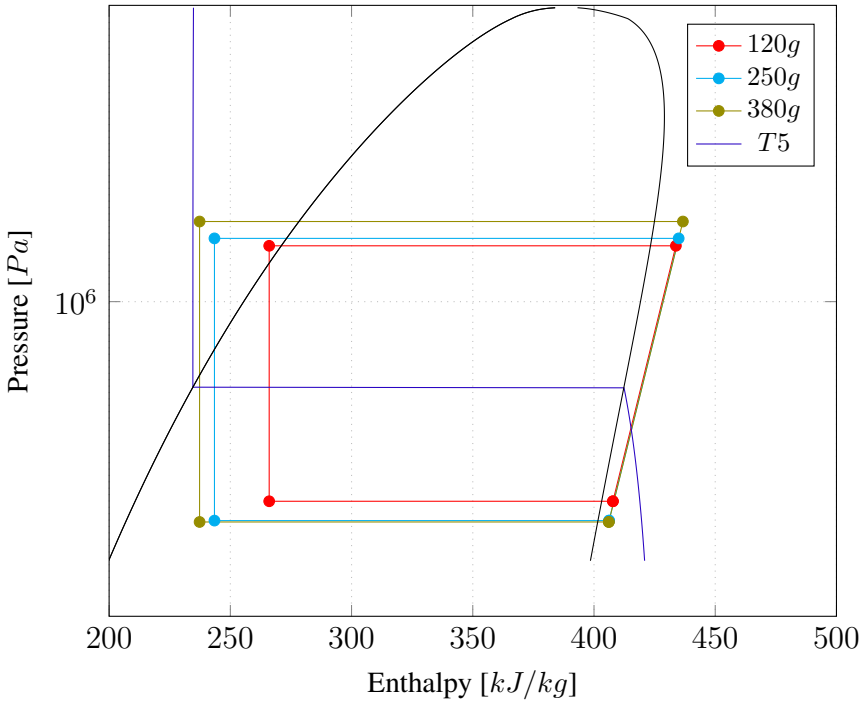

Figure 40 – Mass optimization for maximum COP in pressure x enthalpy diagram

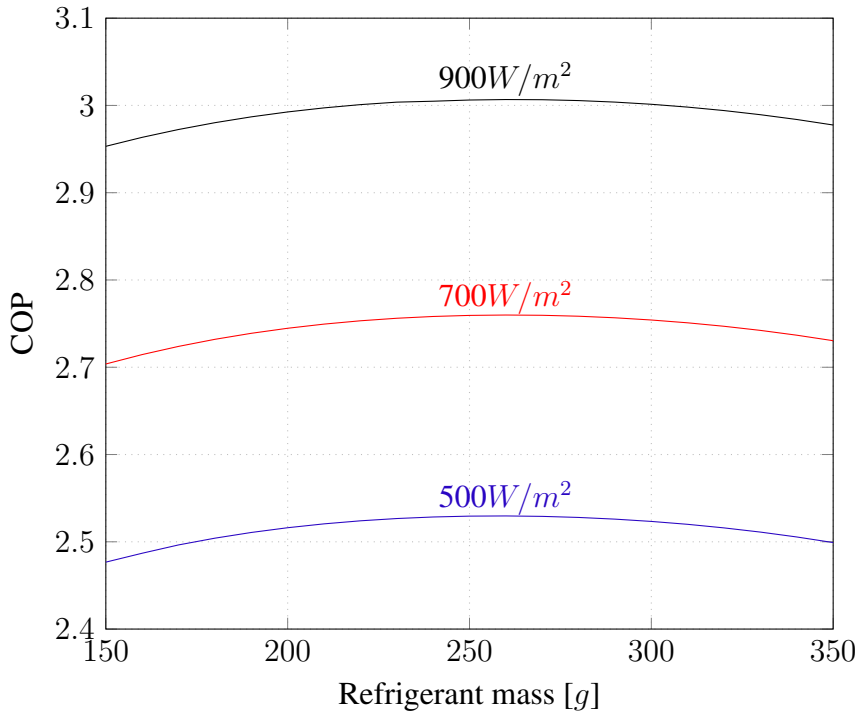

Figure 41 – COP in function of mass of R134a for three different solar irradiation

Table 12 – Optimized refrigerant mass considering COP

R134a	R1234yf	R290	R600a	R513A	R454C	R455A
260 g	250 g	105 g	125 g	280 g	210 g	200 g

5.2 DX-PVT-SAHP simulation

The energy analysis was based on the COP as a function of ambient temperature with values between 15 ^oC and 35 ^oC, COP, compressor electric consumption and power output of PV cells as a function of solar irradiation with values between 50W/m^2 to 1,000 W/m^2 for the environment conditions fixed and listed in Tab. 6 showed in Fig. 42, Fig. 43, Fig. 44, Fig. 45, Fig. 46 and Fig. 47. The system COP increased under the influence of increasing ambient temperature, which is consistent with the conclusions reported in the study of Duarte, Paulino, Pabon, *et al.* (2019). An increase in the evaporation temperature enhances the heat-transfer rate in the condenser, thereby raising the COP of the system. Among all the refrigerants evaluated, R1234yf delivered the best overall performance. For pure refrigerants, R1234yf showed the highest performance while R600a performed the worst, according to Fig. 42. For refrigerant blends, R455A achieved the best result whereas R454C exhibited the poorest performance, according to Fig. 43. The system COP, compressor electric consumption and power output of PV cells were increased under the influence of increasing solar irradiation. Further, according to Fig. 44, R1234yf presented the best results of COP among the compared low GWP pure refrigerants, increasing the COP value from 2.21 at 50 W/m^2 to 4.06 at 1000 W/m^2, this finding of COP superiority over other fluids was also reported by Kim *et al.* (2023). It was observed a very similar performance of R1234yf with R290 under low solar irradiation from 50W/m^2 to 200W/m^2. Considering the refrigerant blends in Fig. 45, R455A presented the best COP results for all solar irradiation ranges, presenting a result 21.39% higher than R454C for a solar irradiation of 500 W/m^2. R513A and R454C presented similar performance for high solar irradiation of 1,000 W/m^2, while for low and medium solar irradiation values, R513A presented a better result compared to R454C.

Additionally, in Fig. 46, R134a presented the highest compressor electric consumption from solar irradiation higher than 200 W/m^2 followed by R290, R600a and R1234yf. R1234yf presented the lowest compressor electric consumption among the compared low GWP pure refrigerants of 215 W at 50 W/m^2 to 283 W at 1000 W/m^2. Regarding the refrigerant mixtures in Fig. 47, R455A presented the lowest results in compressor electrical energy consumption for all solar irradiation ranges, presenting a value 16.02% lower than the result obtained for R513A for a solar irradiation of 500 W/m^2. R513A and R454C presented similar performance for low solar irradiation of up to 400 W/m^2, while for higher values, R513A presented a higher compressor

electrical energy consumption compared to R454C. In both Fig. 46 and Fig. 47 as solar irradiation increases the power consumption of compressor also increases and the PVT surface temperature rises resulting in the refrigerant entering the compressor to evaporate at a higher pressure and temperature with higher specific volume of the suction vapor, this effect makes the compressor handle more volume flow for the same refrigerant mass flow increasing the power consumption to achieve the condensing pressure. Additionally, the power output of PV cells is similar for all the refrigerants and is proportional to solar irradiation as stated in the research of Yogaraja *et al.* (2024). This behavior can be explained because as solar irradiation increases, the number of photons absorbed by the PV cells increases, leading to a higher generation of electricity. The results showed that R1234yf has the best energetic performance ammong the compared refrigerants in agreement with the results reported by Bellos and Tzivanidis (2019).

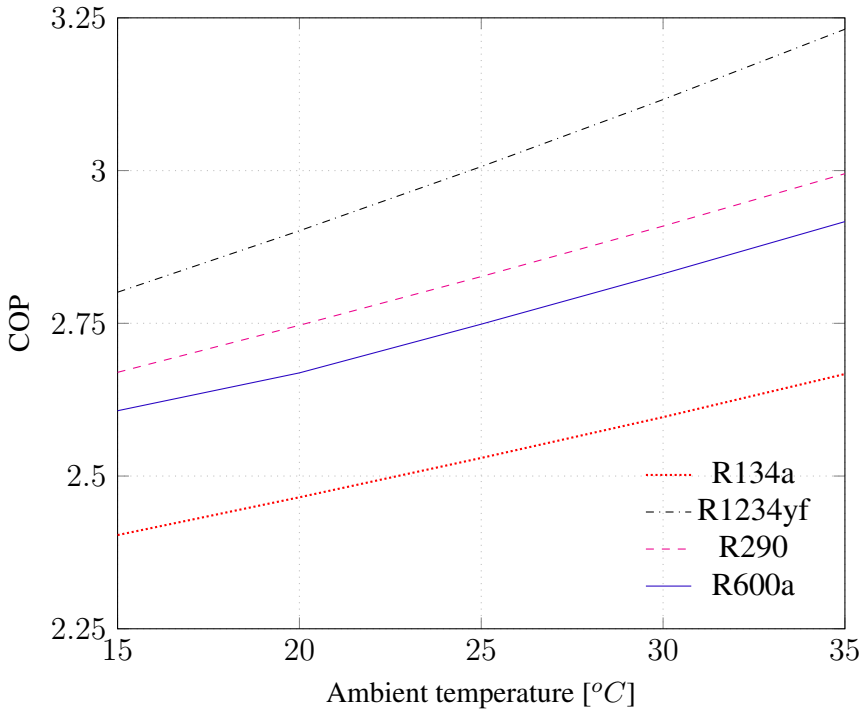

Figure 42 – COP in function of ambient temperature of pure refrigerants

The calculation of SPF was performed assuming that the heat pump operated to heat $200L$ of water from the ambient temperature to 50^oC every day of the year for Belo Horizonte, Brazil. After the heating period, the equipment would shut down, and the photovoltaic panel would continue to produce electricity. The SPF was calculated as the ratio of the annual accumulated thermal energy for heating the water to the electricity consumed by the compressor, minus the energy produced by the PV panel as represented in Fig. 48 for the month of January 2024.

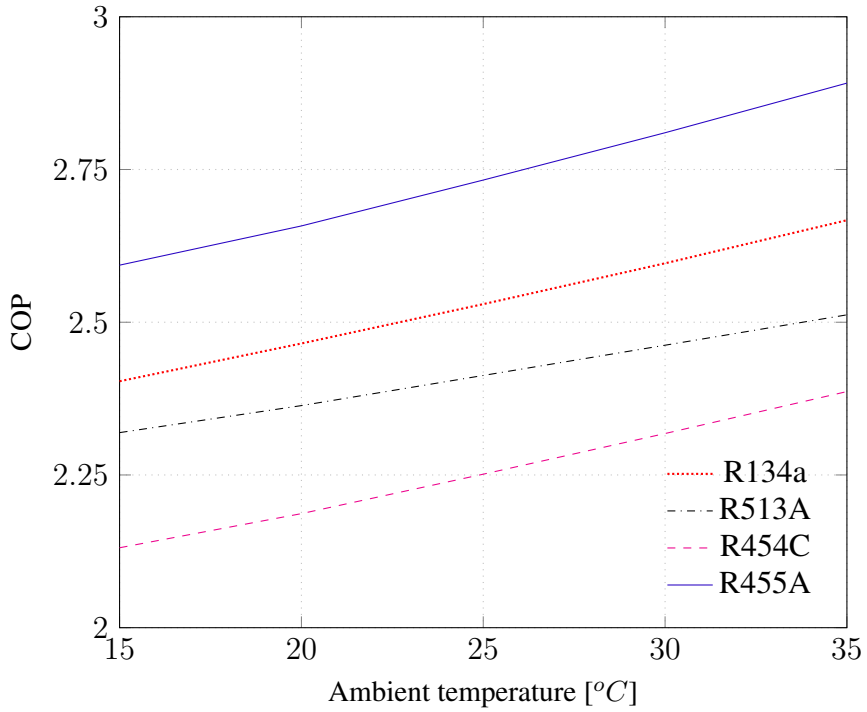

Figure 43 – COP in function of ambient temperature of refrigerant blends

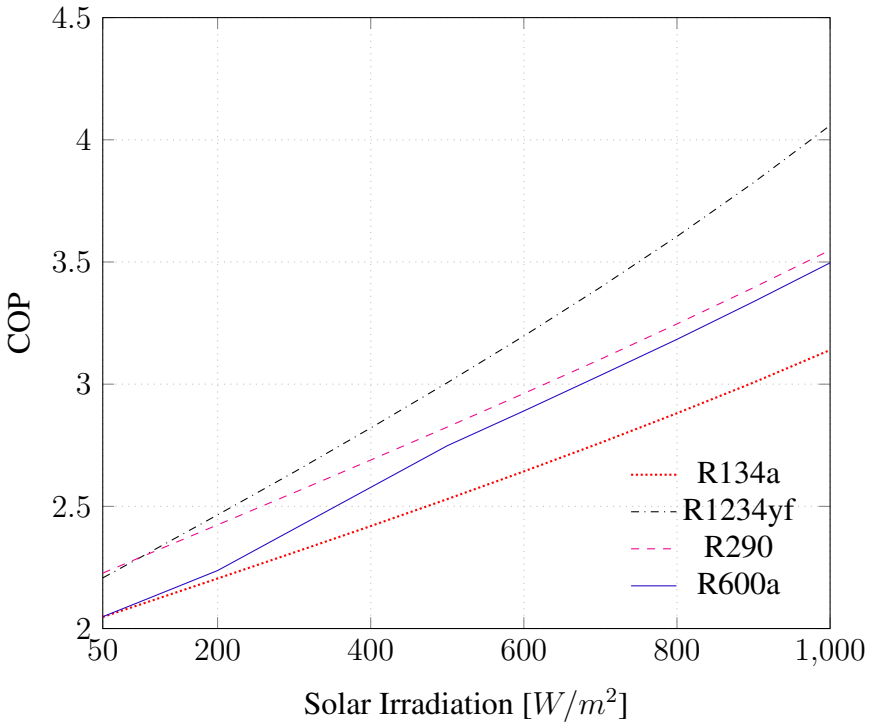

Figure 44 – COP in function of solar irradiation of pure refrigerants

The SPF, direct emissions and indirect emissions in TEWI calculation are shown in Tab. 13, Fig. 49 and Fig. 50. Direct emissions are calculated by the first term on the right side of the Eq. 4 and indirect emissions are calculated by the second term on the right side of the Eq. 4. The refrigerants with the lowest direct emissions used in TEWI calculation are the R290 and R600a

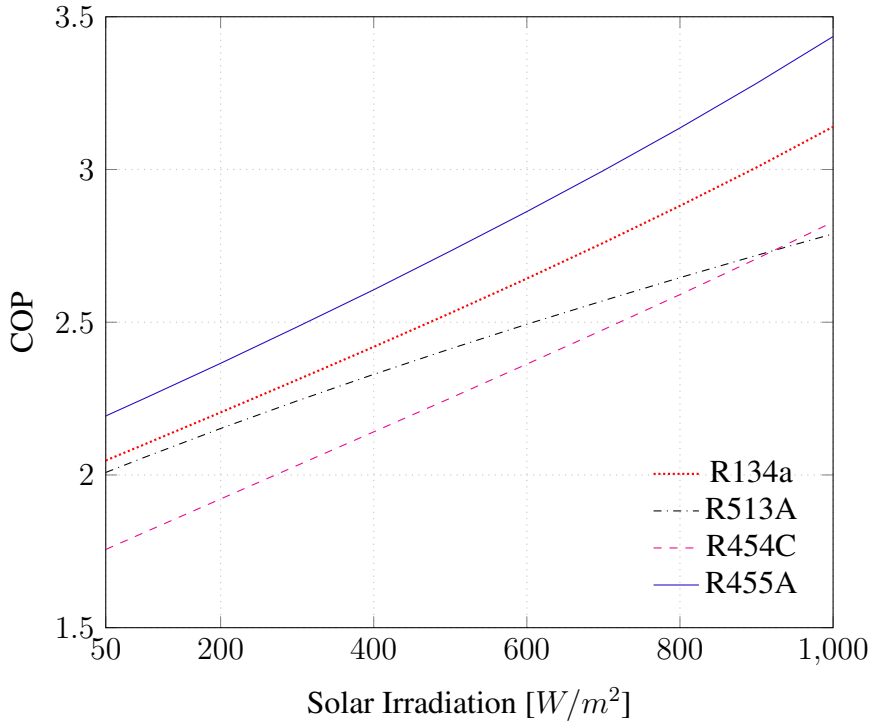

Figure 45 – COP in function of solar irradiation of refrigerant blends

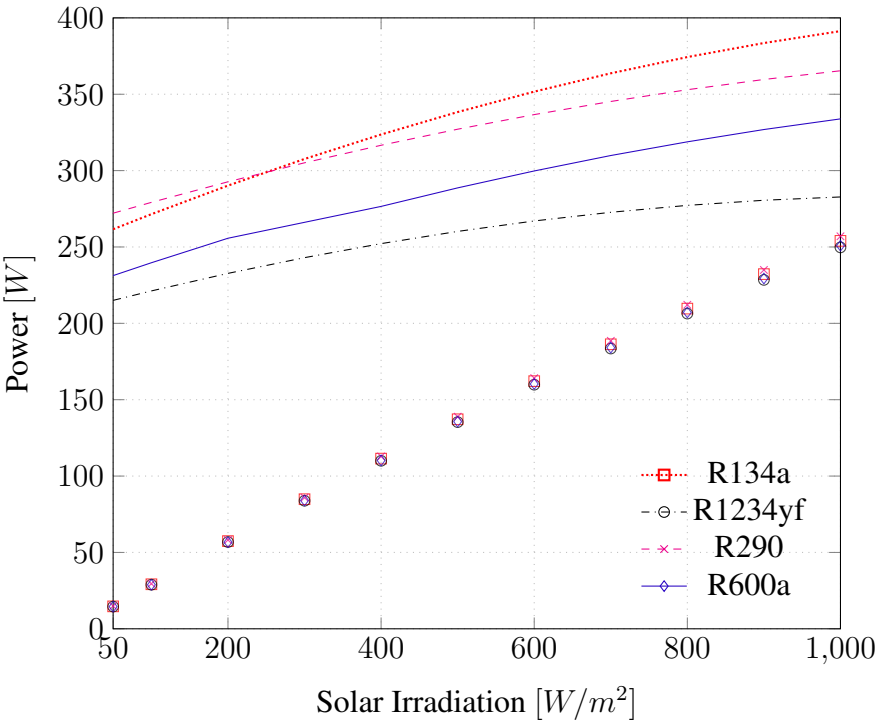

Figure 46 – Power output of PV cells (marks) and compressor electric consumption (lines) in function of solar irradiation of pure refrigerants

due to their low GWP value and low charge of refrigerant. The worst value of direct emissions due to its elevated GWP was presented by the R134a that was 1179 greater than the value of R290 and R600a. Furthermore R1234yf presented the best result of indirect emissions in TEWI

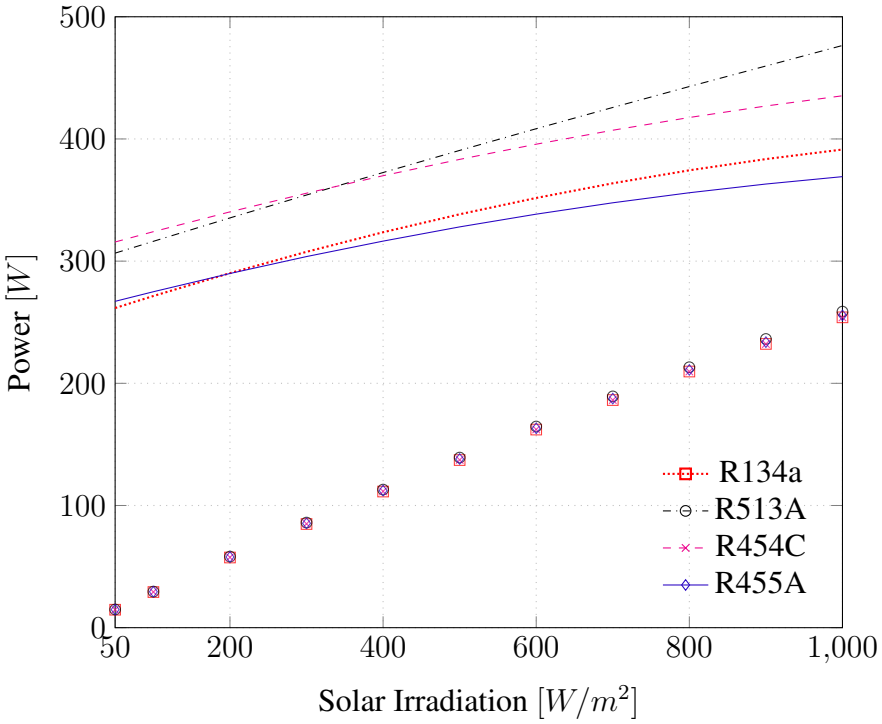

Figure 47 – Power output of PV cells (marks) and compressor electric consumption (lines) in function of solar irradiation of refrigerant blends

calculation due to its superior SPF results followed by R290. R513A and R454C presented the worst results of indirect emissions due to their values of SPF lower than all other compared refrigerants. The direct emissions for R134a corresponds to 36.1% and the indirect emissions corresponds to 63.9% of the total TEWI. The direct emissions for R1234yf, R290 and R600a corresponds to less than 1% of the total TEWI value due to their low GWP value. The best TEWI value calculated by the sum of direct emissions and indirect emissions was presented by R1234yf due to its low GWP value combined with the best SPF among all refrigerants which is in a good agreement with the performance presented in Fig. 44. Additionally, R1234yf presented a 49.59% lower TEWI than R513A that presented the worst value of TEWI. A comparative study of refrigerants carried out by Kim *et al.* (2023) concluded that R134a presented a TEWI value 30% higher than that of R1234yf, in addition, another study conducted by Duarte, Paulino, Pabon, *et al.* (2019) found similar TEWI values for the fluids R290 and R600a, which is in agreement with the results presented in this article. Furhtermore, the comparative study of TEWI values considered the case in which one to four photovoltaic panels were used in conjunction with an electric heater to provide the heating demand as stated in Tab. 13. Even four PV panels operating under the same environmental conditions achieved worst SPF and TEWI results compared to all refrigerants operating in the DX-PVT-SAHP. The DX-PVT-SAHP operating with R1234yf

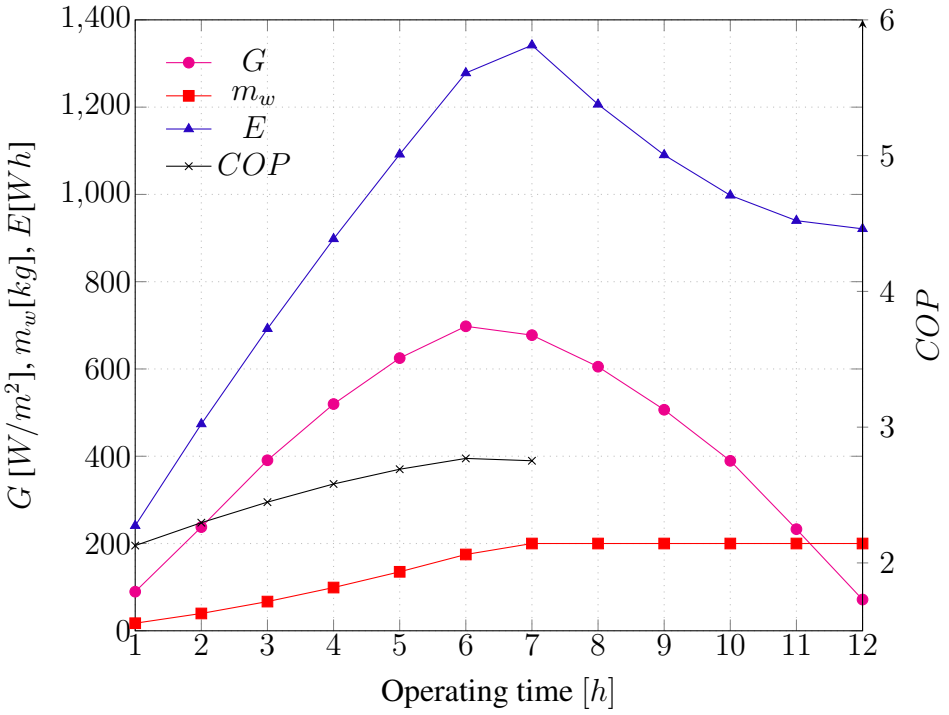

Figure 48 – DX-PVT-SAHP operating performance in January 2024 for R134a

combined with photovoltaic generation of electricity for the grid would avoid 1.6 tons of CO_2 emissions compared to an electric heater over a 15-year period. Furthermore, the electrical heater operating with 1 PV would avoid 314 kg of CO_2 emissions compared to an electric heater without a PV over a 15-year period.

Table 13 – Annual SPF and TEWI for a 15-year period in Belo Horizonte

Ref. or System	SPF	Direct emission (kg CO_2)	Indirect emission (kg CO_2)	TEWI (kg CO_2)
R134a	5.86	167.31	295.73	463.04
R1234yf	9.39	0.45	184.51	184.96
R290	7.45	0.14	232.63	232.77
R600a	7.05	0.14	245.70	245.84
R513A	5.07	71.82	341.56	413.38
R454C	4.57	13.99	379.43	393.42
R455A	6.93	13.05	250.24	263.29
1PV	1.18	0.00	1472.98	1472.98
2PV	1.50	0.00	1159.12	1159.12
3PV	2.05	0.00	845.26	845.26
4PV	3.26	0.00	531.41	531.41
Electric heater	0.97	0.00	1786.83	1786.83

The payback analysis presented in Fig. 51 was performed by comparing the DX-PVT-SAHP operating with the low-GWP refrigerant R1234yf, which presented the highest SPF

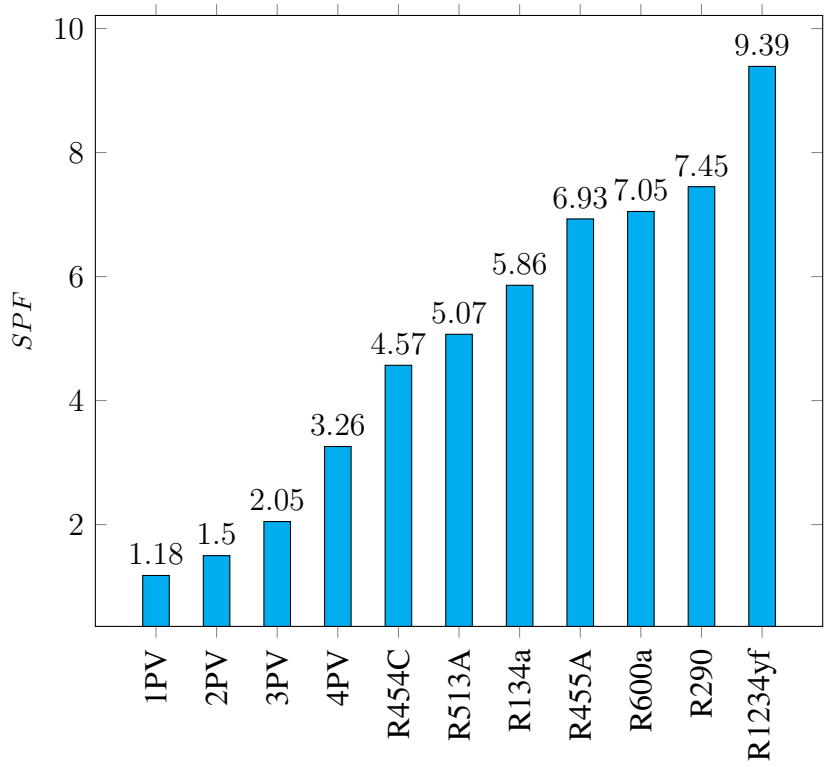

Figure 49 – Annual SPF of DX-PVT-SAHP and PV operating in Belo Horizonte-MG

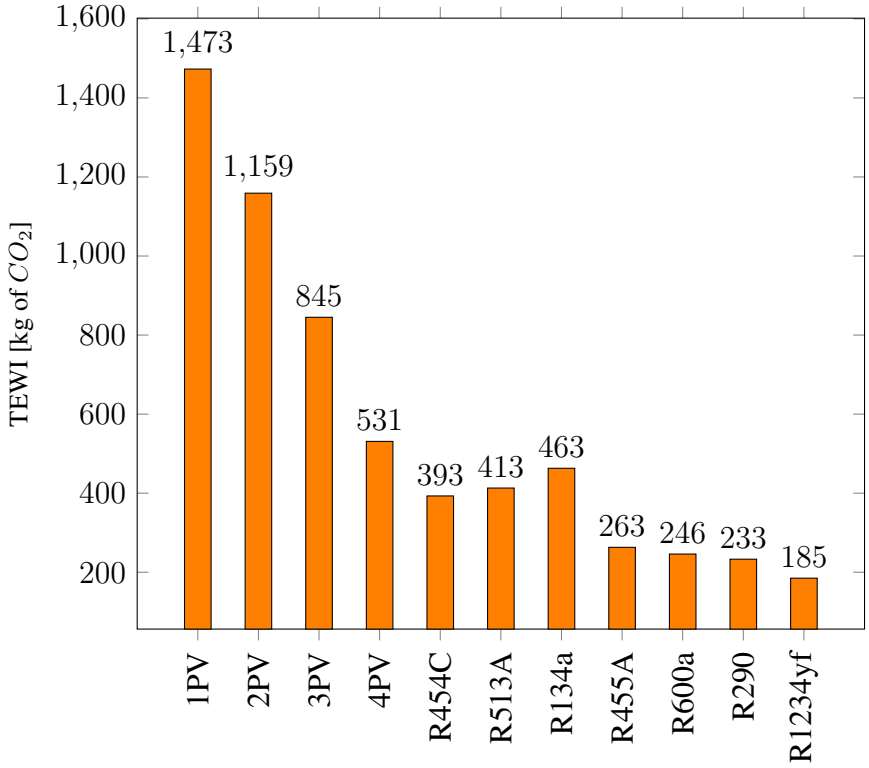

Figure 50 – TEWI of DX-PVT-SAHP and PV operating in Belo Horizonte-MG

and lowest TEWI, with an electric water heater supported only by the photovoltaic panel. The results indicated that the payback period of the investment, when considering the energy savings

achieved by the DX-PVT-SAHP system, was 2.8 years. In contrast, when considering the installation of a photovoltaic panel for electricity generation combined with the use of an electric heater, the payback period extended to 5.4 years, demonstrating that considering the energy savings of DX-PVT-SAHP using R1234yf has a payback time approximately twice as fast as the electric water heater supported by the photovoltaic panel. Additionally, for the case that two, three and four PV were used with the electric heater the calculated payback were 4.0, 3.5 and 3.3 years, respectively. The result of the payback for the electric water heater is in a good agreement with Fukurozaki, Zilles, and Sauer (2013) that developed a research of payback time estimated in 2.47 – 3.13 years for a 1.2 kWp PV system for Belo Horizonte. The component with the lowest allowable operating pressure in the heat pump is the 3/8" diameter copper tube, which has a maximum working pressure of 8.3 MPa. The refrigerants considered in this study have the following critical pressures (in MPa): R134a = 4.0593; R1234yf = 3.3822; R290 = 4.2512; R600a = 3.629; R513A = 3.6478; R454C = 4.3188; R455A = 4.6538. Since all the fluids operate under subcritical cycles, none of them reach pressures that would necessitate the use of specialized piping for the heat pump. Therefore, the selection of a standard commercial copper tube is sufficient to accommodate all the refrigerants analyzed.

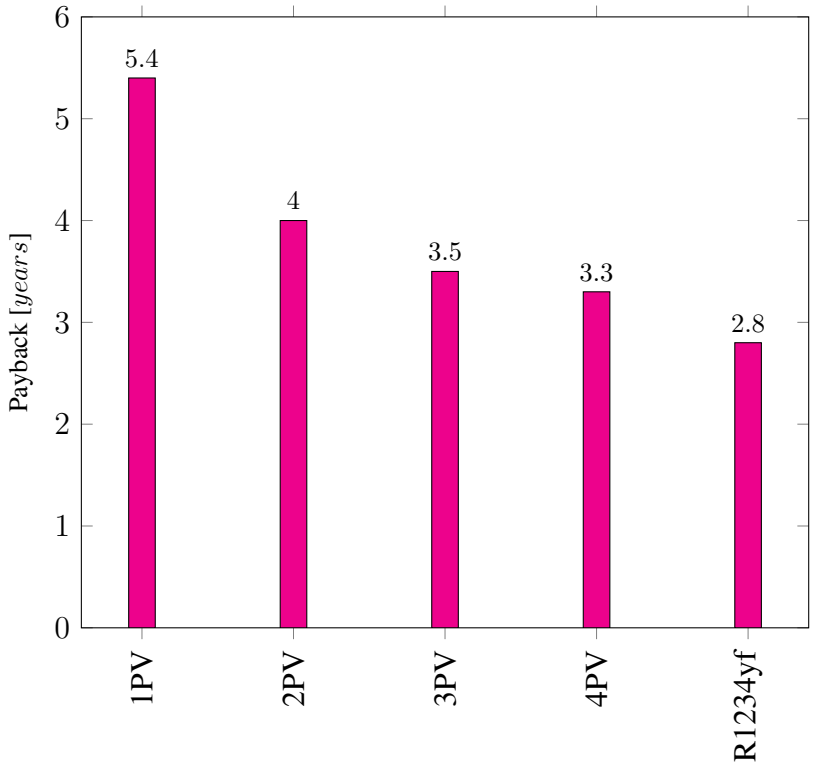

Figure 51 – Payback of DX-PVT-SAHP and PV operating in Belo Horizonte-MG

The monthly SF of DX-PVT-SAHP operation for the cities of Belo Horizonte-MG (BH),

Florianópolis-SC (FL) and São Luís (MA) were compared. For all the refrigerants the best SF occurred in September for the cities of Belo Horizonte-MG and São Luís and in February for Florianópolis. Fig. 52 showed that R1234yf presented better SF over R134a for all months of the year in all the compared cities. Additionally in relation to the greatest SF difference, in Belo Horizonte in December, R1234yf presented 8.14% higher SF than R134a, in Florianópolis in August, R1234yf presented 15.45% higher SF than R134a and in São Luís in June, R1234yf presented 8.22% higher SF than R134a. Fig. 53 showed that R290 presented better SF over R134a for all months of the year in all the compared cities. Additionally in relation to the greatest SF difference, in Belo Horizonte in June, R290 presented 5.32% higher SF than R134a, in Florianópolis in August, R290 presented 8.86% higher SF than R134a and in São Luís in June, R290 presented 5.93% higher SF than R134a. Fig. 54 showed that R600a presented better SF over R134a for all months of the year in all the compared cities. Additionally in relation to the greatest SF difference, in Belo Horizonte in May, R600a presented 4.31% higher SF than R134a, in Florianópolis in August, R600a presented 12.41% higher SF than R134a and in São Luís in January, R600a presented 4.03% higher SF than R134a. Fig. 55 showed that R134a presented better SF over R513A for all months of the year in all the compared cities. Additionally in relation to the greatest SF difference, in Belo Horizonte in September, R134a presented 3.64% higher SF than R513A, in Florianópolis in July, R134a presented 12.37% higher SF than R513A and in São Luís in August, R134a presented 2.96% higher SF than R513A. Fig. 56 showed that R134a presented better SF over R454C for all months of the year in all the compared cities. Additionally in relation to the greatest SF difference, in Belo Horizonte in December, R134a presented 7.14% higher SF than R454C, in Florianópolis in July, R134a presented 13.18% higher SF than R454C and in São Luís in February, R134a presented 6.88% higher SF than R454C. Fig. 57 showed that R455A presented better SF over R134a for all months of the year in all the compared cities. Additionally in relation to the greatest SF difference, in Belo Horizonte in June, R455A presented 3.77% higher SF than R134a, in Florianópolis in September, R455A presented 4.83% higher SF than R134a and in São Luís in January, R455A presented 4.60% higher SF than R134a. The highest SF observed among the evaluated cities and refrigerants was 1.0, recorded in September in São Luís with the DX-PVT-SAHP operating with R1234yf. This indicated that, during that month, the electrical and thermal energy produced by the DX-PVT-SAHP fully met the water heating demand without requiring any additional energy from the grid. Moreover, the worst SF of 0.59 occurred with the DX-PVT-SAHP operating with R454C in the city of

Florianópolis, in June, a result 41% lower than the best SF. The results confirm that the fluid achieving the highest COP, combined with the highest solar irradiation, yielded the greatest SF. Conversely, the fluid with the lowest COP under the lowest solar irradiation conditions resulted in the smallest SF.

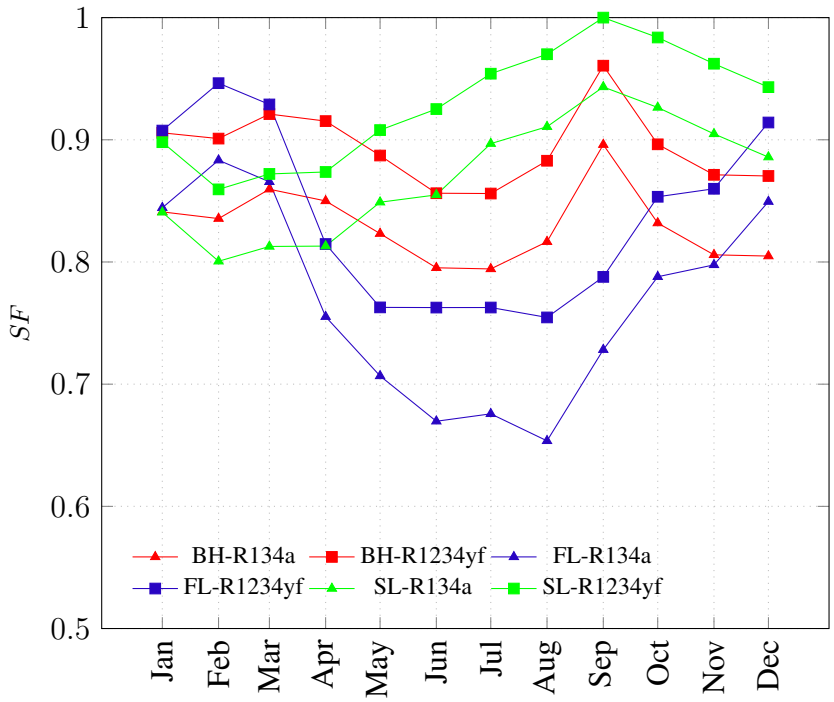

Figure 52 – Variation of monthly SF of the DX-PVT-SAHP operating with R134a and R1234yf

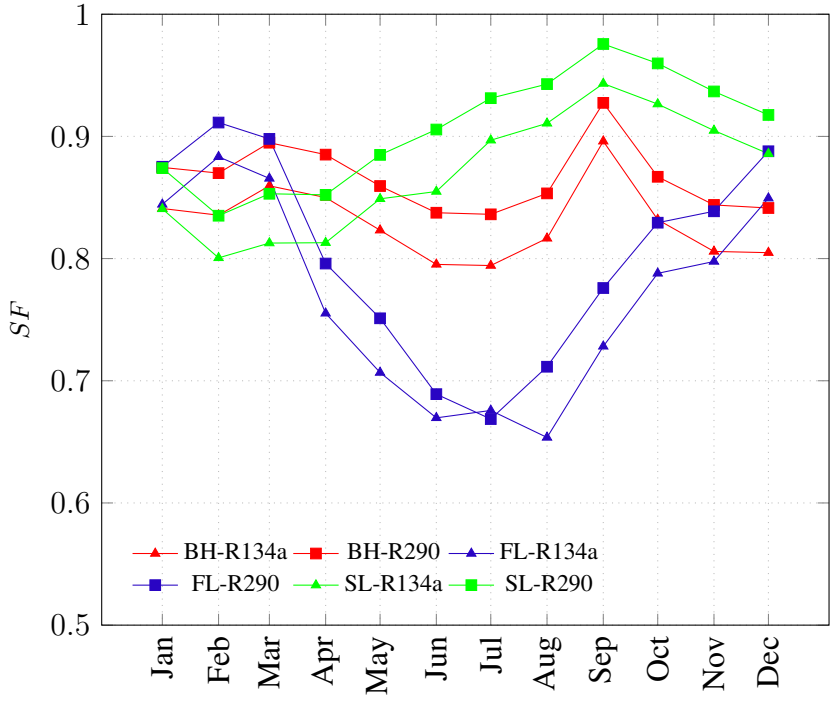

Figure 53 – Variation of monthly SF of the DX-PVT-SAHP operating with R134a and R290

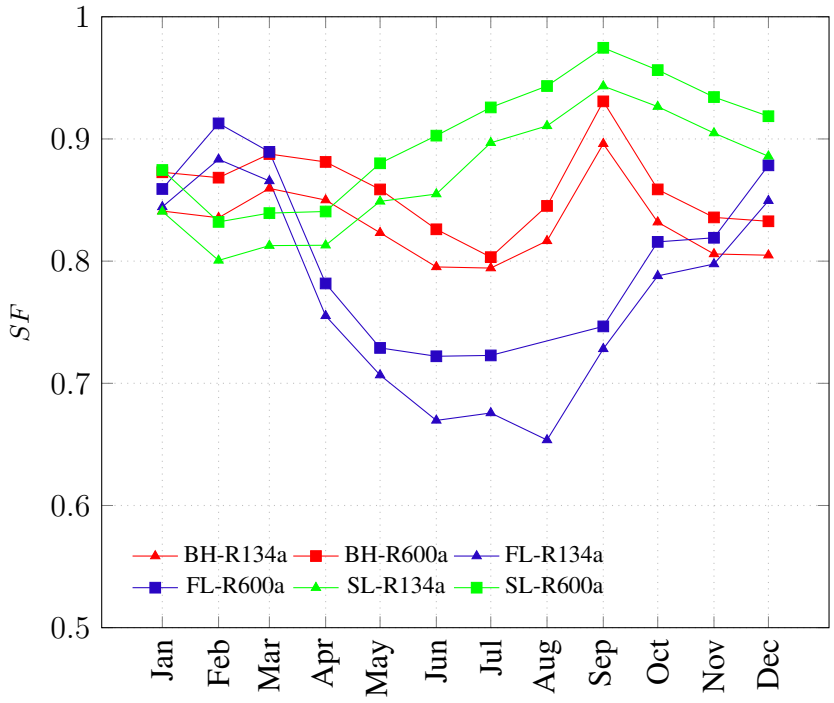

Figure 54 – Variation of monthly SF of the DX-PVT-SAHP operating with R134a and R600a

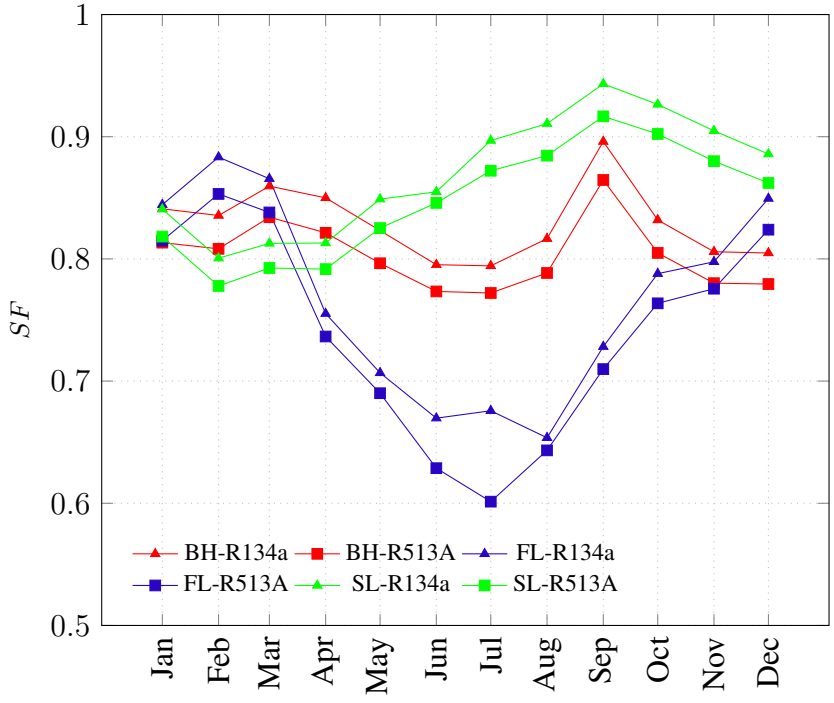

Figure 55 – Variation of monthly SF of the DX-PVT-SAHP operating with R134a and R513A

5.2.1 Influence of compressor selection in COP

This section evaluates the impact of compressor selection on the COP, recognizing that commercial compressors cannot always be chosen to exactly match the desired cooling capacity at specific operating conditions. As shown in Fig. 58, the variable-speed (R134a$^{(VS)}$) and fixed-

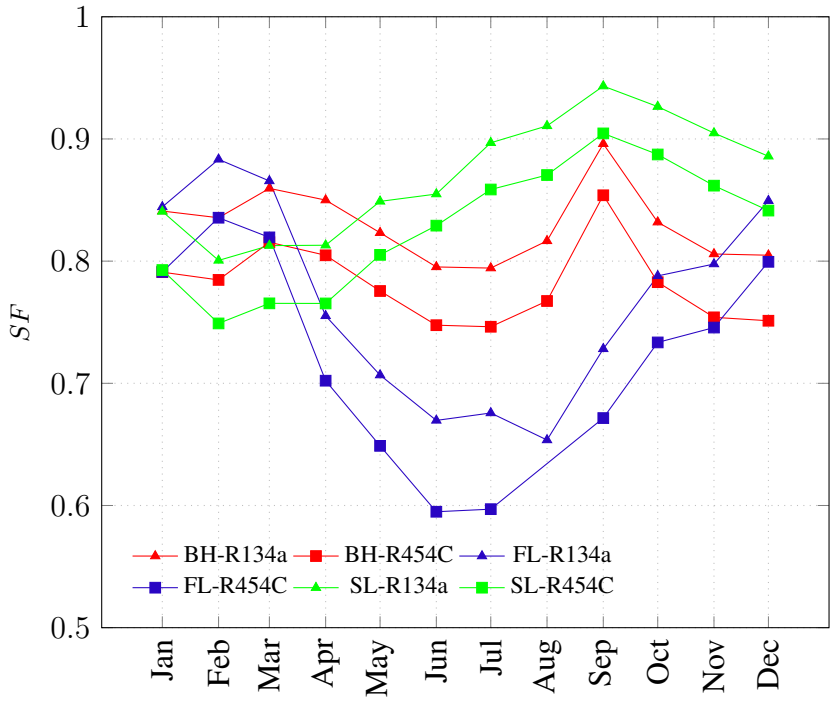

Figure 56 – Variation of monthly SF of the DX-PVT-SAHP operating with R134a and R454C

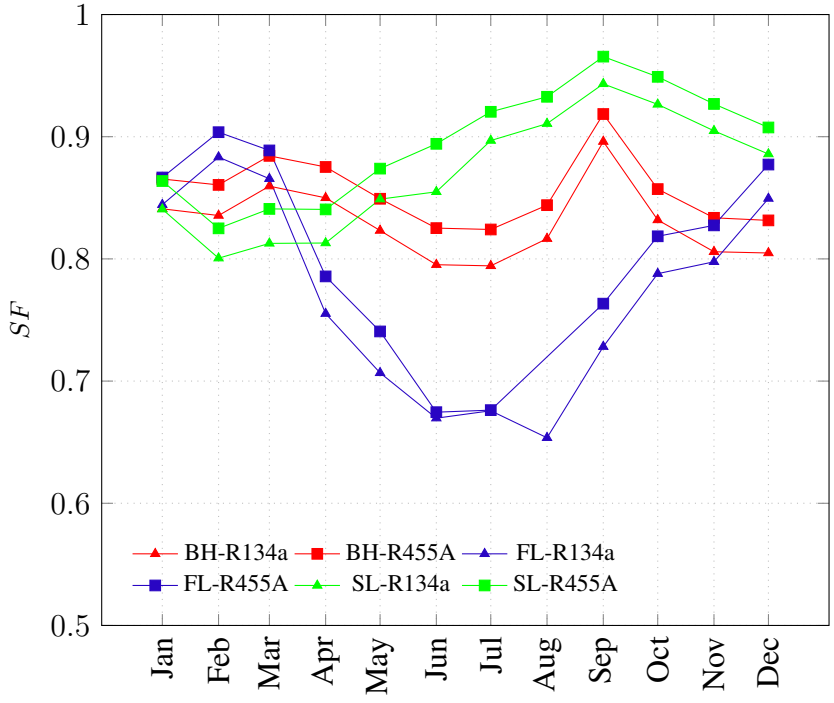

Figure 57 – Variation of monthly SF of the DX-PVT-SAHP operating with R134a and R455A

speed (R134a$^{(FS)}$) compressors, although similar in cooling capacity and displacement volume, display different energy efficiencies. Under the defined operating conditions, the variable-speed compressor achieves significantly better performance compared to the fixed-speed unit. Furthermore, for the R1234yf compressors, efficiency differences are also evident, as selecting

between two available models yields distinct COP values under identical operating conditions. As shown in Fig. 58, the compressor with lower displacement volume and cooling capacity (R1234yf$^{(1)}$) achieves superior performance compared to the compressor with higher displacement volume and cooling capacity (R1234yf$^{(2)}$). It can be concluded that compressor selection plays a decisive role in determining the efficiency of the DX-PVT-SAHP system. For instance, adopting the compressor with the highest cooling capacity for R1234yf may alter the ranking of the best-performing refrigerant, leading to R290 being identified as the optimal choice.

In this chapter, a series of results addressing energetic, economic, and environmental aspects were obtained using the developed mathematical model. In the next chapter, the main conclusions of the study will be presented.

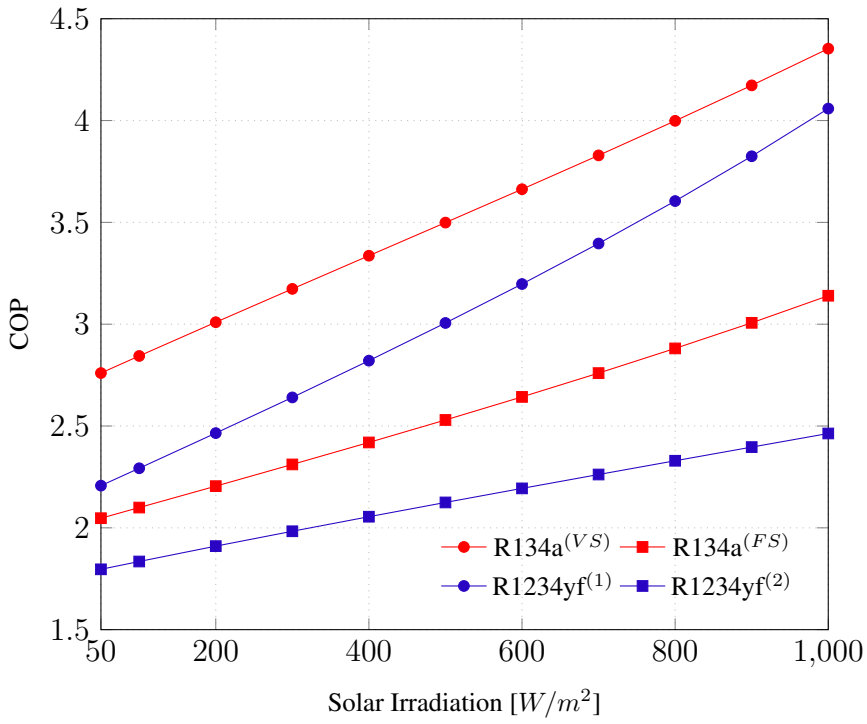

Figure 58 – COP in function of compressor selection

6 CONCLUSION

In the present thesis a numeric model of a DX-PVT-SAHP was presented and validated experimentally. The condenser and the PVT evaporator were modeled based in a moving boundary model and the compressor was modeled using a gray box model. The validation was developed based on seven steady state operational conditions. The COP mean uncertainty value was ± 0.10 and the maximum value was ± 0.15 that corresponds to 3.4% of the measured result. The thesis presented the results of a research conducted under various operating circumstances of solar irradiation, ambient temperature and mass flow rate. The comparison of low GWP refrigerants under energetic, environmental and economical performance was demonstrated.

The optimized refrigerant charges for R134a, R1234yf, R290, R600a, R513A, R454C, and R455A were 260 g, 250 g, 105 g, 125 g, 280 g, 210 g, and 200 g, respectively. These values indicate the specific amount of refrigerant required to achieve the best system performance for each fluid.

Furthermore, R1234yf exhibited the highest COP among all evaluated refrigerants, with its COP increasing from 2.21 at 50 W/m² to 4.06 at 1000 W/m². This demonstrates that its performance benefits become more pronounced under higher solar irradiance.

In addition, the lowest TEWI value was obtained with R1234yf, owing to its low GWP combined with the highest SPF among the compared refrigerants. By contrast, R513A and R454C showed the highest indirect emissions because their SPF values were lower than those of all other refrigerants analyzed.

It is also noteworthy that, even when four PV panels operated under identical environmental conditions, their SPF and TEWI results were inferior to those of all refrigerants used in the DX-PVT-SAHP system. This comparison reinforces the advantages of the integrated system over standalone PV-based water heating.

Moreover, the results showed that the investment payback period, when considering the energy savings provided by the DX-PVT-SAHP system, was 2.8 years. In comparison, installing a photovoltaic panel for electricity generation combined with an electric heater resulted in a payback period of 5.4 years. Consequently, the DX-PVT-SAHP using R1234yf offers a payback

time nearly twice as fast as that of an electric water heater supported by a photovoltaic panel.

With respect to the solar fraction, the highest value (SF = 1.0) occurred in September in São Luís–MA when operating the DX-PVT-SAHP with R1234yf. Conversely, the lowest SF (0.59) was observed in Florianópolis in June when R454C was used, highlighting the combined influence of refrigerant selection and local climatic conditions.

Overall, the findings confirm that the refrigerant providing the highest COP under conditions of high solar irradiance yielded the greatest SF. Conversely, the refrigerant with the lowest COP combined with the lowest solar irradiance resulted in the smallest SF, emphasizing the strong dependence of system performance on both thermal and environmental factors.

Finally, the electrical power generation was similar for all refrigerants and increased proportionally with solar irradiance, indicating that the choice of refrigerant has minimal impact on the photovoltaic efficiency of the system.

As the installation size increases, the viability of the DX-PVT-SAHP is enhanced. Therefore, the results of the present thesis indicate the feasibility of extending the analysis to applications that require larger volumes of water, such as hotels and swimming pools.

The present thesis represents the first study on a DX-PVT-SAHP system conducted at UFMG. The constructed prototype demonstrated satisfactory operating conditions and was able to deliver results that were validated by the numeric model, providing a basis for future research and publications. Furthermore, several opportunities for continued research arise from potential modifications to the system, such as replacing the thermostatic expansion valve with an electronic expansion valve; comparing the electrical output of the PV panel when operating as part of the PVT evaporator to that of an isolated PV panel; and investigating a control device capable of adjusting the water pump mass flow rate in response to variations in solar irradiance in order to maintain a constant outlet temperature, among other possibilities.

References

ABBASI, Bardia; LI, Simon; MWESIGYE, Aggrey. Investigation of the thermodynamic performance of a direct-expansion solar-assisted heat pump under very cold climatic conditions with and without glazing. **International Journal of Refrigeration**, v. 158, p. 329–344, 2024.

AGREEMENT, Paris. Paris agreement. In: HEINONLINE, 2017. REPORT of the conference of the parties to the United Nations framework convention on climate change (21st session, 2015: Paris). Retrived December. **Proceedings of** [...]. Paris-FR: [s.n.], 2015. v. 4, p. 2.

ANASTAS, Adam; MWESIGYE, Aggrey. Investigation of a photovoltaic thermal-direct expansion solar-assisted heat pump (PVT-DXSAHP) collector with different photovoltaic characteristics in cold climates. **American Journal of Undergraduate Research**, v. 22, n. 1, 2025.

ANDRADE, Angel; ZAPATA-MINA, Juan; RESTREPO, Alvaro. Exergy and environmental assessment of R-290 as a substitute of R-410A of room air conditioner variable type based on LCCP and TEWI approaches. **Results in Engineering**, v. 21, p. 101806, 2024. ISSN 2590-1230.

ARNESSON, Hugo *et al.* Comprehensive energy, economic, and environmental analysis of a hybrid photovoltaic-thermal (PVT) heat pump system. **Energy**, p. 136563, 2025.

ASHRAE, Handbook. Fundamentals-2013 American Society of Heating. **Refrigerating and Air Conditioning Engineers, Atlanta**, 2013.

BELL, Ian H. *et al.* Pure and pseudo-pure fluid thermophysical property evaluation and the open-source thermophysical property library CoolProp. **Industrial and Engineering Chemistry Research**, v. 53, n. 6, p. 2498–2508, 2014.

BELLOS, Evangelos; TZIVANIDIS, Christos. Multi-objective optimization of a solar assisted heat pump-driven by hybrid PV. **Applied Thermal Engineering**, v. 149, p. 528–535, 2019.

BELMAN-FLORES, Juan Manuel *et al.* Experimental study of R1234yf as a drop-in replacement for R134a in a domestic refrigerator. **International Journal of Refrigeration**, v. 81, p. 1–11, 2017.

BOTTICELLA, Francesco; VISCITO, Luca. Seasonal performance analysis of a residential heat pump using different fluids with low environmental impact. **Energy Procedia**, v. 82, p. 878–885, 2015.

BRAGA, Carlos HM *et al.* Energetic, economic and environmental (3E) analysis of R290, R454C and R465A for drop-in split type air conditioning running on R22. **Case Studies in Thermal Engineering**, v. 69, p. 105988, 2025.

BUKER, Mahmut Sami; RIFFAT, Saffa B. Solar assisted heat pump systems for low temperature water heating applications: a systematic review. **Renewable and Sustainable Energy Reviews**, v. 55, p. 399–413, 2016.

CHAICHANA, Chatcahwan; AYE, Lu; CHARTERS, William WS. Natural working fluids for solar-boosted heat pumps. **International Journal of Refrigeration**, v. 26, n. 6, p. 637–643, 2003.

CHAPRA, Steven C. **Applied numerical methods with MATLAB for engineers and scientists**. [S.l.]: McGraw-Hill, 2018.

CHATA, FB Gorozabel; CHATURVEDI, SK; ALMOGBEL, AJEC. Analysis of a direct expansion solar assisted heat pump using different refrigerants. **Energy Conversion and Management**, v. 46, n. 15-16, p. 2614–2624, 2005.

CHATURVEDI, S.K.; GAGRANI, V.D.; ABDEL-SALAM, T.M. Solar-assisted heat pump - a sustainable system for low-temperature water heating applications. **Energy Conversion and Management**, v. 77, p. 550–557, 2014.

CHEN, Hongbing; RIFFAT, Saffa B; FU, Yu. Experimental study on a hybrid photovoltaic/heat pump system. **Applied Thermal Engineering**, v. 31, n. 17-18, p. 4132–4138, 2011.

CHEN, Hongbing; ZHANG, Lei, *et al.* Performance study of heat-pipe solar photovoltaic/thermal heat pump system. **Applied Energy**, v. 190, p. 960–980, 2017.

CHOW, Tin Tai *et al.* Potential use of photovoltaic-integrated solar heat pump system in Hong Kong. **Applied Thermal Engineering**, v. 30, n. 8-9, p. 1066–1072, 2010.

DANNEMAND, Mark; PERERS, Bengt; FURBO, Simon. Performance of a demonstration solar PVT assisted heat pump system with cold buffer storage and domestic hot water storage tanks. **Energy and Buildings**, v. 188, p. 46–57, 2019.

DENG, Weishi; YU, Jianlin. Simulation analysis on dynamic performance of a combined solar/air dual source heat pump water heater. **Energy Conversion and Management**, v. 120, p. 378–387, 2016.

DRAVID, Arun Nilkanth *et al.* Effect of secondary fluid motion on laminar flow heat transfer in helically coiled tubes. **AICHE Journal**, v. 17, n. 5, p. 1114–1122, 1971.

DUARTE, Willian M; PAULINO, Tiago F; PABON, Juan JG, *et al.* Refrigerants selection for a direct expansion solar assisted heat pump for domestic hot water. **Solar Energy**, v. 184, p. 527–538, 2019.

DUARTE, Willian M; PAULINO, Tiago F; TAVARES, Sinthya G; CANÇADO, Kássio N, *et al.* Comparative study of geothermal and conventional air conditioner: a case of study for office applications. **Journal of Building Engineering**, v. 65, p. 105786, 2023.

DUARTE, Willian M; PAULINO, Tiago F; TAVARES, Sinthya G; MAIA, Antonio AT, *et al.* Feasibility of solar-geothermal hybrid source heat pump for producing domestic hot water in hot climates. **International Journal of Refrigeration**, v. 124, p. 184–196, 2021.

DUARTE, Willian Moreira. **Numeric model of a direct expansion solar assisted heat pump water heater operating with low GWP refrigerants (R1234yf, R290, R600a and R744) for replacement of R134a**. 2018. PhD thesis – Universidade Federal de Minas Gerais.

DUARTE, Willian Moreira; PABON, Juan Jose Garcia, *et al.* Nonisentropic phenomenological model of a reciprocating compressor. **International Journal of Air-Conditioning and Refrigeration**, v. 27, n. 04, p. 1950039, 2019.

EPE, EMPRESADE PESQUISA ENERGÉTICA. **Balanço Energético Nacional (BEN) 2023: Ano base 2022**. [S.l.: s.n.], 2023.

EPE, EMPRESADE PESQUISA ENERGÉTICA. PNE 2050-Plano Nacional de Energia. **Brasília: Plano Nacional de Energia**, 2020.

ESBRÍ, Joaquín Navarro *et al.* Effect of mean void fraction correlations on a shell-and-tube evaporator dynamic model performance. **Science and Technology for the Built Environment**, v. 21, n. 7, p. 1059–1072, 2015.

FAN, Yi *et al.* Scientific and technological progress and future perspectives of the solar assisted heat pump (SAHP) system. **Energy**, v. 229, p. 120719, 2021.

FANG, Guiyin; HU, Hainan; LIU, Xu. Experimental investigation on the photovoltaic–thermal solar heat pump air-conditioning system on water-heating mode. **Experimental Thermal and Fluid Science**, v. 34, n. 6, p. 736–743, 2010.

FINE, JP; FRIEDMAN, J; DWORKIN, SB. Detailed modeling of a novel photovoltaic thermal cascade heat pump domestic water heating system. **Renewable Energy**, v. 101, p. 500–513, 2017.

FONSECA, Vinícius David *et al.* Mass flow prediction in a refrigeration machine using artificial neural networks. **Applied Thermal Engineering**, v. 214, p. 118893, 2022.

FUKUROZAKI, SH; ZILLES, Roberto; SAUER, Ildo Luís. Energy payback time and CO2 emissions of 1.2 kWp photovoltaic roof-top system in Brazil. **Int. J. Smart Grid Clean Energy**, v. 2, n. 2, p. 164–169, 2013.

GHOUBALI, Redouane *et al.* Simulation study of a heat pump for simultaneous heating and cooling coupled to buildings. **Energy and Buildings**, v. 72, p. 141–149, 2014.

GUARRACINO, Ilaria *et al.* Systematic testing of hybrid PV-thermal (PVT) solar collectors in steady-state and dynamic outdoor conditions. **Applied Energy**, v. 240, p. 1014–1030, 2019.

HAWLADER, M.N.A.; CHOU, S.K.; ULLAH, M.Z. The performance of a solar assisted heat pump water heating system. **Applied Thermal Engineering**, v. 21, n. 10, p. 1049–1065, 2001.

HEREZ, Amal *et al.* Review on photovoltaic/thermal hybrid solar collectors: classifications, applications and new systems. **Solar Energy**, v. 207, p. 1321–1347, 2020. ISSN 0038-092X.

HU, Hainan; WANG, Rui; FANG, Guiyin. Dynamic characteristics modeling of a hybrid photovoltaic–thermal heat pump system. **International Journal of Green Energy**, v. 7, n. 5, p. 537–551, 2010.

HU, Wei; HE, Wei, *et al.* Experimental study of photovoltaic heat pump system based on modular phase change material. **Energy Conversion and Management**, v. 322, p. 119133, 2024. ISSN 0196-8904.

HUMIA, Gleberson M *et al.* Solar irradiation and refrigerant charge effects on performance of direct expansion solar assisted heat pumps using CO_2 transcritical cycle. **Applied Thermal Engineering**, v. 267, p. 125725, 2025.

INCROPERA, P; DEWITT, D. **Fundamentals of Heat and Mass Transfer (Portuguese edition)**. [S.l.: s.n.], 2008.

INMET. **National Institute of Meteorology: Weather data**. 2024.

JAMES, A *et al.* Experimental studies on photovoltaic-thermal heat pump water heaters using variable frequency drive compressors. **Sustainable Energy Technologies and Assessments**, v. 45, p. 101152, 2021.

JI, Jie *et al.* Distributed dynamic modeling and experimental study of PV evaporator in a PV/T solar-assisted heat pump. **International Journal of Heat and Mass Transfer**, v. 52, n. 5, p. 1365–1373, 2009. ISSN 0017-9310.

KAMEL, Raghad S; FUNG, Alan S. Modeling, simulation and feasibility analysis of residential BIPV/T+ ASHP system in cold climate—Canada. **Energy and Buildings**, v. 82, p. 758–770, 2014.

KHLIYEVA, Olga *et al.* Environmental and energy comparative analysis of expediency of heat-driven and electrically-driven refrigerators for air conditioning application. **Applied Thermal Engineering**, v. 219, p. 119533, 2023. ISSN 1359-4311.

KIM, Jinyoung *et al.* Energy, economic, and environmental evaluation of a solar-assisted heat pump integrated with photovoltaic thermal modules using low-GWP refrigerants. **Energy Conversion and Management**, v. 293, p. 117512, 2023.

KONG, XQ; LI, Y, *et al.* Modeling evaluation of a direct-expansion solar-assisted heat pump water heater using R410A. **International Journal of Refrigeration**, v. 76, p. 136–146, 2017.

KONG, XQ; ZHANG, D, *et al.* Thermal performance analysis of a direct-expansion solar-assisted heat pump water heater. **Energy**, v. 36, n. 12, p. 6830–6838, 2011.

KUANG, YH; SUMATHY, K; WANG, RZ. Study on a direct-expansion solar-assisted heat pump water heating system. **International Journal of Energy Research**, v. 27, n. 5, p. 531–548, 2003.

LAUGHMAN, Christopher R *et al.* A comparison of transient heat pump cycle models using alternative flow descriptions. **Science and Technology for the Built Environment**, v. 21, n. 5, p. 666–680, 2015.

LAZZARIN, Renato M. Dual source heat pump systems: Operation and performance. **Energy and Buildings**, v. 52, p. 77–85, 2012.

LEE, Yohan; JUNG, Dongsoo. A brief performance comparison of R1234yf and R134a in a bench tester for automobile applications. **Applied Thermal Engineering**, v. 35, p. 240–242, 2012.

LEMMON, E. W. *et al.* **NIST Standard Reference Database 23: Reference Fluid Thermodynamic and Transport Properties-REFPROP, Version 10.0, National Institute of Standards and Technology**. [S.l.: s.n.], 2018.

LEONFORTE, Fabrizio *et al.* Energy assessment and monitoring of a novel photovoltaic-thermal collector designed for solar-assisted heat pump systems. **IET Renewable Power Generation**, v. 14, n. 13, p. 2323–2330, 2020.

LI, Hong; SUN, Yue. Operational performance study on a photovoltaic loop heat pipe/solar assisted heat pump water heating system. **Energy and Buildings**, v. 158, p. 861–872, 2018.

LI, Shanshan; LI, Shuhong; ZHANG, Xiaosong. Comparison analysis of different refrigerants in solar-air hybrid heat source heat pump water heater. **International Journal of Refrigeration**, v. 57, p. 138–146, 2015.

LI, Weilin; CHU, Yiyi, *et al.* A transient model for the thermal inertia of chilled-water systems during demand response. **Energy and Buildings**, v. 150, p. 383–395, 2017.

LIANG, Ruobing *et al.* Performance modeling and analysis of a PVT-HP system with the roll-bond plate as the evaporator during winter conditions. **Applied Thermal Engineering**, v. 224, p. 120102, 2023.

LIU, Yang; ZHANG, Heng; CHEN, Haiping. Experimental study of an indirect-expansion heat pump system based on solar low-concentrating photovoltaic/thermal collectors. **Renewable Energy**, v. 157, p. 718–730, 2020.

LIU, Yiyang; QUAN, Zhenhua, *et al.* Numerical analysis and optimization study of photovoltaic/thermal-air source evaporator based on micro heat pipe arrays. **Solar Energy**, v. 269, p. 112314, 2024. ISSN 0038-092X.

LLOPIS, Rodrigo *et al.* R-454C, R-459B, R-457A and R-455A as low-GWP replacements of R-404A: Experimental evaluation and optimization. **International Journal of Refrigeration**, v. 106, p. 133–143, 2019. ISSN 0140-7007.

MAIA, AAT; KOURY, RNN; MACHADO, L. Development of a control algorithm employing data generated by a white box mathematical model. **Applied Thermal Engineering**, v. 54, n. 1, p. 120–130, 2013.

MAKHNATCH, Pavel; KHODABANDEH, Rahmatollah. Selection of low GWP refrigerant for heat pumps by assessing the life cycle climate performance (LCCP). In: 11TH International Energy Agency Heat Pump Conference Montreal, May 12-16, 2014. **Proceedings of** [...]. Montreal-CA: [s.n.], 2014.

MANZOLINI, Giampaolo *et al.* Tiles as solar air heater to support a heat pump for residential air conditioning. **Applied Thermal Engineering**, v. 102, p. 1412–1421, 2016.

MARTINS, Leonardo VS *et al.* Assessment of total equivalent warming impact (TEWI) of alternative refrigerants for retrofit of R22 in single split air conditioning system. **Journal of Building Engineering**, v. 88, p. 109085, 2024.

MCTI: MINISTRY OF SCIENCE, Technology; INNOVATION. **Fator médio - Inventários corporativos Banco de dados**. 2024.

MOHANRAJ, M *et al.* Comparison of energy performance of heat pumps using a photovoltaic–thermal evaporator with circular and triangular tube configurations. In: SPRINGER. BUILDING simulation. **Proceedings of** [...]. Berlin-GE: [s.n.], 2016. v. 9, p. 27–41.

MOHANRAJ, M. *et al.* Research and developments on solar assisted compression heat pump systems – A comprehensive review (Part A: Modeling and modifications). eng. **Renewable and sustainable energy reviews**, v. 83, p. 90–123, 2018. ISSN 1364-0321.

MOSTAFA, A.; HASSANAIN, M.; ELGENDY, E. An experimental study of R-454C pull-down performance as a drop-in refrigerant in a walk-in cold store system. **International Journal of Refrigeration**, v. 130, p. 170–178, 2021. ISSN 0140-7007.

MOTA-BABILONI, Adrián; GIMÉNEZ-PRADES, Pau, *et al.* Semi-empirical analysis of HFC supermarket refrigeration retrofit with advanced configurations from energy, environmental, and economic perspectives. **International Journal of Refrigeration**, v. 137, p. 257–271, 2022. ISSN 0140-7007.

MOTA-BABILONI, Adrián; HARO-ORTUNO, Jorge, *et al.* Experimental drop-in replacement of R404A for warm countries using the low GWP mixtures R454C and R455A. **International Journal of Refrigeration**, v. 91, p. 136–145, 2018.

NOGUEIRA, Filipe; MACHADO, Luiz, *et al.* Performance evaluation of a PVT-DX-SHAP operating with refrigerants R134a and R290. **Proceeding of 28th International Congress of Mechanical Engineering**, to appear, 2025.

NOGUEIRA, Filipe; MAIA, Antônio A.T., *et al.* Energetic, economic and environmental analysis of a direct expansion photovoltaic solar assisted heat pump with low-GWP refrigerants. **Solar Energy**, v. 302, p. 114042, 2025. ISSN 0038-092X.

OECD/IEA. **The Future of Heat Pumps**. [S.l.: s.n.], 2022. P. 110.

ORUÇ, Vedat; DEVECIOĞLU, Atilla G. Experimental investigation on the low-GWP HFC/HFO blends R454A and R454C in a R404A refrigeration system. **International Journal of Refrigeration**, v. 128, p. 242–251, 2021.

PALM, Björn. Hydrocarbons as refrigerants in small heat pump and refrigeration systems–a review. **International Journal of Refrigeration**, v. 31, n. 4, p. 552–563, 2008.

PAULA, Cleison Henrique de *et al.* Energetic, exergetic, environmental, and economic assessment of a cascade refrigeration system operating with four different ecological refrigerant

pairs. **International Journal of Air-Conditioning and Refrigeration**, v. 29, n. 03, p. 2150025, 2021.

PAULA, Cleison Henrique de *et al.* Optimal design and environmental, energy and exergy analysis of a vapor compression refrigeration system using R290, R1234yf, and R744 as alternatives to replace R134a. **International Journal of Refrigeration**, v. 113, p. 10–20, 2020.

PAULINO, Tiago F. *et al.* Modeling and experimental analysis of the solar radiation in a CO_2 direct-expansion solar-assisted heat pump. **Applied Thermal Engineering**, v. 148, p. 160–172, 2019.

PEI, G *et al.* Performance of the photovoltaic solar-assisted heat pump system with and without glass cover in winter: a comparative analysis. **Proceedings of the Institution of Mechanical Engineers, Part A: Journal of Power and Energy**, v. 222, n. 2, p. 179–187, 2008.

PETRUCCI, Giovanni Augusto *et al.* Energy analysis of a direct expansion heat pump assisted by a thermal photovoltaic panel for hot water production in several regions of Brazil. **Energy Conversion and Management**, v. 319, p. 118969, 2024. ISSN 0196-8904.

PROTOCOL, Montreal; LAYER, Ozone. **Refrigeration, Air Conditioning and Heat Pumps Technical Options Committee**. **UN Environment Programme**, 2022.

QU, Minglu *et al.* Experimental study on the operating characteristics of a novel photovoltaic/thermal integrated dual-source heat pump water heating system. **Applied Thermal Engineering**, v. 94, p. 819–826, 2016.

RABELO, Sabrina N *et al.* Economic analysis and design optimization of a direct expansion solar assisted heat pump. **Solar Energy**, v. 188, p. 164–174, 2019.

RASMUSSEN, Bjarne Dindler; JAKOBSEN, Arne. Review of compressor models and performance characterizing variables. **Fifteenth International Compressor Engineering Conference at Purdue University**, 2000.

REES, Simon. **Advances in ground-source heat pump systems**. [S.l.]: Woodhead Publishing, 2016.

REIS, Humberto O *et al.* Optimal high-pressure correlation for transcritical CO2 cycle in direct expansion solar assisted heat pumps. **Journal of Building Engineering**, v. 97, p. 110616, 2024.

RESENDE, Sara I. M. *et al.* Dynamic modeling of an R290 direct-expansion solar-assisted heat pump: Performance analysis for efficient hot water production under different conditions. **Journal of Building Engineering**, v. 100, p. 111687, 2025.

RIJVERS, Len; RINDT, Camilo; KEIZER, Corry de. Numerical Analysis of a Residential Energy System That Integrates Hybrid Solar Modules (PVT) with a Heat Pump. **Energies**, v. 15, n. 1, p. 96, 2021.

ROHSENOW, Warren M; HARTNETT, James P; CHO, Young I, *et al.* **Handbook of Heat Transfer**. [S.l.]: Mcgraw-hill New York, 1998. v. 3.

SANTOS, A. *et al.* Air conditioning system integrated with thermal energy storage for buildings in tropical climates. **Processes**, v. 12, n. 11, p. 2388, 2024.

SANTOS, J. O. *et al.* Comparação econômica entre o sistema de refrigeração fotovoltaico por compressão de vapor e chillers de absorção com coletores solares térmicos. In: CBENS 2018: VII Congresso Brasileiro de Energia Solar. **Anais** [...]. Gramado-PR: [s.n.], 2018.

SANZ, Asier *et al.* A solar dually PVT driven direct expansion heat pump one-year field operation results at continental climate. **Energies**, v. 15, n. 9, p. 3205, 2022.

SHAH, Mirza M. A general correlation for heat transfer during film condensation inside pipes. **International Journal of Heat and Mass Transfer**, v. 22, n. 4, p. 547–556, 1979.

SHAH, Mirza M. Improved correlation for heat transfer during condensation in mini and macro channels. **International Journal of Heat and Mass Transfer**, v. 194, p. 123069, 2022.

SHARMA, Deepak Kumar *et al.* Analysis of water and refrigerant-based PV/T systems with double glass PV modules: an experimental and computational approach. **Solar Energy**, v. 268, p. 112296, 2024.

SPORN, P; AMBROSE, ER. The heat pump and solar energy. In: WORLD symposium on applied solar energy. **Proceedings of** [...]. Arizona-US: [s.n.], 1955.

SUN, Licheng; MISHIMA, Kaichiro. An evaluation of prediction methods for saturated flow boiling heat transfer in mini-channels. **International Journal of Heat and Mass Transfer**, v. 52, n. 23-24, p. 5323–5329, 2009.

TAYLOR, Barry N; KUYATT, Chris E, *et al.* **Guidelines for evaluating and expressing the uncertainty of NIST measurement results**. [S.l.]: US Department of Commerce, Technology Administration, National Institute of Standards and Technology, 1994. v. 1297.

TSAI, Huan-Liang. Modeling and validation of refrigerant-based PVT-assisted heat pump water heating (PVTA–HPWH) system. **Solar Energy**, v. 122, p. 36–47, 2015.

UNEP. **Ozone and Climate Protection: Low-Global Warming Potential Alternatives - OzonAction Special Issue 2017**. [S.l.: s.n.], 2017.

VALLATI, A *et al.* Energy analysis of a thermal system composed by a heat pump coupled with a PVT solar collector. **Energy**, v. 174, p. 91–96, 2019.

WANG, Gang *et al.* Experimental study on a novel PV/T air dual-heat-source composite heat pump hot water system. **Energy and Buildings**, v. 108, p. 175–184, 2015.

WU, Di; HU, Bin; WANG, R.Z. Vapor compression heat pumps with pure low-GWP refrigerants. **Renewable and Sustainable Energy Reviews**, v. 138, p. 110571, 2021. ISSN 1364-0321.

XU, Guoying; DENG, Shiming, *et al.* Simulation of a photovoltaic/thermal heat pump system having a modified collector/evaporator. **Solar Energy**, v. 83, n. 11, p. 1967–1976, 2009.

XU, Guoying; ZHANG, Xiaosong; DENG, Shiming. Experimental study on the operating characteristics of a novel low-concentrating solar photovoltaic/thermal integrated heat pump water heating system. **Applied Thermal Engineering**, v. 31, n. 17-18, p. 3689–3695, 2011.

YANG, Bin; BRADSHAW, Craig R.; GROLL, Eckhard A. Modeling of a semi-hermetic CO2 reciprocating compressor including lubrication submodels for piston rings and bearings. **International Journal of Refrigeration**, v. 36, n. 7, p. 1925–1937, 2013. ISSN 01407007.

YAO, Jian; CHEN, Erjian, *et al.* Theoretical analysis on efficiency factor of direct expansion PVT module for heat pump application. **Solar Energy**, v. 206, p. 677–694, 2020.

YAO, Jian; LIU, Wenjie, *et al.* Two-phase flow investigation in channel design of the roll-bond cooling component for solar assisted PVT heat pump application. **Energy Conversion and Management**, v. 235, p. 113988, 2021.

YILDIZ, A; YILDIRIM, R. Investigation of using R134a, R1234yf and R513A as refrigerant in a heat pump. **International Journal of Environmental Science and Technology**, v. 18, n. 5, p. 1201–1210, 2021.

YOGARAJA, J *et al.* Performance of direct expansion photovoltaic-thermal evaporator assisted compression heat pump water heaters using a zeotropic mixture. **Solar Energy**, v. 271, p. 112435, 2024.

ZANETTI, Emanuele *et al.* Performance and control of a CO2 dual source solar assisted heat pump with a photovoltaic-thermal evaporator. **Applied Thermal Engineering**, v. 218, p. 119286, 2023.

ZHANG, Songyuan; GUANB, Xin; GUO, Zhibo. Design and economic analysis of photovoltaic-double resource heat pump. **Energy Procedia**, v. 16, p. 977–982, 2012.

ZHANG, Xingxing; ZHAO, Xudong, *et al.* Characterization of a solar photovoltaic/loop-heat-pipe heat pump water heating system. **Applied Energy**, v. 102, p. 1229–1245, 2013.

ZHAO, Xudong *et al.* Theoretical study of the performance of a novel PV/e roof module for heat pump operation. **Energy conversion and Management**, v. 52, n. 1, p. 603–614, 2011.

ZHOU, Chao *et al.* Experimental study on the cogeneration performance of roll-bond-PVT heat pump system with single stage compression during summer. **Applied Thermal Engineering**, v. 149, p. 249–261, 2019.

ZIVI, Sa M. **Estimation of steady-state steam void-fraction by means of the principle of minimum entropy production**, 1964.